IEEE Access
Multidisciplinary | Rapid Review | Open Access Journal

Received 11 November 2022, accepted 28 November 2022, date of publication 1 December 2022,
date of current version 8 December 2022.

Digital Object Identifier 10.1109/ACCESS.2022.3226272

TOPICAL REVIEW

Array Antennas for mmWave Applications: A Comprehensive Review

B. G. PARVEEZ SHARIFF[1], TANWEER ALI[1], (Senior Member, IEEE), PALLAVI R. MANE[1], (Senior Member, IEEE), AND PRADEEP KUMAR[2]

[1]Department of Electronics and Communication, Manipal Institute of Technology, Manipal Academy of Higher Education, Manipal 576104, India
[2]Department of Electrical, Electronic and Computer Engineering, University of KwaZulu-Natal, Durban 4041, South Africa

Corresponding author: Tanweer Ali (tanweer.ali@manipal.edu)

ABSTRACT The demand for wide bandwidth has driven us to focus on the higher spectrum, the millimeter wave (mmWave) spectrum. The mmWave offers several advantages, such as wide bandwidth, low latency, and higher data rate, but the signal at these frequencies significantly suffers high atmospheric attenuation and path loss. To overcome these issues, array antennas are used as it provides high gain, better directivity, and bandwidth. This paper presents a detailed review of array antennas based on feeding methods and discusses reconfigurable arrays. The series-fed array results in a narrow bandwidth, high return losses, and low gain that can be resolved with tapered structures, coplanar waveguide (CPW), and SIW technique. Similarly, transmission losses, coupling losses, and high side lobe-levels in parallel-fed arrays can be addressed with multilayer structures, coplanar strips with CPW, pill-box transmission, ridge gap waveguide (RGWG), graphene material, and magnetoelectric dipoles. The merits of series and parallel feed methods are availed with the hybrid feed method. These feeding methods with arrays are extended to reconfigurable array along with active RF switch with stubs, continuous or discrete phase shifter, butler matrix, and/or graphene nanoplates. The parameter performance metrics of these arrays are summarized and concluded with the future scope.

INDEX TERMS Array antenna, series-fed, parallel-fed, hybrid-fed, reconfigurable array, mmWave, 5G.

I. INTRODUCTION

The millimeter wave (mmWave) spectrum is the current focus by many topological wireless applicational areas due to its wide bandwidth and low latency [1]. But these advantages come at the expense of higher atmospheric attenuation, short propagation, and higher path loss [2], [3], [4]. To mitigate these issues, comprehension of channel characteristics is essential. Various channel models such as WINNER I, WINNER II model, single-frequency floating-intercept (FI) model, single-frequency close-in (CI) free space reference distance model, alpha-beta-gamma (ABG) model, multi-frequency CI model, and so on [5], [6] are developed to study atmospheric and path loss conditions in an urban and sub-urban area. All these models suggest a need for high gain, directional, and/or beamforming antennas that can resolve the issue of high path loss propagation at mmWave bands [7], [8].

Array antennas can address the above issues because they have numerous advantages: higher gain, directional radiation, wide-angle beam scanning, adaptive beamforming, multiple beams, and wide bandwidth compared to single-element or omnidirectional antennas. With all these advantages, the array antenna suffers from two major issues: higher side-lobe level and grating lobes due to improper element spacing. A lot of research has been conducted on the various types of array antennas. Ely Levine [9] has empirically tested and proved that the gain and directivity of microstrip array antenna of 16, 64, 256, and 1024 elements have improved over the frequency range of 10 to 35 GHz. But it is also evident that as the number of radiating elements increases the radiation loss, dielectric loss, and ohmic loss increase, whereas surface wave losses remain constant. The radiation loss can be controlled with the co-planar waveguide (CPW) designs [10]. The

The associate editor coordinating the review of this manuscript and approving it for publication was Ravi Kumar Gangwar.

substrate-integrated waveguide (SIW) technology reduces the surface wave by reducing the leaky waves and guiding them in the desired direction. These are highly efficient and low-loss antennas, which could operate at higher TE modes and address the issue of radiation losses and surface wave losses encountered in microstrip antennas [11]. SIW requires a high degree of precision milling, especially when designing at mmWave, because the size and distance of via get smaller. SIW antenna with a microstrip feed line makes the design compact and easy to implement [12]. The significant bandwidth improvement with low side-lobe level (SLL) and mutual coupling can be obtained from the tapered/Vivaldi antenna with its low-profile design [13]. The demand for high gain and wide bandwidth influenced the researcher to study the various combination of structures, and one such combination is the magnetoelectric dipole with microstrip patch element of SIW [14], [15].

The feeding network to these antennas should have low radiation losses, be compact, and be easy to feed. Based on that, the feed network can be categorized as series, parallel, or hybrid (a combination of series and parallel). The significance of these feeding methods to various antennas is discussed in section 4.

The frequency, radiation, and/or polarization of an array antenna can be changed to reconfigurable arrays with an additional switching RF circuit. The RF diodes with bandpass filter [16] and orthogonal orientation of radiating element [17] can make the array frequency tunable. The power of equal magnitude with different phases applied to a set of elements or individual elements obtained through phase shifter [18], butler matrix [19], active RF diodes [20], or graphene nanoplate [21] could able to steer the beam in the desired direction. The graphene material is gaining prominence in the field of antennas due to its flexibility, resistive and good conductivity [22]. The orientation of polarization can be altered by superimposing the two different polarization through different feeds [23] [24]. These reconfigurable array structures are discussed in section 5.

This article presents a comprehensive review of array antenna based on the feeding method and reconfigurability. The key contribution of this article is as follows:

- It provides an overview of design methods of series-fed array antennas and methods to overcome the narrow bandwidth and return losses.
- It provides the comprehension of parallel-fed arrays, design structure, and methods to overcome the radiation losses from the feeding network.
- The comprehensive benefit of series and parallel feed combination as hybrid structure in array antenna.
- Overview of reconfigurable structure, feeding methods, and RF circuits to obtain reconfigurability (frequency, radiation, or polarization).

The organization of the paper is as follows: Section 2 introduces the standard parameters to be considered in the design of the array antenna. Section 3 discusses the array antenna for mmWave, followed by a review of a non-reconfigurable array based on the feeding method and reconfigurable arrays in sections 4 and 5. The overall discussion, followed by the conclusion and future scope, is presented in sections 6 and 7.

II. STANDARD PARAMETERS FOR ARRAY ANTENNAS AT mmWAVE

The 3rd generation partnership project (3GPP) and researchers has standardized the performance metric of parameters for an array antenna such as gain, bandwidth, radiation, SLL, grating lobes, beam steering, beam forming, multiple beams [25] as shown in Figure 1 to meet the demand of mmWave applications and 5G [26], [27]. The array antennas designed should meet the following standards: it must have high gain great than 20 dBi to overcome the path loss factor in propagation. It should operate at Q, U, E and W band with narrow beam half-power-beamwidth (HPBW) of less than 10°. The SLL should be < -20 dB with no grating lobes. The maximum beam steering ability of $\pm$ 180° with continues scan or discrete scan with multi beam support to connect the multiple users simultaneously.

FIGURE 1. Parameter standards for array antenna.

III. ARRAY ANTENNAS FOR mmWAVE

This article comprehensively reviews array antennas categorized based on non-reconfigurable and reconfigurable antennas. In contrast, non-reconfigurable antennas are categorized based on the feeding methods, such as series-fed, parallel-fed, or hybrid-fed (parallel-series fed) array antennas, as shown in Figures 2 and 3.

The series feed structure has advantages over parallel feed as it takes less space, and compact and microstrip line losses are low. Here the radiating elements are arranged in series

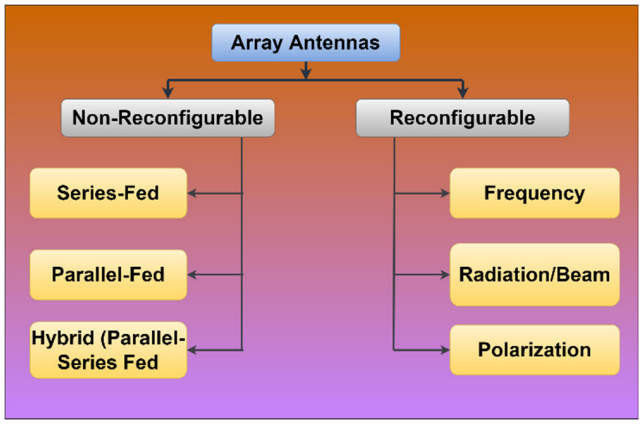

FIGURE 2. Classification of array antennas as non-reconfigurability and reconfigurability.

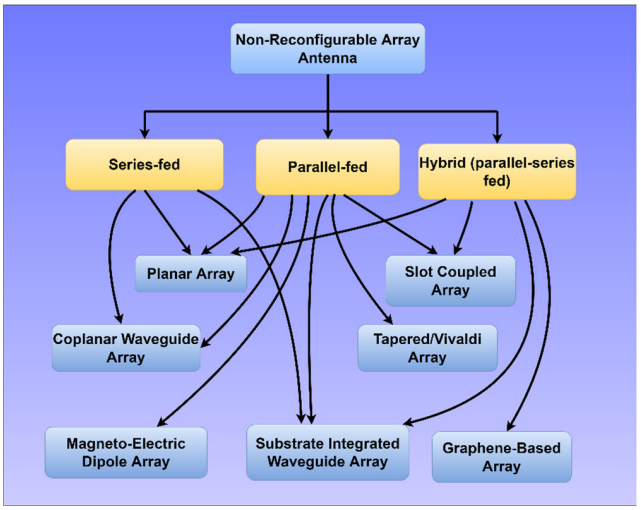

FIGURE 3. Classification of non-reconfigurable array antennas.

and interconnected by microstrip lines. The feeding can be provided at the first element or at the center through coaxial, microstrip, or with SIW. Most of the power in the uniformly shaped and uniformly spaced array is radiated by the first few elements. This is due to improper distribution of power; as a result, the series-feeding method suffers from narrow impedance bandwidth and high SLL. The large SLL can be reduced by modifying the conventional series feed structure to tapered structures [28]. The series-fed method has another issue of high return loss. This can be resolved by terminating the microstrip line with a matched radiating element that can radiate the residual power from the microstrip line.

On the other hand, the design of parallel feed structure is relatively simple compared to series-fed. The power to all the radiating elements can be equally divided through the T-junction distributor. Hence, the magnitude and phase of each element can be controlled. It results in wide bandwidth, better gain, reduced SLL, and better radiation patterns. But parallel feed structure introduces high radiation loss due to multiple feed arms, which affects the overall radiation efficiency of the array antenna. Therefore, most of the reconfigurable antennas utilize the advantages of both the series and parallel feed methods by combining these into a hybrid feed.

The reconfigurable antennas are categorized based on frequency, radiation pattern, and polarization reconfigurability. The frequency reconfigurable antenna finds its application in cognitive radio [29], satellite application [30], and aircraft [31]. These use active devices like a p-i-n diode to operate as a switch to connect a portion of antenna to resonate at a different frequency. Radiation reconfigurable array antennas able to steer the beam at different angle in azimuthal plane (ϕ) or elevation plane (θ) and or able to generate multiple beam with the aid of continuous phase shifters [32], [33], active devices (diodes) with EBG structure [34], or butler matrix (BM) [35]. The polarization reconfigurable array could be able to reconfigure the polarization from linear to circular or right-hand circular polarization (RHCP) to left-hand circular polarization (LHCP) and vice versa.

IV. NON-RECONFIGURABLE ARRAY ANTENNAS

The non-reconfigurable array antennas are categorized based on the feeding methods to the radiating element as shown in Figure 3. The series-fed, parallel-fed, and hybrid (parallel-series) fed, are further categorized based on the technological structure adapted such as planar, slot-coupled, coplanar waveguide (CPW), substrate integrated wave guide (SIW), Vivaldi antenna, Magneto-Electric dipole, Graphene-based. The impedance for the microstrip transmission line can be calculated using equations (1) to (4), where W_f is the width of the feed line, h, and εr are the height and relative permittivity of the substrate.

For $W_f/h \leq 1$

$$Z_0 = 100\Omega = \frac{W_f}{h} \leq 1 = \frac{60}{\sqrt{\varepsilon_{eff}}} ln\left[\frac{8h}{W_f} + \frac{W_f}{4h}\right] \quad (1)$$

where

$$\varepsilon_{reff} = \frac{\varepsilon_r + 1}{2} + \frac{\varepsilon_r - 1}{2}\left[\frac{1}{\sqrt{1 + 12\frac{h}{W_f}}} + 0.04\left(1 - \frac{W_f}{h}\right)^2\right] \quad (2)$$

For $W_f/h \geq 1$

$$Z_0 = 50\Omega = \frac{W_f}{h} \geq 1 = \frac{120\pi\sqrt{\varepsilon}_{eff}}{\left[\frac{W_f}{h} + 1.393 + 0.667ln\left[\frac{W_f}{h} + 1.444\right]\right]} \quad (3)$$

where

$$\varepsilon_{reff} = \frac{\varepsilon_r + 1}{2} + \frac{\varepsilon_r - 1}{2}\left[\frac{1}{\sqrt{1 + 12\frac{h}{W_f}}} + 0.04\left(1 - \frac{W_f}{h}\right)^{-\frac{1}{2}}\right] \quad (4)$$

A. SERIES-FED ARRAY ANTENNAS

This section reviews planar, slot coupled, coplanar waveguide, and substrate integrated-waveguide array antennas.

1) PLANAR ARRAY

The planar antennas are mostly designed on a single substrate with microstrip elements, making them a low-profile antenna. A simple eight-dipole array antenna is proposed on planar structure in [36] to reduce the line losses and enhance the bandwidth. Here the reflectors and directors are replaced by eight dipoles tilted at an angle of 45° towards the ground plane, which has also been tapered toward the end of the strip. This antenna is comparable with the log-periodic dipole antenna (LPDA) structure, but its performance is much better than LPDA in terms of gain and bandwidth. The Rogers RO4003C substrate is used with a thickness of 0.2032 mm. The left half of the dipoles are connected in series to a microstrip etched on top of the substrate. The other half of the dipoles are connected to the microstrip line etched on the bottom of the substrate. A strip line on top is fed by a quarterwave-transformer, whereas the bottom strip line is connected to the ground. This resulted in 27.1-30.6 GHz bandwidth at S11 < -10 dB, SSL of -14.7 and -7 dB in E- and H-plane. The design is optimized by changing the length and spacing between elements resulting in a nonuniform structure. The length and spacing between dipoles decrease from the ground plane till the end of the structure. A parametric study is performed by varying on length and spacing between dipoles to optimize the performance. This resulted in a better gain of 10.8 dBi, a bandwidth of 23.5-51.9 GHz, with SLLs -24.9 and -19.4 in E- and H-plane as shown in Figure 4(a, c and d). These results show that the non-uniform structure has resolved the issue of narrow bandwidth, SLL, and gain. The prototype fabrication is shown in Figure 4(b).

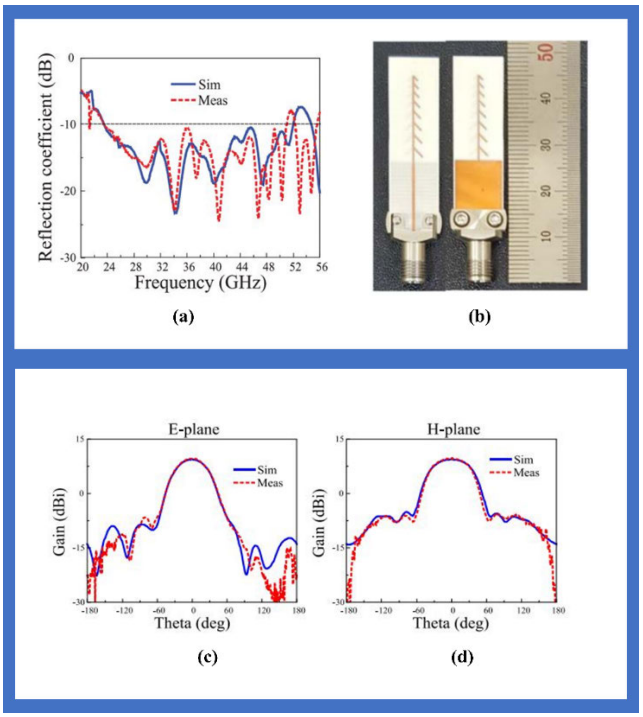

FIGURE 4. (a) Reflection coefficient bandwidth at S11 < -10 dB of non-uniform structure. (b) Prototype fabrication of non-uniform array antenna. Radiation pattern of non-uniform antenna at 24 GHz (c) E-plane, (d) H-plane. [36].

Another high gain antenna with ladder-like structure is designed in [37]. The initial design begins with the rectangular patch fed by a 50 Ω microstrip line. Later the feed is optimized to a quarterwave-transformer to improve the reflection coefficient S11 and to decrease the return loss. Further, multiple patches are replicated, connected by a 50 Ω microstrip line forming a ladder structure. The edges of extreme four corner patches are trimmed to enhance the S11. The parametric study is performed to obtain the optimum length and width of feed, as well as the length of strip line connected to patches. From the current distribution Figure 5(f) it can be noted that the maximum current is concentrated over the feed line and at the edges of few patches. The bandwidth at S11 < -10 dB is 27.06 – 28.35 GHz as shown in Figure 5(a) along with prototype fabrication (Figure 5(b)). The radiation pattern is omnidirectional in E and H – planes are shown in Figure 5(c-d).

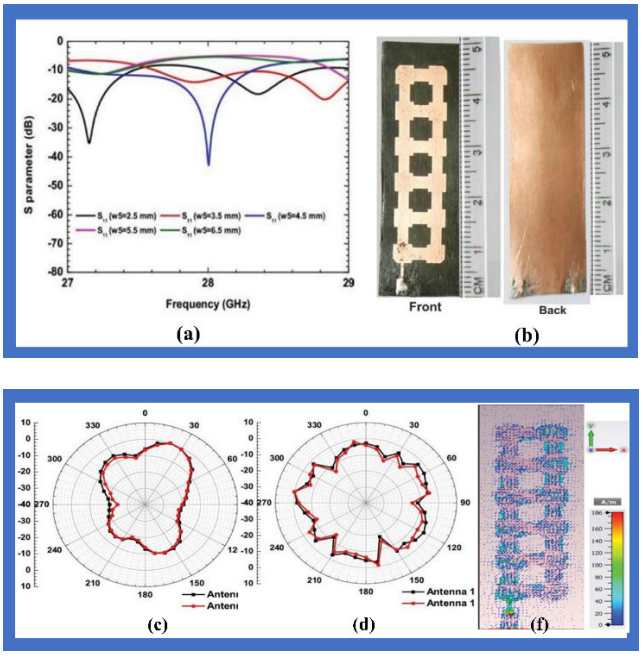

FIGURE 5. (a) Reflection coefficient$_{S11}$ parameter. (b) Prototype fabrication of array antenna. Radiation pattern of array, (c) E-plane, (d) H-plane, (f) Current distribution [37].

Another low-profile series-fed antenna array is proposed with a horn shape stub to the left of the microstrip line [38]. The traveling wave in the microstrip line has symmetrical fringing fields and magnetic current, which is periodic at λg (guided wavelength). Due to this periodic nature, the magnetic current cancels when the microstrip line is unable

TABLE 1. Merits and demerits of series-fed planar array structures.

References	Design Structure	Technique adapted	Merits	Demerits
Series Feeding Method				
[36]	Planar array	Non-uniform structure and spacing with tapered dipole radiator	• Wide bandwidth • Suppressed SLL • Narrow beamwidth in E- and H-plane.	• Lack of standard method to calculate variable spacing and length of the element.
[37]		Non-uniform structure and uniform spacing, ladder structure radiator	• Wide bandwidth • High efficiency	• Omnidirectional radiation • Unequal power distribution
[38]		Uniform structure and spacing tapered stubs radiator	• Reduced mismatch losses • Wide bandwidth • Narrow beamwidth • Low cross-polarization due to asymmetrical arrangement.	• Dominant SLL • Unequal power distribution.

to radiate. In this design, a simple technique is adopted to eliminate the anti-phase magnetic current by introducing stub at a period of λg, as shown in Figure 6(a-b). The stub element can be rectangular, triangular, or any shape, but here trapezoidal shape is considered as it performs slightly better than others. The design of the proposed structure has a microstrip line with four trapezoidal stubs to the left of the strip line at a distance of λg on top of the Rogers 5880 substrate with the ground plane at the bottom. The structure is fed by a coaxial cable at the center of the microstrip line. The cancellation of anti-phase magnetic current in the proposed structure is demonstrated via the simulated current distribution image in HFSS, which is compared with the pure microstrip line current distribution. The parametric analysis is performed on the microstrip length and dimension of a stub.

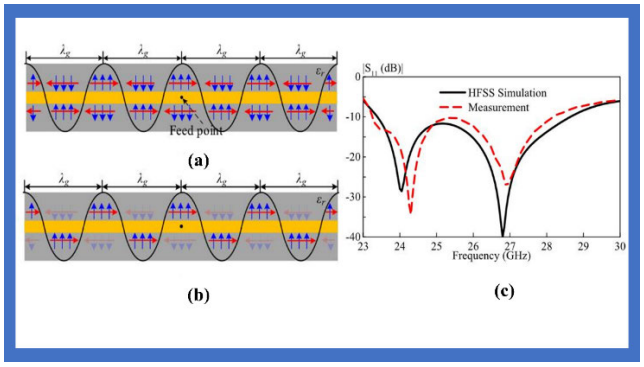

FIGURE 6. Transmission line fields, (a) Fringing electric field and equivalent magnetic current of a pure microstrip line. (b) schematic for effective radiation. λ g represents the guide wavelength. Blue arrow-Fringing electric field. Red arrow-Equivalent magnetic current. (c) Simulated and measured reflection coefficient [38].

The results reveal that there are two resonant modes at 25.3 GHz and 28.5 GHz. The first is sensitive to the stub, and the second is due to the variation in length of the microstrip line. The parametric study was also performed on the number of stubs, which directly impacts the antenna's gain and bandwidth. With this design, the SLL is -13 dB. The microstrip line is tapered to improve the SLL and impedance matching further. It has improved SLL to −28.4 dB but with a slight gain reduction. The design of 1 × 4 is extended to a 4 × 4 structure with four subarrays connected by a microstrip line. The bandwidth at reflection coefficient S11 < −10 dB has resulted in 23.39-28.2 GHz with a gain of 17.5 dBi as shown in Figure 6(c). The radiation pattern is in broadside with HPBW of 25° and 18° in E-and H-plane with SLL of −11.9 and −16.8 dB in H-plane at 24.3 and 26.9 GHz, as shown in Figure 7(a-b). The prototype fabrication is shown in Figure 7(c-d). The merits and demerits of the series-fed planar array structures are presented in Table 1.

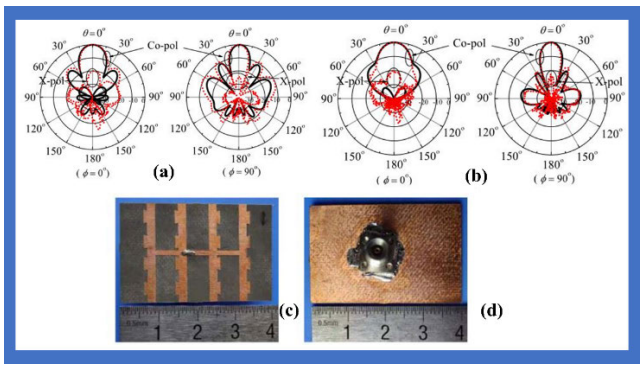

FIGURE 7. Simulated and measured radiation pattern at (a) 24.3 GHz, (b) 26.9 GHz. Prototype fabrication of array antenna (c) top view, (d) bottom view [38].

2) SLOT COUPLED ARRAY

In slot coupled antenna, the radiating element and microstrip excitation line are etched on different layers of substrate. When the feeding network is excited, the power to the radiator is coupled through the slot. A wide band, circularly polarized, the multi-layer antenna is proposed in [39]. The structure has three substrates of Rogers RO4003, with a top substrate having four 45° right inclined rectangular patches on top, aligned in a straight line, and the bottom layer has a ground plane with slots to couple the power. These slots are of inverted V-shape underneath the radiating patch. The bottom of the second substrate has a 50 Ω microstrip feed line terminated with a stub.

The third substrate is at the bottom, with a conductive layer on top that acts as a reflector to improve the directivity and gain. The proper position of an inclined patch and inverted V-slot will result in circular polarization. Here the elements are placed at half wavelength. To further improve the design bandwidth, the patches are etched with the slit in the middle, which creates additional current paths resulting in degenerate mode generation at the fundamental frequency. The current, in this case, adds up at 0° and 180° angles and cancels at 90° and 270°, resulting in RHCP. The bandwidth at reflection coefficient S11 < -10 dB has 27.5-30 GHz, as shown in Figure 8(a). The gain is 10.2 dBi throughout the band. The radiation is in the broadside with HPBW of 70° in E-plane and 18° in H-plane as 27.9 GHz as shown in Figure 8(b-c). The prototype fabrication is shown in Figure 8(d-e).

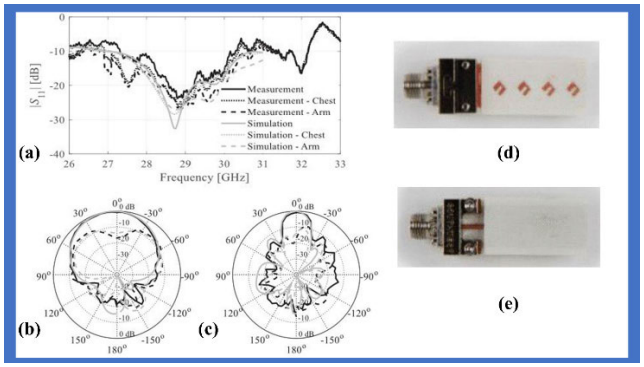

FIGURE 8. (a) Simulated and measured reflection coefficient. Simulated and measured radiation pattern at 27.5 GHz (b) E-plane, (c) H-plane. Proposed prototype fabrication of array antenna (d) top view, (e) bottom view [39].

To control the radiated power and matching of each element in a traveling wave mode in a series-fed structure, an alternate approach to uniform structure is a non-uniform structure array proposed in [40]. The proposed structure has non-uniform shapes and spacing of elements along the microstrip line which is to obtain a uniform aperture field for different radiated-to-available power ratios (RAPR). The radiated power from each element is calculated as the difference between input power, output power, and ohmic losses. To match this requirement three different shape of elements are proposed, type 1: rectangular patch with input and output port, type 2: rectangular patch with input port and inset feed at the output port, type 3: rectangular patch with inset feed input port and slit-coupled output port. The RAPR in type 3 is controlled by varying the gap in a slit-coupled port.

The parametric analysis is performed on the dimensions of all three types of elements to match the required RAPR. The proposed array has one type 1, three type 2, and three type 3 elements of varied shapes from left to right to match the RAPR. The microstrip line is terminated with an inset feed rectangular patch to avoid reflections by radiating the residual power. The power is coupled through a WR-10 waveguide which requires microstrip-to-waveguide transition (MWT). The obtained bandwidth at reflection coefficient S11 < −10 dB is 75-77.5 GHz with a gain of 15 dBi as shown in Figure 9(a). The SLL is maintained at −17 dB (Figure 9(b)), and the radiation is in broadside with HPBW of 20° in the E-plane as shown in Figures 10(a). The prototype fabrication is shown in Figure 10(b-c).

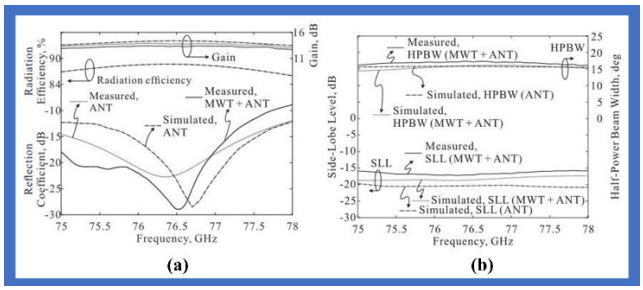

FIGURE 9. (a) Simulated and measured reflection coefficient and gain. (b) Simulated and measured SLL and HPBW [40].

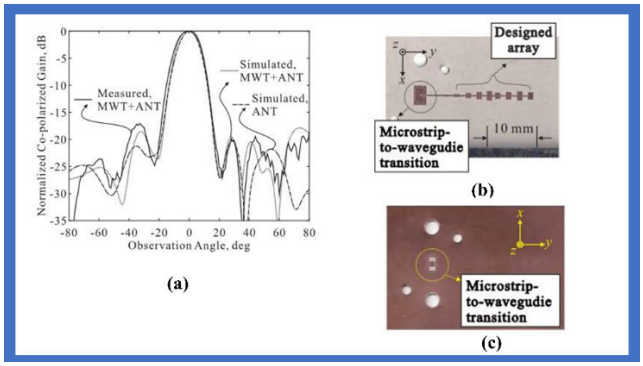

FIGURE 10. (a) Simulated and measured radiation pattern of proposed array in the E-plane at 76.5 GHz. Prototype fabrication of proposed array, (b) top view, (c) bottom view [40].

3) COPLANAR WAVEGUIDE ARRAY

In thinner substrates, surface radiation losses are high. To mitigate this issue grounded coplanar waveguide technique can be used. In microstrip design, the coplanar waveguide has a transmission line/radiator in the center with a ground plane on either side, all on the same plane. This arrangement facilitates easy mounting of RF devices and reduces radiation losses. If the additional ground plane is added at the bottom of the substrate, it results in grounded CPW (GCPW) [10].

In [41], a three-layer series-fed rectangular tapered antenna is proposed. The upper substrate has five tapered rectangular patches to the right and another set of five rectangular tapered patches to the left with a phase shifter. These two sets are fed parallelly by a 50 Ω microstrip line. The patches and feed line on the top of upper substrate are surrounded by grounded CPW. The second and third-layer substrate (RO4350B and RO4450F) has a rectangular slot to couple the power. Metallic vias surround the patches and feed line to form the cavity structure to reduce the surface wave losses so that bandwidth is increased. The bandwidth at reflection coefficient

S11 < -10 dB resulted in 77-85 GHz (Figure 11(a)) with narrow HPBW of 20° in H-plane and wide beamwidth of 120° in E-plane as shown in Figure 12. The gain of antenna is 9.5 dBi. The design is extended to six series-fed cavity-back patch structure as shown in Figure 11(b).

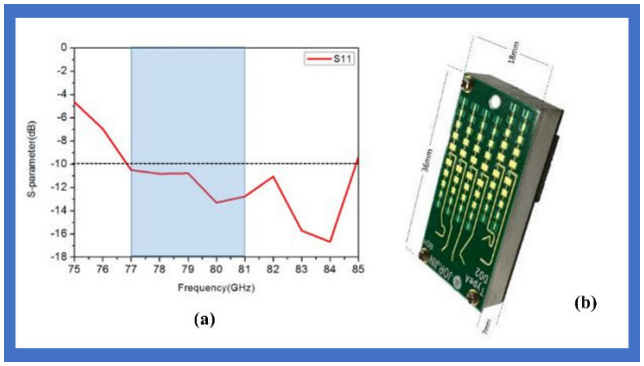

FIGURE 11. (a) simulated reflection coefficient of array antenna. (b) fabricated prototype array antenna [41].

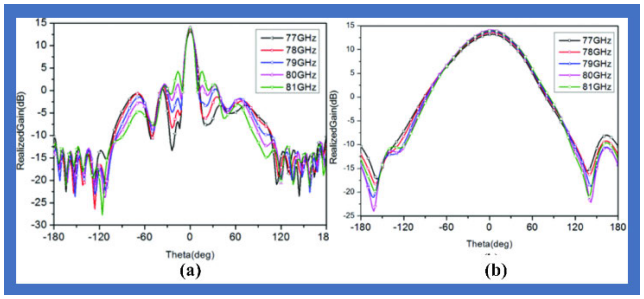

FIGURE 12. Simulated results of radiation pattern. (a) H-plane, (b) E-plane [41].

4) SUBSTRATE INTEGRATED-WAVEGUIDE ARRAY

A cost-efficient slotted substrate-integrated waveguide with an air-filled brass-plated array is proposed in [42]. The structure has a stacked section of RF ground, waveguide, and slotted antenna array. The RF ground is formed at the lower substrate, which uses FR4 covered with a copper sheet on top and bottom. The middle substrate is the waveguide section which uses Rogers 4350B, where the top and bottom are covered with a copper sheet, a rectangular slot is etched on this substrate to form the hollow waveguide, and slot edges are copper coated to form the metallic wall. The top layer is a 5-mill brass sheet with four rectangular slots arranged slightly aft the straight line and five additional slots for soldering. The structure is fed by a microstrip line in the middle layer, which is gently tapered to convert the quasi-TEM mode to the TE_{10} mode of the waveguide. The structure layers are assembled with six screws, which may reduce wave leakage losses. This middle layer acts as a waveguide. The slot width a is calculated using the below equation:

$$a = \frac{c}{2f_c'} \tag{5}$$

where c is the speed of light, f_c is a cutoff frequency in TE_{10} mode. From the current distribution Figure 13(a), it is evident that the waveguide delivers equal power to all the radiating slots.

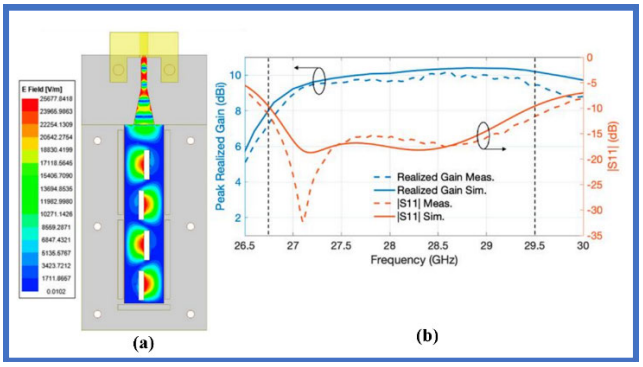

FIGURE 13. (a) Electric current distribution on the MSL and inside the ASIW with radiating slots at 28 GHz. (b) Measured and simulated peak gain and reflection coefficient of ASIW slot array [42].

The structure resonates at 27.2 GHz with bandwidth at reflection coefficient S11 < -10 dB is 26.75-29.5 GHz with a gain of 9.5 dBi as shown in Figure 13(b). The measured and simulated results discrepancy is due to manual soldering and surface roughness. The radiation is in broadside direction with HPBW of 60° and 20° in E- and H-plane with a tilt by 3° and large SLL in H-plane is reported as shown in Figure 14(a). The efficiency of the antenna is calculated by considering the mismatch of the microstrip line, surface roughness, dielectric, and conductor losses, which resulted in 84%. The prototype fabrication is shown in Figure 14(b-c).

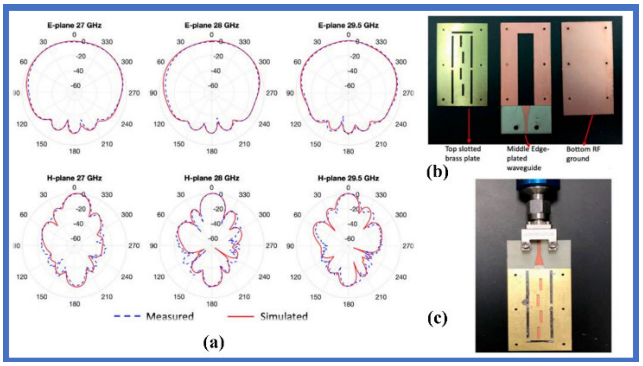

FIGURE 14. (a) Simulated and measured radiation pattern (E-and H-plane) of ASIW slot array at 27 GHz, 28 GHz, and 29.5 GHz. Prototype fabrication of array antenna, (b) fabricated individual layers, (c) assembled prototype [42].

The merits and demerits of slot coupled, CPW, and SIW array structures, with series-fed, are shown in Table 2. Also, the summary of performance metrics of series-fed arrays is shown in Table 3.

B. PARALLEL-FED ARRAY ANTENNAS

1) PLANAR ARRAY

A compact and planar 1 × 4 multi-circular ring wideband array antenna is proposed in [43]. The single element has

TABLE 2. Merits and demerits of slot coupled, CPW, and SIW array structures, with series-fed.

References	Design Structure	Technique adapted	Merits	Demerits
Series Feeding Method				
[39]	Slot coupled array	Multilayer, uniform structure and spacing, inclined radiators.	• Right-hand circular polarization • Wide bandwidth • Narrow beamwidth in H-plane • Reduced transmission losses	• Wide beamwidth in E-plane. • Unequal power distribution. • Power loss due to leaky waves.
[40]		Non-uniform and spacing radiators with terminated patch	• Controlled RAPR • Reduced impedance mismatch due to terminated patch. • Wide bandwidth • Narrow beam in E-plane • Suppressed SLL	• Requires microstrip-to-waveguide transition to feed power • Radiation pattern of the H-plane is missing
[41]	CPW	Multilayer, non-uniform structure and spacing, with center-fed supported by SIW cavity.	• Reduced surface wave due to cavity structure. • Wide bandwidth. • Narrow beamwidth in H-plane.	• Wide beamwidth in E-plane.
[42]	SIW	Multilayer, tapered waveguide	• Reduced leaky waves. • Equal power distribution. • Wide bandwidth. • Operates at TE_{10} mode	• Wide beamwidth in E-plane. • Misalignments of layers lead to devastating results.

TABLE 3. Performance metrics summary of series-fed arrays.

Reference	Dimension (mm^2)	Center frequency (GHz)	Array Elements	Average Gain (dBi)	Bandwidth (GHz)	Side-lobe level (dB)	Efficiency (%)	Radiation Pattern	Beamwidth	Polarization
Series Feed Array										
[36]	34.7x10	28	8x1	10.8	23.3 – 51.9	-24.9 / -19.4		Broadside	40^0 & 50^0 in E - & H-plane	Linear
[37]	51.44 x 18.43	28	6x2	15	27.06 – 28.35		93	Omnidirectional	-	Linear
[38]	26 x 40	27	4 x 4	17.5	23.39 – 28.2	-11.9 / -16.8		Broadside	25^0 & 18^0 in E & H-plane	Linear
[39]	28.7 x 13	28	4 x 1	10.2	27.5 - 30		90	Broadside	70^0 & 18^0 in E- & H-plane	RHCP
[40]	15 x 1.75	77	1 x 8	15	75 – 77.5	-17	85.5	Broadside	16^0 in E-plane	Linear
[41]	36 x 18	77	1 x 10	9.5	77 – 85			Broadside	120^0 & 20^0 in E- & H-plane	Linear
[42]	51.35 x 23.4	28	1 x 4	9.5	26.75 – 29.5		84	Broadside with 3^0 tilt to right	60^0 & 20^0 in E- & H-plane	Linear

three circular rings, in which two are concatenated, and the third ring overlaps on two rings. The power is fed through a 50 Ω microstrip line. The ground plane has defected to the partial ground with slit in the center to improve the bandwidth. The radiation pattern due to partial ground is affected, resulting in bidirectional and poor front-to-back ratio. The parametric analysis is performed on ring size, spacing, position, length of the ground plane, and length of the slit in the ground plane to perform better. The antenna has resonated at dual frequencies at 28.8 GHz and 38.4 GHz. As the length of the ground slit increases, the resonant frequency is drifted slightly higher, whereas it is reverse in the case of ring spacing. The single element is extended to a 4-element array fed by full corporate feed to divide the power equally to all the elements as seen from the current distribution Figure 15(a). It can be noted that the maximum current is in the feedline and radiator. The bandwidth at reflection coefficient S11 < -10 dB resulted in 26.2-36.7 GHz as shown in Figure 15(b). The radiation pattern is bidirectional with HPBW of 20° and 70° in E-and H-plane with gain of 10 dBi as shown in Figure 16(a-b). The prototype fabrication is shown in Figure 16(c).

Similar to the earlier design, a 1×4 ring-shaped array antenna is proposed in [44]. The single element is a circular patch with a circular slot, forming a ring-shaped structure on Rogers 5880 substrate fed by a 50 Ω microstrip line.

To improve the bandwidth, the ground plane is optimized to the partial ground with a slit at the center for better impedance match. The parametric analysis on ring size, ground slit width, and length is performed. The design is extended to 4 element arrays fed by corporate feed with three power dividers with a horizontal and vertical strip of 100Ω and

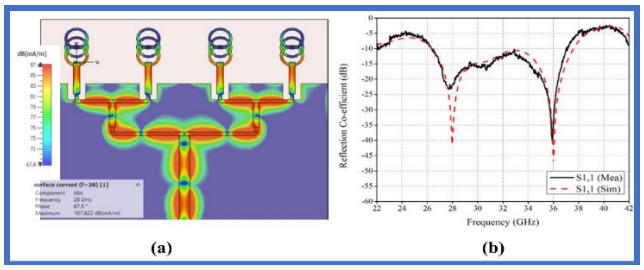

FIGURE 15. (a) Surface current distribution of array antenna. (b) Simulated and measured reflection coefficient S11 [43].

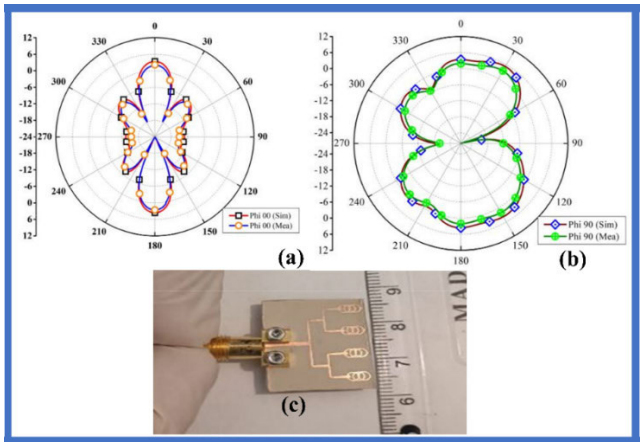

FIGURE 16. Radiation pattern at 28 GHz, (a) E-plane, (b) H-plane. (c) Prototype fabrication of array antenna [43].

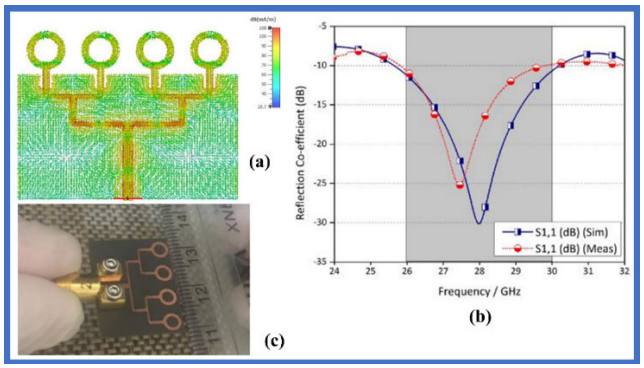

FIGURE 17. (a) Surface current distribution of array antenna. (b) Simulated and measured reflection coefficient of array antenna. (c) Prototype fabrication of array [44].

70Ω impedance. The surface current distribution indicates the maximum current concentrating in the feed, power divider, and ring, as in Figure 17(a). The bandwidth at S11 < -10 dB is 26-30 GHz, as shown in Figure 17(b). Due to partial ground, the major back lobe's radiation pattern resulted in bidirectional radiation with HPBW of 70° and 12° in H- and E-plane as shown in Figure 18(a-b). The prototype fabrication is shown in Figure 17(c).

Another four-element triangular slot array antenna is proposed in [45]. The single element is a rectangular patch on top

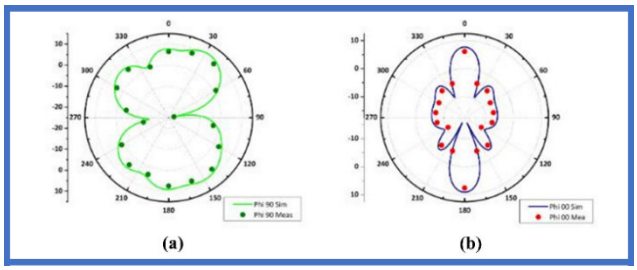

FIGURE 18. Simulated and measured radiation pattern. (a) H-plane, (b) E-plane [44].

of Rogers 5880 substrate fed by a 50 Ω microstrip line with a partial ground plane on the bottom of the substrate to improve the bandwidth. The antenna resonated at 33 GHz with S11 of −14 dB. To improve the impedance match and bandwidth, a triangular slot is etched on the patch, resulting in S11 of −20 dB, which is further improved by modifying the center feed to offset feed. This induces a capacitance effect and reduces the inductance effect on the patch, resulting in resonance at 28 GHz and 38 GHz with a bandwidth of 25-47 GHz. The parametric analysis of feed width, patch length, and width are performed to obtain the optimum dimensions.

Figure 19(a) shows the surface current distribution, indicating the maximum current at the edges of the slot and feed line. The design is extended to four element arrays fed by a T-junction power divider. The reflection coefficient and isolation analysis of microstrip feed, T-junction, and bend are performed and set well below the limits. The bandwidth of four element array at S11 < -10 dB is 26-45 GHz with gain and efficiency of 10 dBi and 78%, as shown in Figure 19(b). The radiation pattern is nearly omnidirectional in the E- and H-plane, as shown in Figure 20(a-b). The prototype fabrication is shown in Figure 20(c-d).

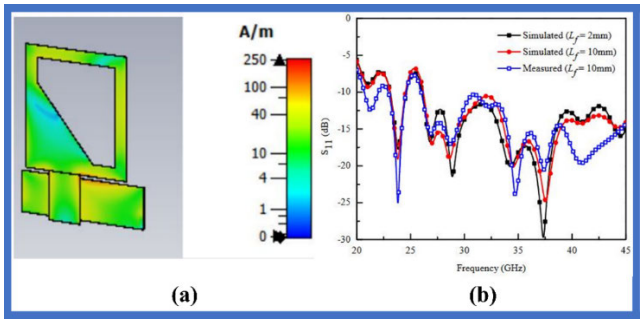

FIGURE 19. (a) Surface current distribution of proposed antenna at 27 GHz. (b) Simulated and measured reflection coefficient S11 [45].

The narrow beamwidth with a highly directional radiation pattern is the need of a 5G application. In [46], an array of 1 × 4 bowtie-shape structures with a curved surface formed using the Bezier curve designed to resonate in the frequency range of 23.41 – 33.92 GHz. The initial design is a single bowtie shape element (triangular shape) etched on the top of the substrate fed by a 50 Ω microstrip line. An asymmetrical

TABLE 4. Merits and demerits of planar array structures with parallel feed.

References	Design Structure	Technique adapted	Merits	Demerits
Parallel Feeding Method				
[43]	Planar	Uniform structure and spacing of radiators with defected ground	• Equal power distribution. • Wide bandwidth • Narrow beamwidth in E-plane	• Bidirectional radiation due to defected ground. • Wide beamwidth in H-plane. • Dominant transmission line losses due to multiple feed arms. • Dominant SLL in E-plane
[44]		Uniform structure and spacing radiators with defected ground	• Equal power distribution. • Wide bandwidth • Narrow beamwidth in H-plane.	• Bidirectional radiation due to defected ground. • Wide beamwidth in E-plane. • Dominant transmission line losses due to multiple feed arms. • Dominant SLL in E-plane.
[45]		Uniform structure and spacing radiators, with defected ground and offset feed	• Equal power distribution. • Dual-band resonance. • Wide bandwidth	• Nearly omnidirectional radiation pattern. • Dominant transmission line losses due to multiple feed arms. • Dominant SLL in E-and H-plane.
[46]		Uniform structure and spacing bowtie-shape radiator, with defected ground	• Equal power distribution. • Wide bandwidth. • Narrow beam width in H-plane.	• Wide beamwidth with end-fire radiation in E-plane. • Transmission line losses due to multiple feed arms. • Dominant SLL in end-fire direction.

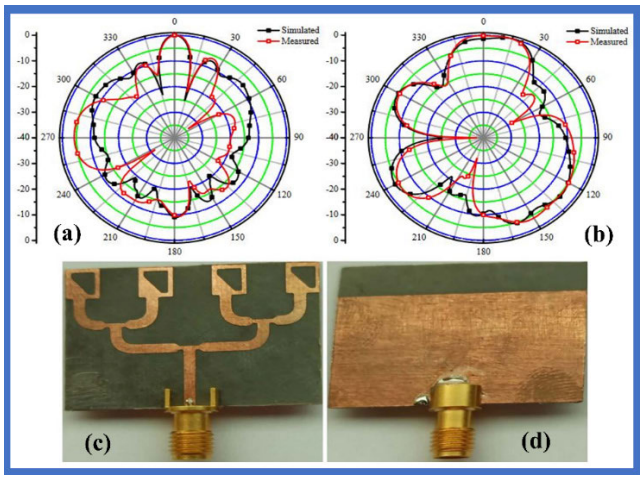

FIGURE 20. Simulated and measured radiation pattern at 28.5 GHz, (a) E-plane, (b) H-plane. Proposed antenna array (c) top view, (d) bottom view [45].

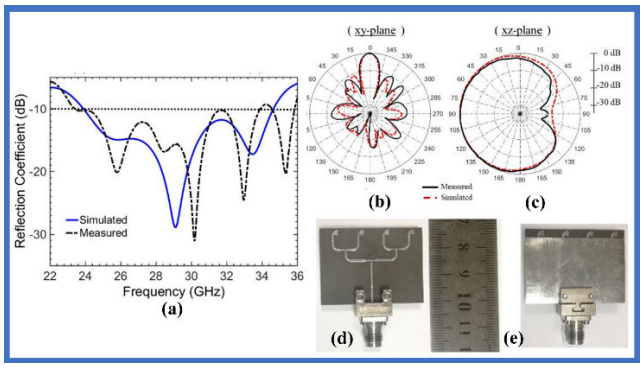

FIGURE 21. (a) Simulated and measured reflection coefficient S11. Simulated and measure radiation pattern at 28 GHz, (b) H-plane, (c) E-plane. Prototype fabricated array antenna, (d) top view, (e) bottom view [46].

shape is etched on the bottom of the substrate connected to the ground. Further, the design is optimized with the curved shape, and through parametric study, the dimension of the antenna is modified to resonate at 28 GHz. The design is extended to four elements, with half of the bowtie element etched on top of RT5880 substrate, which are parallel-feed, and the other half are etched on the bottom, which are connected to the partial ground plane. The current distribution indicates that the maximum current is concentrated in the feed and at the center edges of the antenna, which indicates the radiation along the x-axis. The radiation is in end-fire and broadside direction in E- and H-plane with HPBW of 90° and 14° (in Figure 21) with gain, bandwidth, and efficiency of 10.7dBi, 35.53%, and 90%. The resulting bandwidth at S11 < -10 dB of 24 – 33.8 GHz as displayed in Figure 21 with the prototype fabrication. The merits and demerits of planar array structures with parallel-fed method are discussed in Table 4.

2) SLOT COUPLED ARRAY

The wide bandwidth is obtained by resonating a circular patch with a quasi-TM_{21} mode [47]. Here, the design has four layers on two substrates (TLY-5). The upper substrate top layer has a 4×4 circular patch which has one vertical slit and two horizontal slits. The bottom of substrate 1 has

rectangular strips which are connected to circular patches through metallic vias. The top of substrate 2 is ground plane with slot to couple the power to the radiator, and bottom has a parallel feed structure. Both substrates are joined with the bonding film (RO4450B). When the four 2 × 2 feed structures are arranged symmetrical to each other, it results in linear polarization (LP) and, arranged orthogonally, results in circular polarization (CP).

The 4 × 4 LP resulted in a gain of 19.74 dBi and 19.22% (27 – 32.5 GHz) bandwidth at S11 < −10 dB as shown in Figure 22(a), whereas CP has shown a gain, bandwidth, and 3 dB axial ratio of 14.69 dBi, 58.46% (23 – 39 GHz) and 13.68% (27.25 – 31.25 GHz) as displayed in Figure 22(b). The radiation pattern is very narrow with HPBW of 17.5°, 16°, and 15° in E and H – planes at 27, 29.5, and 32 GHz, as shown in Figure 23. The prototype fabrication is shown in Figure 24.

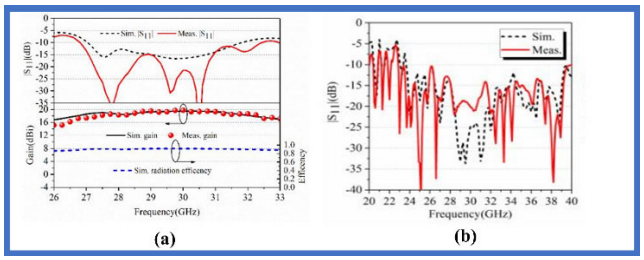

FIGURE 22. (a) Experimental results of the 4 × 4 LP array antenna. (b) Reflection efficient of 4 × 4 CP array antenna [47].

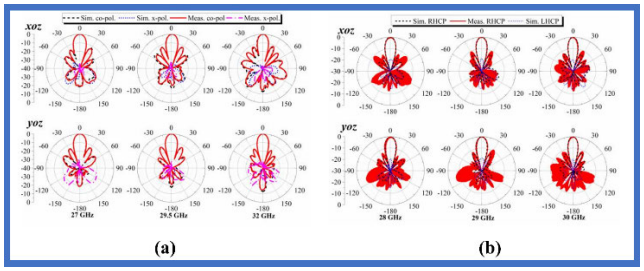

FIGURE 23. Simulated and measured normalized radiation patterns. (a) 4 × 4 LP array antenna (b) 4 × 4 CP array [47].

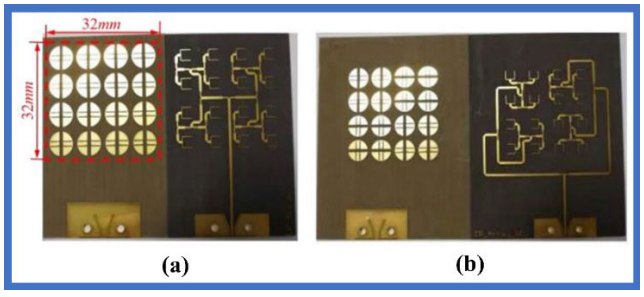

FIGURE 24. Fabricated prototype, (a) 4 × 4 LP planar array antenna, (b) 4 × 4 CP array antenna [47].

3) COPLANAR WAVEGUIDE ARRAY

The microstrip antenna with parallel feed experiences feed line losses. To counter this issue, a combination of coplanar strips (CPS) and coplanar waveguides (CPW) can be used to design the feed structure for mmWave. In [48], CPS and CPW lines are realized because their impedance is constant irrespective of substrate thickness. It also increases the isolation as the electric-field lines lie between the signal line and the ground line on the same plane. The design has eight radiating elements, where a differential CPS line connects every two radiating patches. By combining two CPS, a CPW line is formed. For array configuration, a bridge is constructed to transit CPS to CPW and vice versa. The gold of 2 μm is used for the patch and feed line. The array is designed to resonate at 65 GHz, obtained the bandwidth at reflection coefficient S11 < −10 dB is 51 – 53.5 GHz and 57 – 65 GHz, as displayed in Figure 25(a). The gain is not constant, it varies from 12 to 14.5 dBi in the band of interest. The radiation pattern resulted in an end-fire at 90 deg, with HPBW of 60° in end-fire and 30° in E- and H-plane, as seen in Figure 25(b-c). The prototype fabrication is shown in Figure 25(d).

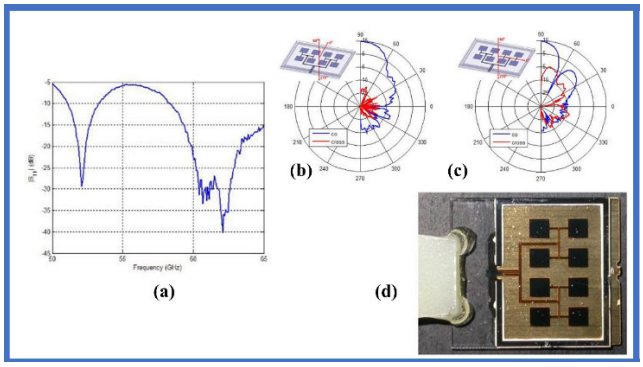

FIGURE 25. (a) Measured reflection coefficient S11. Measured radiation pattern, (b) E-plane and H-plane (c). (d) Prototype fabrication of proposed antenna array [48].

A monopole antenna array with the defected ground to improve the bandwidth is presented in [49]. Here the rectangular patch is optimized to increase the bandwidth by trimming the corners of the patch along the width, with the slot in the patch amended with an inverted T-shape structure. Such optimization to the patch has drifted the operating frequency to a higher value. To bring down the operating frequency, the ground plane is modified with circular slots, rectangular slots, and rings, resulting in the defected ground plane (DGS). The power to the patch is coupled through a quarter-wave transform with defected co-planar waveguide (CPW). The current distribution is maximum in the feed line and ground which is a good characteristic. Thus, with such a design optimum bandwidth at S11 < −10 dB is 10.9% obtained over the frequency of 57.2 – 63.8 GHz as shown in Figure 26(a), with the gain of 11.6 dBi on a planar structure of size 20.64 × 20 mm^2. The radiation pattern is narrow with

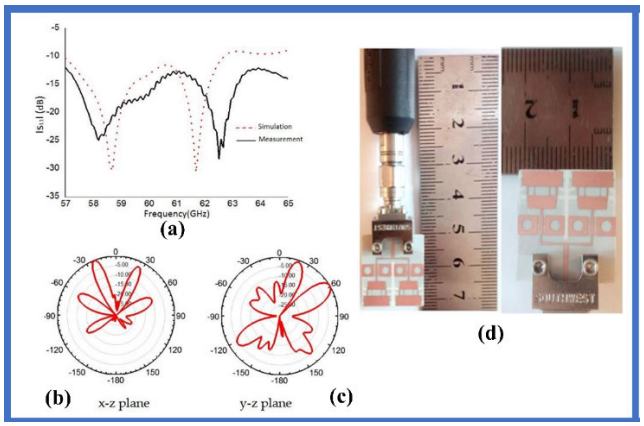

FIGURE 26. (a) Measured and simulated reflection coefficient. Radiation pattern, (b) E-plane (second), (c) H-plane (third). (d) Prototype fabrication [49].

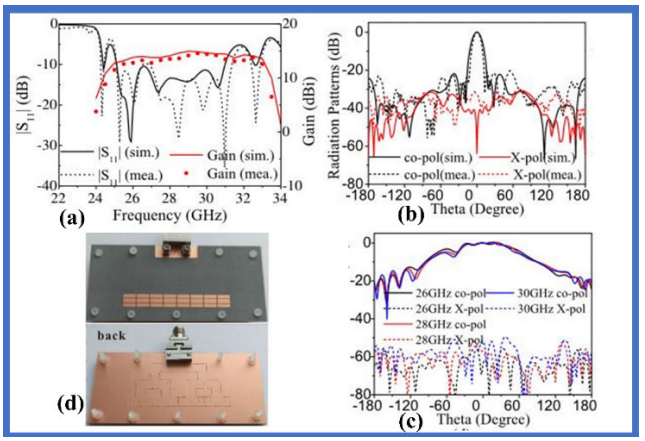

FIGURE 27. (a) Simulated and measure S11 and gain of 1 x 8 antenna array. Simulated and measured radiation pattern, (b) E-plane at 26 GHZ, (c) H-plane [50]. (d) Fabricated prototype of the 1 × 8 SIW antenna array [50].

multiple beams in E & H – plane indicated in Figure 26(b-c). The Prototype fabrication is shown in Figure 26(d).

4) SUBSTRATE INTEGRATED-WAVEGUIDE ARRAY

To achieve higher gain at mmWave, the array of radiating elements should be increased, which intern increase the complexity and profile of the antenna. The microstrip array structure experience dielectric and surface current losses, which limits the antenna's performance. The losses associated with feed network radiation and surface waves also affect overall efficiency. These issues are addressed in [50] by operating a patch array of 1 × 8 antenna at higher-order mode (TM_{30}) with a reduced number of array elements, making it a low-profile antenna suitable for 5G applications. The slot-coupled substrate-integrated waveguide (SIW) feeds unequal power to array elements, resulting in lower sidelobe levels. The higher-order mode is realized by etching multiple horizontal slits in the rectangular patch. The antenna has achieved the larger bandwidth at S11 < -10 dB of 27.9% (25.2 – 31.3 GHz) and a gain of 14.6 dBi operating at 28 GHz with low sidelobe levels of -15 dB as shown in Figure 27(a). The radiation pattern is directional on the broadside tilted at $+20°$ with HPBW of 18° and 120° in the E- and H-plane, as shown in Figure 27(b-c). The prototype fabrication is shown in Figure 27(d).

In another approach, a four-element array of Jin-shaped Chinese characters is designed on top of a substrate [51]. The SIW feed technique is used to feed the signal to four elements through the slot created on layer 2. The metallic vias connecting the ground plane split the equal power into four arms of SIW. The metallic vias between the slots act as isolating elements, and a parametric study is performed by increasing the number of vias along the length. The achieved bandwidth at S11 < -10 dB is 24.5 – 27.5 GHz, with an average gain of 12 dB, as shown in Figure 28(a). The radiation pattern is directional on the broadside with an HPBW of 60° and 15° in the E- and H-plane, as seen in Figure 28(b-c).

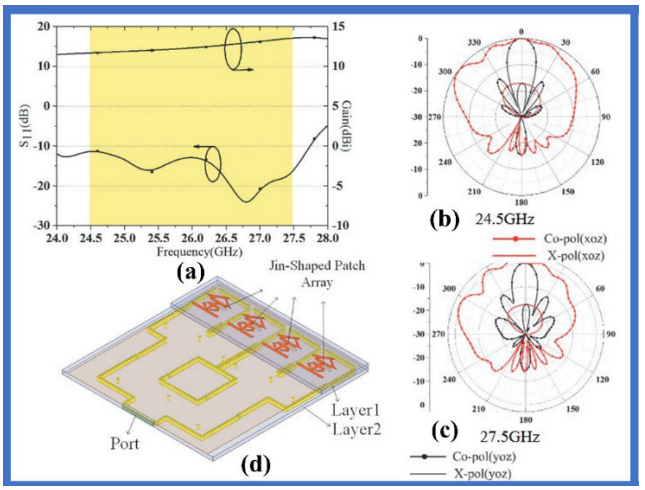

FIGURE 28. (a) Simulated reflection coefficient S11 and gain of proposed antenna array. Simulated radiation pattern of antenna array, (b) at 24.5 GHz, (c) at 27.5 GHz. (d) 3D design of proposed antenna [51].

The simulated design of the proposed antenna is shown in Figure 28(d).

An H-shaped slot array antenna with high gain is proposed in [52]. The initial design is a single-element antenna with a square patch size of half wavelength fed by coaxial feed, which resulted in a gain of 8dBi. But to match the required frequency, the rectangular slot with two rectangular slits on either side of the patch is introduced, shifting the frequency higher to match the desired resonance. A metallic vias is inserted to connect to the ground to limit the resonant current. The parametric study on the length and width of the slot is performed, and it realized that slot width does not affect frequency shift, whereas slot length has an effect.

Further, the planar design is extended to multilayer design with two substrates (Rogers 5880) joined by prepreg layer (RO4550T) to enhance the performance. The lower substrate top and bottom have a ground plane, the upper substrate

top layer has an H-shaped patch, and the bottom layer has two matching stubs to improve the impedance match. One match stub is connected to the feed line, and the other is connected to the ground through metallic vias (shorted pin) as seen from Figure 29(a). The matching stub length and width acts as inductance and capacitance which affects the impedance match, for which parametric analysis is performed. This design is extended to four element array which is fed by one coaxial feed of a 1×4 power divider. To reduce the leakage losses and phase distortion, the edges of the design are covered with metallic vias connected to the ground forming a magnetic wall as seen from the current distribution Figure 29(b). The resulting bandwidth at reflection coefficient S11 < -10 dB is 27.8-28.4 GHz as shown in Figure 30(a). The radiation pattern is in broadside with HPWB of 34° and 31° in E- and H-plane with a gain of 12.5 dBi as shown in Figure 30(b-c). The prototype fabrication is shown in Figure 29(c).

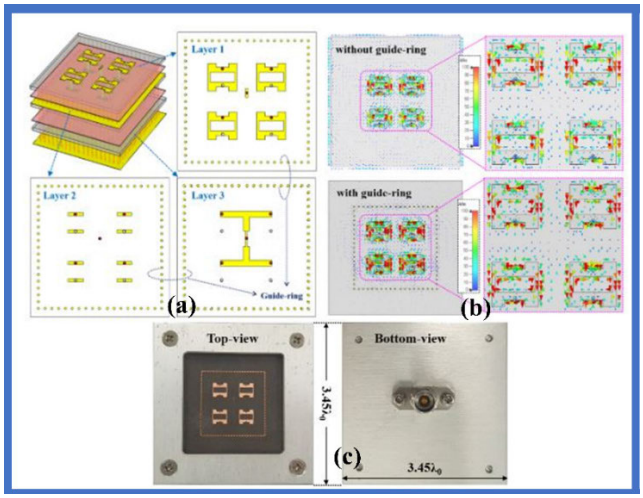

FIGURE 29. Proposed 2 × 2 array antenna. (a) Multilayer view, (b) Surface current on elements with and without guide-ring (SIW). Proposed prototype fabricated array antenna [52].

In the next design, the SIW is backed by a cavity (SIWC) for better performance with an eight-element array antenna [53]. The design has three layers with two substrates which use Rogers 4003C with copper coated on both sides. The bottom substrate top layer has an I-shaped SIW cavity to which the coaxial feeding network is connected. This power is equally distributed to the second layer, which has four SIW-cavity chambers with rectangular slots on top of the upper substrate, which will further equally distribute the power to the 2×2 subarray on the top layer. The top layer has four 2×2 subarrays, with each element having two slots. The structure is designed such that the equal phase and magnitude is coupled to all the cavities as seen from Figure 31(a), this is possible by placing all the coupling slots at equal distance from SIW in layer 2, but still the 2° phase error has been observed in the simulated results. With additional metallic vias in the cavity, excitation is improved, generating TE_{320} mode.

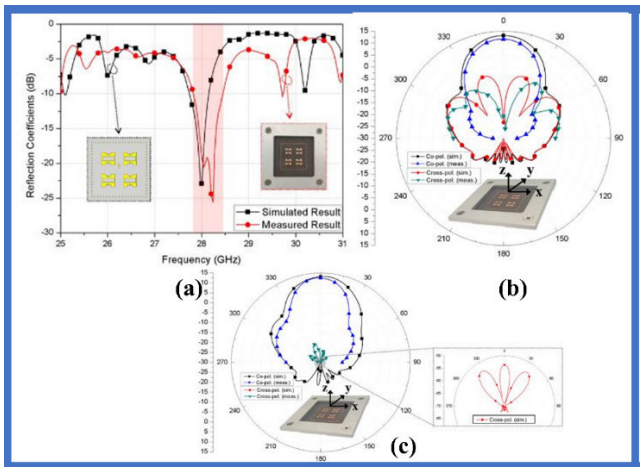

FIGURE 30. (a) Simulated and measured reflection coefficient S11. Simulated and measured radiation pattern of proposed array antenna, (b) E-plane, (c) H-plane [52].

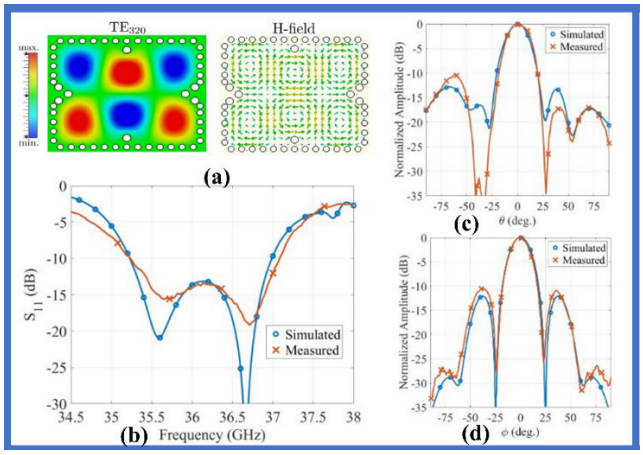

FIGURE 31. (a) Electric and magnetic fields of fundamental mode of cavity. Simulated and measured reflection coefficient S11. Radiation pattern of proposed array at 35.4 GHz, (c) E-plane, (d) H-plane [53].

The performance of single and double-slot radiators is verified, and a parametric study is performed on length, width, and position, which reveals its significance in improvement in bandwidth, tuning, and resonance. The resulting bandwidth at reflection coefficient S11 < -10 dB is 35.25-37.1 GHz, as shown in Figure 31(b). The radiation is in the broadside with HPBW of 20° with SLL of -10 dB in E- and H-plane as shown in Figure 31(c-d). The prototype fabrication is shown in Figure 32. The merits and demerits of slot coupled, CPW, SIW array structures with parallel feed are discussed in Table 5.

5) VIVALDI ANTENNA ARRAY

In the planar array antennas, the ground plane may be defected (DGS) to improve efficiency and enhance the isolation between the radiating elements. But the DGS is not significant in the tapered antennas (also called Vivaldi antennas). A notch between the tappers can improve the isolation.

TABLE 5. Merits and demerits of slot coupled, CPW, SIW array structures with parallel feeding method.

References	Design Structure	Technique adapted	Merits	Demerits
Parallel Feeding Method				
[47]	Slot coupled	Multilayer, uniform structure and spacing radiators	• Equal power distribution. • Low transmission line losses due to distributed layers. • Linear and circular polarization with change in radiator orientation. • Wide bandwidth. • Narrow beamwidth in E- and H-plane.	• Power loss due to leaky wave. • Dominant SLL. • Change in HPBW with change in frequency.
[48]	CPW	Uniform structure and spacing radiator, fed by CPW and CPS	• Equal power distribution. • Low transmission line losses. • Wide bandwidth. • Narrow beamwidth in H-plane.	• Structure is expensive due to usage of gold in patch and feed line. • Wide beamwidth in E-plane. • Dominant SLL.
[49]		Uniform structure and spacing radiators, with defected ground	• Equal power distribution. • Low transmission line losses due to CPW feed.	• Dominant SLL. • Complex design.
[50]	SIW	Multilayer structure with SIW feed	• Reduced dielectric and surface current losses. • Reduced leaky wave. • Operates at higher TM_{30} mode. • Unequal power distribution results in suppressed SLL. • Narrow beamwidth in E-plane.	• Complex structure. • Wide beamwidth in H-plane. • Misalignments of layers lead to devastating results.
[51]		Multilayer structure with SIW feed, and Jin-shaped radiator	• Reduced dielectric and surface current losses. • Reduced leaky wave. • Equal power distribution. • Narrow beamwidth in H-plane.	• Complex structure. • Wide beamwidth in E-plane. • Dominant SLL.
[52]		Multilayer, uniform structure and spacing, with coaxial feed and SIW cavity	• Equal power divider. • Reduced leaky wave. • Narrow beamwidth in E- and H-plane.	• Narrow bandwidth. • Complex structure. • Misalignments of layers lead to devastating results.
[53]		Multilayer, uniform structure and spacing, with coaxial feed and SIW cavity	• Equal power distribution. • Operates at a higher mode of TE_{320}. • Reduced leaky wave losses. • Wide bandwidth. • Narrow beam in E- and H-plane	• Phase error of 2^0. • Dominant SLL. • Complex structure. • Misalignments of layers lead to devastating results.

So, a notch is introduced between the left and right taper [54]. Here, 1×8 antipodal Vivaldi antenna (AVA) is proposed, which has eight radiating elements of left tapered fed by an equal power divider etched on top of the substrate, and eight right tapered shapes are etched at the bottom of the substrate, which is connected to the ground plane. The top and bottom taper follows exponential and elliptical shapes obtained by equations (6) and (7),

$$x_1 = k_1 * e^{360y} + k_2 (7.88mm \leq y \leq 16.5mm) \quad (6)$$

$$x_2 = -k_1 * e^{360y} + k_2 (7.88mm \leq y \leq 16.5mm) \quad (7)$$

where x_1 and x_2 are the sizes of quadrant shape elements.

From Figure 33(b), the maximum current concentration is distributed in the radiator and in the feed of AVA – CS compared to AVA, which results in a maximum gain. The AVA with decoupling notch structure (AVA-CS) has increased the bandwidth at S11 < -10 dB from 23.5 – 30.2 GHz to 22.8 – 31.3 GHz compared to AVA, as shown in Figure 35. The mutual coupling with AVA – CS design has been reduced with increased isolation level S12 of -40 dB at 28.5 GHz as in Figure 34(a-b) and gain of 12.5 dBi, whereas -30 dB of S12 at 28.7 GHz and gain of 7.8 dBi for AVA. The radiation pattern is directional with HPBW of 60° in E and H – planes at 26 GHz, as seen in Figure 34(c-d). The prototype fabrication is shown in Figure 33(c-d).

Another design of AVA array antenna with a modified structure resonates at dual-band, i.e., from 24.5 – 29 GHz and 30.5 – 40 GHz [55]. Here AVA antenna is corrugated in a comb structure, improving the isolation and radiation pattern. The top of the patch is etched with a tapered shape formed by a circular arc and exponential curve. The bottom has a mirror shape of an upper patch that is connected to the ground. Further, the patches are corrugated.

This modification has been downshifted to the resonance frequency. To achieve the desired frequency response, the corrugated structure is optimized. The single AVA corrugated structure is enhanced to a 1×4 array structure, which is fed by a full corporate feed. The rectangular slots are added in the ground plane to improve the frequency response. From Figure 35(b), it can be observed that the addition of

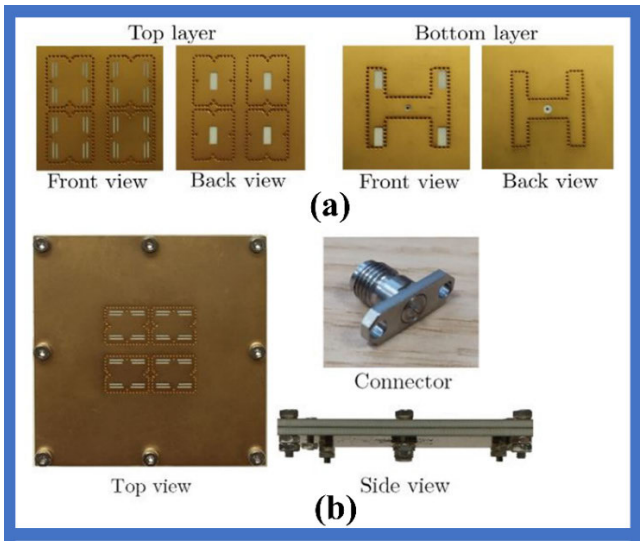

FIGURE 32. Prototype fabrication of array antenna (right) (a) Layer details, (b) Complete assembly and connector details [53].

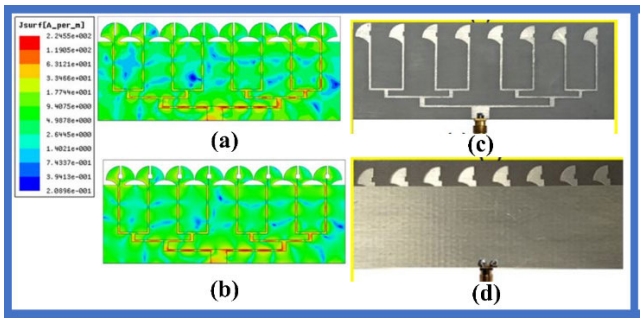

FIGURE 33. Surface current distribution (right), (a) 26 GHz (AVA array), (b) 26 GHZ (AVA – CS array). Prototype fabrication of proposed Vivaldi array antenna, (c) top view, (d) bottom view [54].

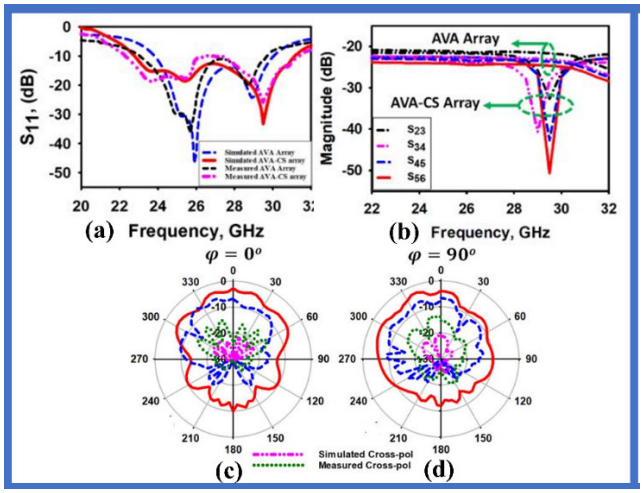

FIGURE 34. (a) Comparison of simulated and experimentally validated reflection co-efficient (S11) of AVA array and AVA-CS array (left). (b) Comparison of AVA and AVA-CS array simulated mutual coupling characteristics (middle). Radiation pattern at 26 GHz (right) (c) E – plane, (d) H – plane [54].

a corrugation shape has increased the current concentration level, improving the radiation efficiency. The bandwidth at

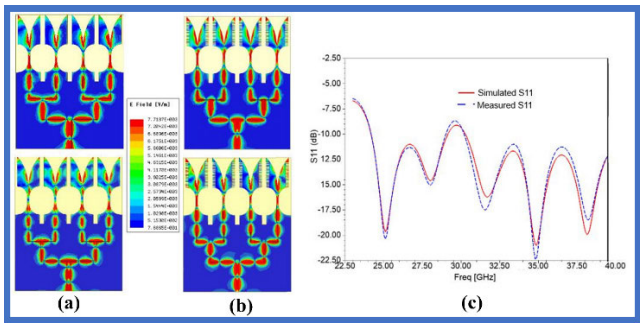

FIGURE 35. Surface current distribution with and without corrugation of AVA array at 25 GHz and 34 GHz (a-b). (c) Simulated and measured reflection coefficient S11 of proposed AVA array with corrugations [55].

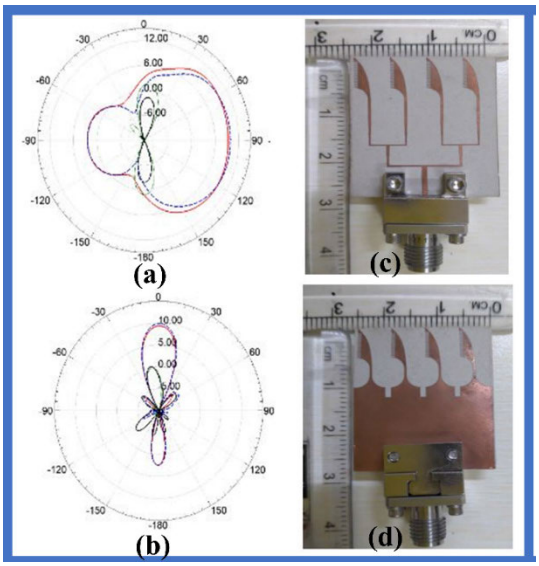

FIGURE 36. Simulated co and cross-polarization of (a) E – Plane, (b) H – Plane. Prototype fabrication of AVA corrugated array antenna (c) top view, (d) bottom view [55].

reflection coefficient S11 < -10 dB is shown in Figure 35(c). The radiation pattern results in end-fire radiation in the E-Plane with HPBW of 80°, whereas radiation is directional in the broadside with HPBW of 20° in H – Plane as seen from Figure 36(a-b). The prototype fabrication is shown in Figure 36(c-d).

Another antipodal Vivaldi for multiband with a 1×8 array of leaf-shaped structure is proposed for Ku-band and 5G application in [56]. The single-element antenna is developed in three stages. In the first stage, a swell strip line radiator with a curved shape is etched, fed by a quarter-wave transformer on the top of the substrate. The bottom substrate has a mirror image of the radiator connected to partial ground with an extended stub. This resulted in resonance at three bands starting from 19.81 to 38.17. To resonate further at a lower frequency, the radiating area is increased with more swell, bringing down the frequency to 15.04 GHz. This design is optimized by splitting the radiating area into two swell or leaf-shaped structures to obtain the three bands, i.e., 12-18 GHz,

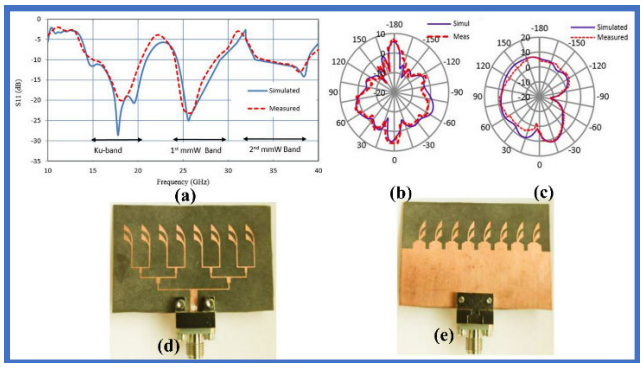

FIGURE 37. (a) Simulated and measured reflection coefficient. Simulated and measured radiation pattern of array antenna, (b) E-plane, (c) H-plane. Prototype fabrication of proposed array antenna, (d) top view, (e) bottom view [56].

18-27 GHz, and 27-40 GHz. The single-element design is extended to eight elements fed by a 1 × 8 power divider with a full corporate feed with seven parallel feed sections. With eight elements, the gain has increased from 3.6 to 12 dBi but affected the radiation direction due to mutual coupling from adjacent elements. Proper spacing of these elements is very important to reduce the mutual couple, which can be calculated by considering the lower resonating frequency ($\lambda_0/2$). The surface current distribution is maximum at the power divider and the edges of the leaf at a lower frequency, and at a higher frequency, the power is at the main power dividers. The measured bandwidth at S11 < -10 dB is 15-21 GHz, 24-28.5 GHz, 35-38 GHz, as shown in Figure 37(a). The radiation pattern is bidirectional and end-fire in E- and H-plane at 90°. The HPBW varies with a frequency range from 8°-30° and 60° - 120° in the E- and H-plane as shown in Figure 37(b-c). The prototype fabrication is shown in Figure 37(d-e).

6) MAGNETO-ELECTRIC DIOPLE ARRAY

The demand for high gain and wide bandwidth, influenced the researcher to study the various combination of structures, one such combination is the magnetoelectric dipole with microstrip patch element, such a design is proposed in [14]. Here the proposed antenna element has two additional patches are connected to microstrip line which is positioned between the ME. In the ME dipole, the microstrip patch acts as an electric dipole, and metallic vias connecting the patch and ground plane work as a magnetic dipole. The high gain is obtained by maximizing the radiation through optimizing the radiating area of the patch and by feeding equal phase power. The current distribution at various frequencies are studied, which shows the power coupled to the microstrip line through slots, distributes to patches for magnetic current radiation.

In this design, power is coupled through substrate-integrated-waveguide (SIW) through an aperture of the substrate to patches when excited through the stack of the pillbox, which delivers equal power to radiating elements. The bandwidth at S11 < -10 dB is 30.7% (53 – 72 GHz) with a gain of 25.1 dBi is achieved at a cost of complex design as it requires a multi-layer substrate as shown in Figure 38(a). The beamwidth is narrow in the broadside direction with 18° in E and H – planes as shown in Figure 38(b-c). The prototype fabrication is shown in Figure 39.

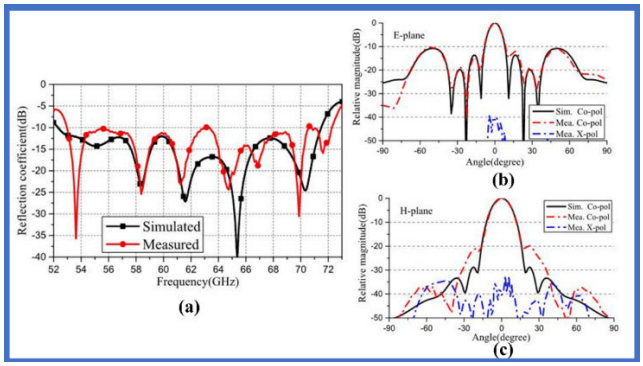

FIGURE 38. (a) Measured and simulated reflection coefficients. Simulated and measured radiation patterns of the proposed antenna array at 55 GHz, (b) E-plane, (c) H-plane [14].

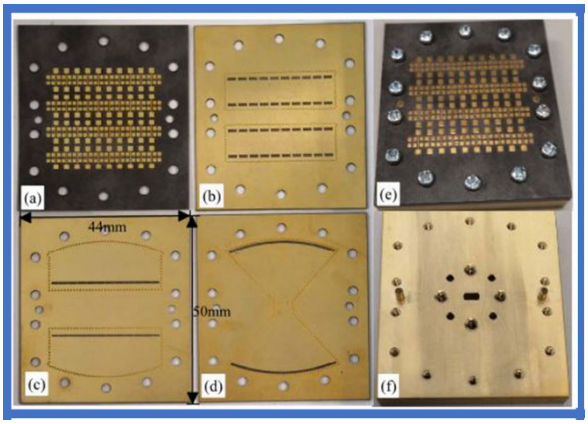

FIGURE 39. Prototype photography (a) substrate1, (b) substrate2, (c) substrate3, (d) substrate4, (e) fabricated antenna array, and (f) WR-15 waveguide flange [14].

The pillbox feed structure is complex, which makes the design high profile. In another approach, a 1 × 4 ME dipole array antenna is designed to obtain narrow beamwidth with dual polarization. Here the single ME dipole structure has four patches on layer five, connected to the ground through metallic vias with a slot in the ground plane. These patches and vias act as ME dipoles [57]. The two microstrip T-junction ports are etched on layers 4 and 2, which are placed on two EBG mushroom structures of layers 3 and 1 orthogonal to each other to obtain dual polarization. The gain of the array is enhanced through an additional layer of a 3 × 3 split ring resonator (SSR) [58] with a characteristic of zero permittivity placed on top of the ME dipole, which acts as meta-lens. This single structure is expanded to a 1 × 4 array. The bandwidth at S11 < -10 dB is 27.5 – 32.8 GHz and 33.5 – 34.5 GHz, as seen in Figure 40(a).

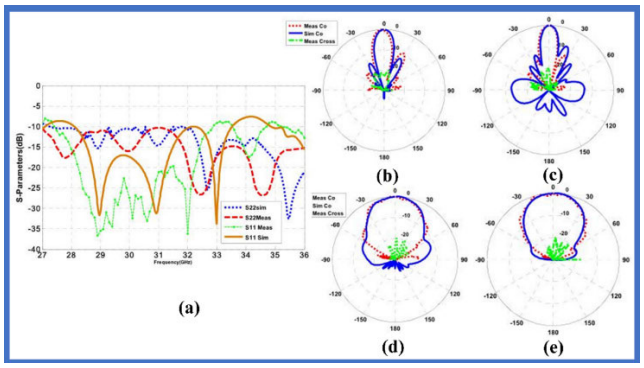

FIGURE 40. (a) Simulated and measured reflection coefficient S11 at port 1 and 2 for dual-polarized ME dipole antenna array. Simulated and measure radiation pattern of ME dipole for port 1 in E – plane (b) 28 GHz, (c) 30 GHz. Simulated and measure radiation pattern of ME dipole for port 1 in H – plane (d) 28 GHz, (e) 30 GHz [57].

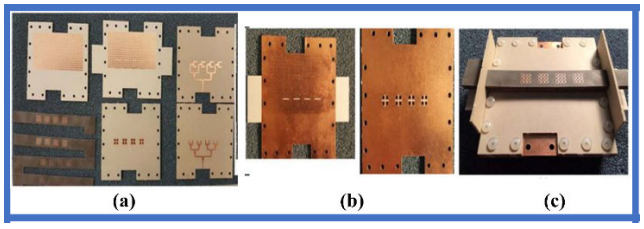

FIGURE 41. Prototype fabrication of proposed array, (a) Layers, (b) Bottom surface of Layer 4 and bottom surface of Layer 7, (c) Final assembled prototype [57].

The gain of the array is 15 dB with an efficiency of 86%. The radiation pattern is narrow in broadside direction with 15° in E-plane and 50° in H-plane (Figure 40(b-e)). The prototype fabrication is shown in Figure 41.

To resolve the issue of substrate losses occur due to the parallel transmission line, a low-loss ridge gap waveguide (RGWG) with magneto-electric (ME) dipole is proposed [59]. The initial design is a 2 × 2 ME dipole with coaxial feed on two Teflon substrate layers with different thicknesses forming the radiating structure. The ME has two rectangular patches separated by a coaxial-feed T-probe that forms a GSG transmission and six metallic vias. Five vias are connected to patches, and one is connected to T-probe. The T-probe is terminated with ring padding for better impedance matching. The bottom of the first substrate is the ground plane that covers the dielectric cavity on the second layer. Metallic vias, four coaxial probes surround this layer, and at the center there is a coupling slot. The third and fourth layers are copper layers filled with air and constitute the feeding network, where third layer is the coupling slot, and the fourth is the short-end RGWG section. During first half of time the current is concentrated in GSG feed (exciting magnetic dipole) and at next half current concentration is at quarter-wavelength patches, which indicates excitation of electric dipole, which makes them work complementary as ME as seen from Figure 42(a-c). The dielectric cavity delivers in-plane equal power to all the ME when exited by RGWC. The cavity is exited at TE_{230} mode as it is the lowest resonant

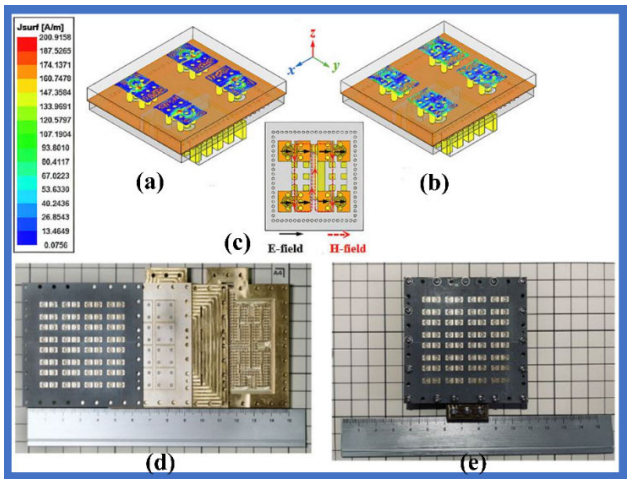

FIGURE 42. Simulated surface current distribution (left) of 2 × 2 ME-dipole sub-array. (a) t = 0, T/2, (b) t = T/4, 3T/4. (c) Equivalent magnetic current and electric current. Prototype fabrication of proposed array antenna, (d) diffusion layer, (e) assembled prototype [59].

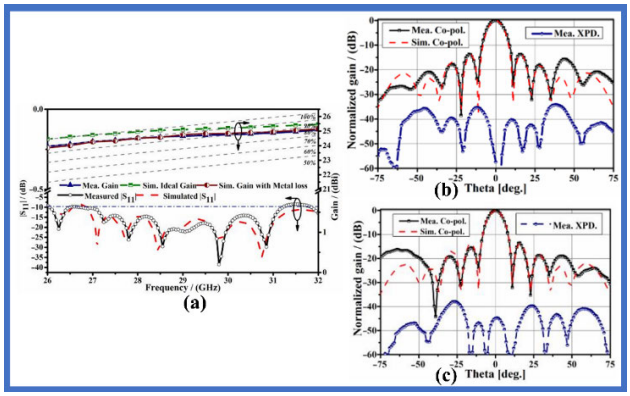

FIGURE 43. (a) Simulated and measured reflection coefficient and gain of 8 × 8-unit hybrid-feed ME-dipole antenna array. Simulated and measured radiation pattern of the 8 × 8 ME array at 27 GHz, (b) E-plane, (c) H-plane [59].

mode. The design is further extended to an 8 × 8 ME dipole array antenna fed by a 1 × 16 RGWG feed network. For this, three RGWG units are used.

The impedance matching and power divide ratio is adjusted by varying the length and height of the ridge in RGWG. A deviation of ±5° and ± 0.2 dB in phase and amplitude is observed at output ports. The resulting bandwidth at S11 < −10 is 27-32 GHz with a gain of 24.6 dBi and an efficiency of 80%, as shown in Figure 43(a). The radiation pattern is in broadside with HPBW of 20° in E- and H-plane at 27 GHz, as shown in Figure 43(b-c). The prototype fabrication is shown in Figure 42(d-e). The merits and demerits of Vivaldi and ME dipole array structures with parallel feed method are presented in Table 6. The summary of performance metrics of parallel feed arrays are presented in Table 7.

C. HYBRID-FED ARRAY ANTENNAS

1) PLANAR ARRAY

The series feed structure has advantages over parallel feed as it takes less space, compact and strip line losses are low.

TABLE 6. Merits and demerits of Vivaldi and ME dipole array structures with parallel feeding method.

References	Design Structure	Technique adapted	Merits	Demerits
Parallel Feeding Method				
[54]	Vivaldi	Uniform structure and spacing tapered radiator with notch	• Equal power divider. • Wide bandwidth. • Reduced surface wave loss due to the notch.	• Wide beamwidth in E- and H-plane. • Dielectric losses. • Low front-to-back ratio.
[55]		Uniform structure and spacing tapered radiator, with corrugated structure	• Equal power distribution. • Wide bandwidth. • Reduced surface wave losses. • Narrow beamwidth in H-plane.	• Wide beamwidth in E-plane. • Dielectric losses. • Low front-to-back ratio.
[56]		Uniform structure and spacing tapered leaf radiator	• Multiband resonance. • Equal power divider. • Wide bandwidth. • Narrow beamwidth in E-plane.	• Wide beamwidth in H-plane. • Dielectric losses. • Dominant SLL in E-plane.
[14]	ME Dipole	Multilayer, uniform structure and spacing of radiator, with pillbox transmission	• Reduced dielectric and surface current losses. • Reduced leaky wave. • Wide bandwidth. • Narrow beamwidth in E- and H-plane.	• Complex structure. • Dominant SLL in E-plane. • Misalignments of layers lead to devastating results.
[57]		Multilayer, uniform structure and spacing radiator, with EBG structure	• Equal power distribution. • EBG as meta-lens improved directivity. • Wide bandwidth. • Dual polarization. • Reduced leaky wave losses. • Narrow beamwidth in E-plane.	• Complex structure. • Dominant SLL in E-plane. • Misalignments of layers lead to devastating results.
[59]		Multilayer, uniform structure and spacing radiator, with RGWG transmission	• Reduced substrate losses. • Equal power and phase distribution. • Operates at a high mode of TE_{230}. • Wide bandwidth. • Very high gain. • Narrow beamwidth in E- and H-plane. • Suppressed SLL.	• Complex structure. • Deviation of $\pm 5^0$ in phase distribution. • Misalignments of layers lead to devastating results.

In contrast, the corporate feed has equal arm length for all the elements, which gives the flexibility of inter-element spacing, and divide the power equally among the elements. Hence, in [60], the benefit of series and corporate feed is exploited to design a 16-element linear array. The design has an 8-element in series forms subarray interconnected by microstrip line of quarter wave transform. Further, the Y-junction power divider feeds two such series of the subarray. The size of a single patch is calculated using the equations of rectangular patch [61], and the impedance of tapered Y-junction is calculated using equations (1) to (4). The simulated bandwidth of the design is 26.4-28.9 GHz at S11 < -10 dB with voltage-standing-wave-ratio (VSWR) of 2 in the desired band, as shown in Figure 44(b). The constructive radiation pattern is on the broadside with the HPBW of 30° and 8° in E- and H-plane (Figure 44(c-d)) with sidelobe level of -11 dB and -20 dB. The average gain of the resulted in 16.4 dBi. The prototype design is shown in Figure 44(a).

In another design, parasitic patches are used on top of an 8×6 array antenna to mitigate the narrow bandwidth due to series feed to obtain wide bandwidth [62]. The design has a two-layer substrate of Rogers RT/Duriod 5880 with a thickness of 0.127 mm. The top of the bottom substrate is engraved with rectangular tapered patches of 8×6 radiating with eight subarrays, each having 06 elements connected in series.

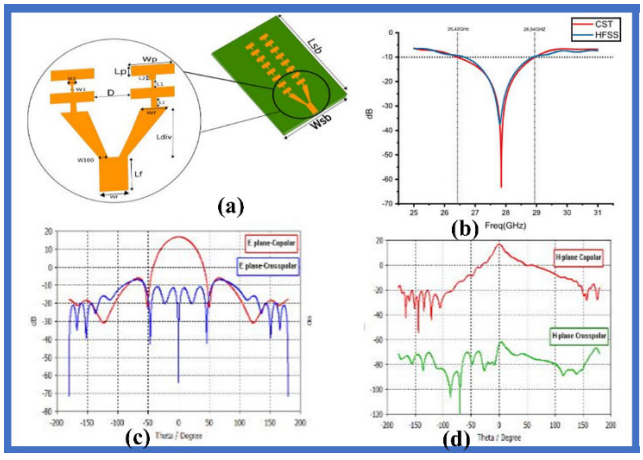

FIGURE 44. (a) Simulated design of proposed array antenna. (b) Reflection coefficient S11. Simulated radiation pattern, (c) E-plane (d) H-plane. [60].

TABLE 7. Performance metrics summary of parallel-fed arrays.

Reference	Dimension (mm^2)	Center frequency (GHz)	Array Elements	Average Gain (dBi)	Bandwidth (GHz)	Side-lobe level (dB)	Efficiency (%)	Radiation Pattern	Beamwidth	Polarization
Parallel Feed Arrays										
[43]	18.25 x 12.5	28/36	1 x 4	10	26.2 – 36.7	-	95	Bidirectional	20^0 & 70^0 in E- & H-plane	Linear
[44]	20 x 22	28	1 x 4	10.2	26 – 30	-	88	Bidirectional	12^0 & 70^0 in E- & H-plane	Linear
[45]	35.5 x 14.85	28/38	1 x 4	10	26 - 45	-	78	Omnidirectional	-	Linear
[46]	14.3 x 37.6	28	1 x 4	10.7	23.41 – 33.92	-10.9	90	End-fire (-90^0) & Broadside	90^0 & 14^0 in E- & H-plane	Linear
[47]	53.15 x 53.15	29.65/29.25	4 x 4	19.74/ 14.69	27 – 32.5 / 23 – 39	-12	88 / 84	Broadside	16^0 in E- & H-plane	Linear/Circular
[48]	10.49 x 12.3	60	4 x 2	13	51 – 53.5 / 57 – 65	-	-	End-fire (+90^0)	60^0 & 30^0 in E- & H-plane	Linear
[49]	20.64 x 20	60	1 x 2	11	57.2 – 63.8	-	-	Multiple beams	10^0 & 15^0 in E- & H-plane	Linear
[50]	80 x 35.2	28	1 x 4	14.6	25.2 – 31.3	-15		Broadside	120^0 in E- & H-plane	Linear
[51]	35.1 x 33.64	26	1 x 4	12	24.5-27.5	-	-	Broadside	60^0 & 15^0 in E- & H-plane	Linear
[52]	36.96 x 36.96	28	2 x 2	12.5	27.8 – 28.4	-	-	Broadside	34^0 & 31^0 in E- & H-plane	Linear
[53]	-	36	4 x 4	17	35.25 – 37.1	-10	-	Broadside	20^0 in E- & H-plane	Linear
[54]	52.35 x 16.95	26	1 x 8	12.5	22.8 – 31.3	-	-	Broadside	60^0 in E & H-plane	Linear
[55]	24 x 28.8	25 / 35	1 x 4	10.6	24.5 – 29 / 30.5 - 40	-	92	End-fire (+90^0)/ broadside	80^0 & 20^0 in E- & H-plane	Linear
[56]	33.31 x 54.96	18 / 26 / 38	1 x 8	11	15 -21 / 24 – 28.5 / 35 – 38	-	86	Bidirectional / End-fire (90^0)	8^0-30^0 & 60^0-120^0 in E- & H-plane	Linear
[14]	50 x 44	60	4 x 10	25.1	52 – 72	-	-	Broadside	18^0 in E- & H-plane	Linear
[57]	-	28	1 x 4	15	27.5 – 32.8 / 33.5 – 34.5	-11	86	Broadside	15^0 & 50^0 in E- & H-plane	Dual Polarization
[59]	57.85 x 57.85	28	8 x 8	24.6	27 - 32	-15	80	Broadside	20^0 in E- & H-plane	Linear

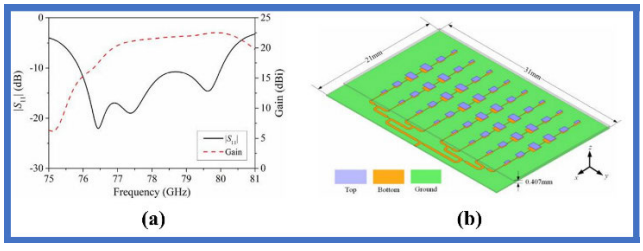

FIGURE 45. (a) Reflection coefficient S11 and gain parameter. (b) Proposed simulated array antenna design [62].

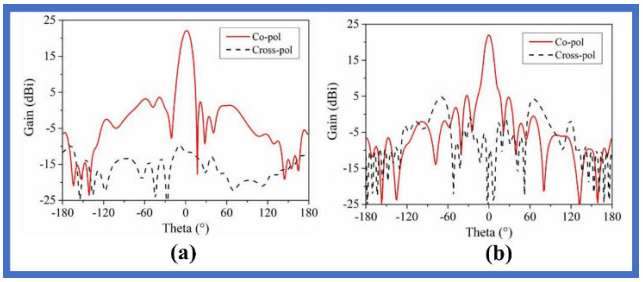

FIGURE 46. Simulated radiation patter of proposed design, (a) E-plane, (b) H-plane. [62].

These subarrays are fed through the corporate feed. The bottom of the substrate is supported by the ground plane. The top of the upper substrate has parasitic patches similar to the radiating element, which aids in enhancing bandwidth at S11 < -10 is 76-80 GHz, as shown in Figure 45(a). The design has resulted in a 20 dBi gain with a narrow HPBW of 13.22° at E-plane and 10.17° at the H-plane as shown in Figure 46. The simulated design is shown in Figure 45(b). The limitation is that the structural analysis is only based on simulated results that are not compared with fabricated results.

2) COPLANAR WAVEGUIDE ARRAY

To improve the bandwidth of the array antenna, a 4×4 hexagonal shape series fed array antenna is proposed for the femtocell to operate at 28 GHz [63]. The initial design is a single-element hexagonal shape patch antenna fed by a

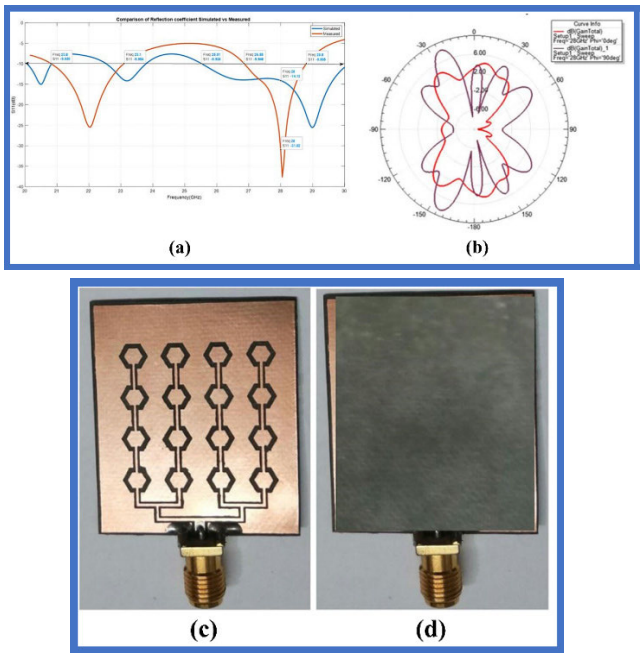

FIGURE 47. (a) Simulated and measured reflection coefficient bandwidth at S11 < -10 dB. (b) Radiation pattern of E- and H-plane. Prototype fabrication of CPW fed hexagonal array, (c) top view, (d) bottom view [63].

50 Ω microstrip feed line surrounded by a coplanar wave guide (CPW) structure. The CPW feed offers low radiation losses, and the various CPW feed details are provided in [10]. The Rogers RT/Duriod 5880 is chosen as substrate with a thickness of 0.02. The dimension of the hexagonal patch is calculated using the equation of a circular patch, and side lengths are obtained by equating the circular patch and hexagonal patch area. The CPW surrounds the patch and feed line. The parasitic analysis is performed to determine the best outer and inner side lengths of the patch and CPW. This single-element antenna is extended to two element parallel feed to enhance the bandwidth from 26.79-29.62 GHz to 25.88-28.93 GHz at S11 < -10 dB. Further, this design is extended to a 1×4 array fed by corporate feed by maintaining the radiator distance of $1.6\lambda g$ to reduce the surface wave coupling.

The number of radiating elements is increased from 4 to 16 through series feed to improve the performance in terms of gain and bandwidth. Here, each 1×4 radiating element has been extended to three other radiating hexagonal patches fed in series. The 4×4 design has resulted in dual-band resonance at S11 < -10 dB, i.e., 22.5-23.6 GHz and 25.51-30 GHz simulated, and 21-23.1 GHz and 26.86-28.8 GHz measured. There are discrepancies in the simulated and measured results of S11, as shown in Figure 47(a). The voltage-standing-wave-ratio (VSWR) at the desired band of interest is 2. The average gain of the proposed design is 8.98 dBi. The radiation is bidirectional in the E- and H-plane, as shown in Figure 47(b). The prototype fabrication is shown in Figure 47(c-d). The overall dimension of the design is 30×35 mm^2.

3) SLOT COUPLED ARRAY

A dual-band multilayer structure with shared space for Ka and E-band is designed in [64]. Here 2×4 array and 8×16 array are proposed to resonate at 28 GHz (Ka-band) and 84 GHz (E-band). The single-element structure has three layers of Rogers 5880 substrate. Layer-1 has a rectangular patch designed to resonate at 28 GHz, which is fed by a 50 Ω microstrip line. This patch has four square slots where parasitic patches are engraved to resonate at 84 GHz. These parasitic patches are supported by another four-square parasitic patches engraved at the bottom of layer-1 to increase the bandwidth at a higher frequency. The feed network for the parasitic patch is at the bottom of layer-3 with a slotted ground plane on layer-2 to couple the power. As the Ka-band and E-band patch shares the same aperture, the impedance for the Ka-band patch is matched through a quarter wavelength transformer. The parametric study on patch sizes and spacing is performed to minimize the coupling and SLL. This three-layer structure is laminated and housed in a metal cavity. Direct feeding of high-frequency signal through microstrip line results in higher reflections, because of which strip line is converted to waveguide port, which is achieved through the antipodal fin-line waveguide to strip line transition. The bandwidth at S11 < -10 dB resulted in 27.6-28.7 GHz and 81-88 GHz, with an approximate beamwidth of 30° in the Ka and E band, which suffered losses due to metal cavity and close spacing of dual-band elements.

The design is extended to array by incorporating additional parasitic patches between Ka elements to reduce the grating lobes at E-band. The element spacing of $0.75\lambda_{ka}$ and $0.56\lambda_E$ is maintained to make it compact. Due to confined space and to reduce the strip line losses, Ka-band patches are connected in series which later fed by parallel network at port. For in-phase excitation of all patches, the port line length is maintained at λg (guided wavelength). Similar series feed is applied to E-band, but due to complex arrangement additional impedance transformation is employed as shown in Figure 48(a-b). The reflection coefficient bandwidth at S11 < -10 dB resulted in 26.5-29 GHz and 82.5-84 GHz as shown in Figure 48(c-d). The gain has increased to 20 dBi and radiation pattern in broadside with HPBW of 15° and 20°, 50° and 30° in E and H-plane for Ka and E-band as shown in Figure 49(a-d). The prototype fabrication of proposed array antenna is shown in Figure 49(e). The limitations of the design are: (1) The performance of E-band array has degraded the bandwidth due to surface wave, (2) The cross-polarization and SLL are significant in the radiation pattern.

4) SUBSTRATE INTEGRATED-WAVEGUIDE ARRAY

A SIWC bandpass filter, power divider, and patch antenna radiator are combined in a single design in a multilayer structure, forming an anti-phase filtering power divider [65], as shown in Figure 50(a). The design has three substrates. The lower substrate is Rogers 5880 of 0.254 thickness surrounded by metallic vias to form three SIWC operating at TE_{110} mode

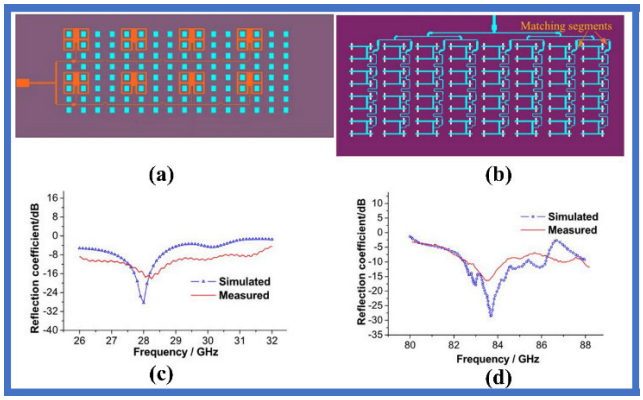

FIGURE 48. Feeding network, (a) Ka band, (b) E band [64]. Reflection coefficient bandwidth at S11 < −10 dB, (c) Ka-band, (d) E-band [64].

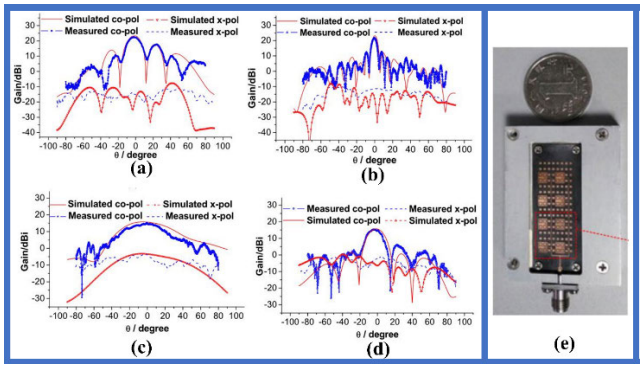

FIGURE 49. Radiation pattern of antenna array, (a) & (b) H-plane and E-plane of E-band, (c) & (d) E- and H-plane of Ka band. (e) Prototype fabrication of array [64].

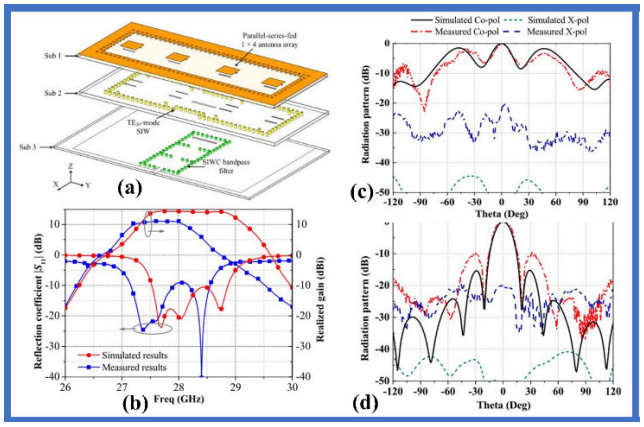

FIGURE 50. (a) 3-D view of proposed mmWave filtering patch antenna array. (b) Measured and simulated reflection coefficient S11 and gain of 1 × 4 filtering patch array antenna. Measured and simulated radiation pattern at 28 GHz, (c) E-plane, (d) H-plane. [65].

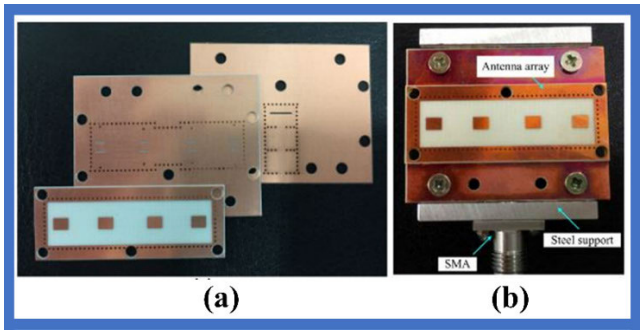

FIGURE 51. Prototype fabrication of 1 × 4 filtering array antenna, (a) expanded view, (b) assembled view [65].

as a bandpass filter. It has an input port to couple the power and a slot at the center to couple the power to the higher layer. The middle substrate is Rogers 4003C, and it has a power coupling slot in the center and metallic vias in two parallel lines operating at TE_{20} mode. The lower and middle substrate shares common ground, forming the power divider. The top layer of the middle substrate has four microstrip line ports. The current at port-2 and -4, port-3 and -5 have even symmetric with in-phase, whereas port-2 and -3, port-4 and -5 has odd symmetric with 180° out-off-phase, results in a differential signal with phase difference. The top substrate is Rogers 4003C, and it has a 1 × 4 patch array formed of 1 × 2 series-fed subarray excited at TE_{10} mode. The bottom of the top substrate has dual coupling slots for each patch.

The measured result shows the dual resonance with reflection coefficient bandwidth S11 < −10 dB of 27.2-27.9 GHz and 28.2-28.5 GHz, which has a discrepancy with the simulated result, and the gain is 10 dBi in the band of interest as shown in Figure 50(b). The radiation pattern is in broadside with HPBW of 60° and 22° in E and H-plane with SLL of −15 dB in H-plane as shown in Figure 50(c-d). The prototype fabrication is shown in Figure 51.

5) GRAPHENE-BASED ARRAY

Graphene has good flexibility and great conductivity and can be used in place of copper. The conductivity of graphene is 1.12×10^6 S/m, measured by the four-probe method. In [66], an 8 × 16 series-parallel fed array antenna is proposed with low side-lobe levels. The single element is a rectangular graphene patch obtained from the CVD method on Rogers 5880 substrate with a thickness of 0.508 mm. The single element is extended to a 16-element array connected in series and fed by a 50 Ω microstrip line. Each element is connected to a microstrip line through a quarter-wave transformer for better impedance match. Such a 16-element structure is further extended to an 8 × 16 array, where the eight microstrip lines are fed by a T-junction power divider with Chebyshev distribution such that each element receives the same phase by which radiation can be in a broadside direction. The analysis of the graphene array is compared with the copper array. The bandwidth at reflection coefficient S11 < −10 dB is 25.5-26.5 GHz, as shown in Figure 52(a). The radiation pattern is highly directional in the broadside with HPBW of 10.3° and 5.1° in the E- and H-plane with SLL of −23.67 and −24.65 dB, as shown in Figure 52(c-d). The gain is high at 25 dBi but relatively less than copper metal. The prototype

TABLE 8. Merits and demerits of planar, CPW, slot-coupled, SIW, graphene-based arrays with hybrid feeding method.

References	Design Structure	Technique adapted	Merits	Demerits
Hybrid Feeding Method				
[60]	Planar	Uniform structure and spacing radiator	• Equal power distribution to subarrays. • Wide bandwidth. • Narrow beamwidth in E- and H-plane.	• Unequal power distribution in series subarrays. • Dielectric, surface wave losses and transmission line losses. • Dominant SLL in E-plane.
[62]		Multilayer, non-uniform structure and uniform spacing radiator, with parasitic elements.	• Equal power distribution to subarrays. • Maintained RAPR. • Wide bandwidth due to parasitic elements. • Very narrow beamwidth in E- and H-plane. • Low transmission line losses.	• Measurement results are missing. • Improper alignment of parasitic elements may lead to devastating results. • Dominant SLL in E- and H-plane.
[63]	CPW	Uniform structure and spacing radiator	• Low transmission line losses. • Equal power distribution to subarrays. • Dual-band resonance. • Wide bandwidth.	• Bidirectional radiation. • Unequal power distribution in series subarray.
[64]	Slot	Multilayer, uniform structure and spacing radiator, with parasitic elements	• Multiband resonance. • Equal power distribution. • Wide bandwidth. • Narrow beamwidth.	• Waveguide to strip line transition required. • Leaky wave and surface wave losses. • High cross-polarization. • Dominant SLL.
[65]	SIW	Multilayer, uniform structure and spacing, with SIW cavity and bandpass filter	• Equal power divider with in-phase and out-of-phase for ports resulting in differential signal with difference phase. • Operates at TE_{10} mode. • Reduced leaky wave losses. • Narrow beamwidth in H-plane. • Suppressed SLL in H-plane.	• Complex structure. • Narrow bandwidth. • Wide beamwidth in E-plane. • Misalignments of layers lead to devastating results.
[66]	Graphene-based	Uniform structure and spacing graphene radiator	• Equal power distribution to subarrays. • Wide bandwidth. • Very narrow beamwidth in E- and H-plane. • Suppressed SLL in E- and H-plane.	• Unequal power distribution in series subarrays.

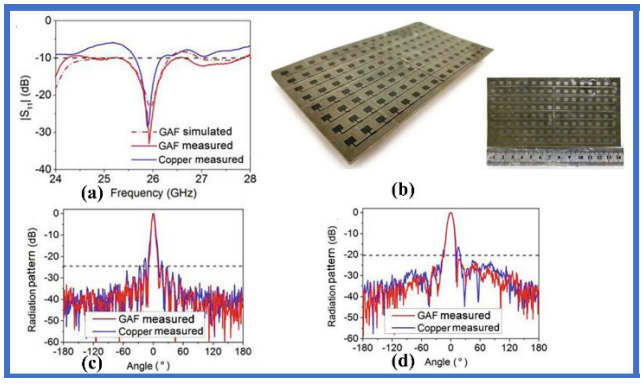

FIGURE 52. (a) Simulated and measured reflection coefficient S11 (b) Prototype fabrication of graphene array antenna (right). Measured radiation pattern, (c) E-plane, (d) H-plane [66].

fabrication is shown in Figure 52(b). The merits and demerits of array structures with hybrid-fed are discussed in Table 8. The summary of performance metrics of these arrays are shown in Table 9.

V. RECONFIGURABLE ARRAY ANTENNAS

The reconfigurable arrays are classified based on frequency, radiation pattern/angle, and/or polarization reconfigurable property of the antenna. This section presents a review of reconfigurable array antennas.

A. FREQUENCY RECONFIGURABLE ARRAY

Frequency reconfigurable characteristic of antenna can be obtained by perturbing the surface current or feeding network integrated with of reconfigurable bandpass filter (BPF). A four-band frequency tunable 16-element array antenna with ring resonator and p-i-n diode, which acts as a band-pass filter (BPF), is proposed in [16]. The structure has three layers and two substrates. The bottom of the lower substrate (RT 5870) has a feeding network connected to BPF, etched on Rogers RO3003 substrate. The top layer of the lower substrate and the bottom layer of the upper substrate share the common ground. The upper substrate (Rogers RO3003) top layer has four subarrays of radiating element (corner trimmed

TABLE 9. Performance metrics summary of hybrid-fed arrays.

Reference	Dimension (mm^2)	Center frequency (GHz)	Array Elements	Average Gain (dBi)	Bandwidth (GHz)	Side-lobe level (dB)	Efficiency (%)	Radiation Pattern	Beamwidth	Polarization
Hybrid-Fed Array										
[60]	88 x 25	28	8 x 2	16.4	26.4 – 28.9	-11 / -20	92	Broadside	30^0 & 8^0in E- & H-plane	Linear
[62]	31 x 21	79	8 x 6	20	76 – 80	-19 / -17	-	Broadside	13.22^0 & 10.17^0 in E- & H-plane	Linear
[63]	30 x 35	22 / 28	4 x 4	8.98	21 -23.1 / 26.86 – 28.8	-	-	Bidirectional with multibeam	-	Linear
[64]	-	28 / 82	8 x 16	20	26.5 – 29 / 82.5 – 84	-10	-	Broadside	15^0 & 20^0 Ka-band, 50^0 & 30^0 E-band in E- & H-plane	Linear
[65]	-	28	1 x 4	10.5	27.2 – 27.9 / 28.2 – 28.5	-15	-	Broadside	60^0 & 22^0 in E- & H-plane	Linear
[66]	145 x 75	26	8 x16	25	25.5 – 26.5	-23.67 / -24.65	-	Broadside	10.3^0 & 5.1^0 in E- & H-plane	Linear

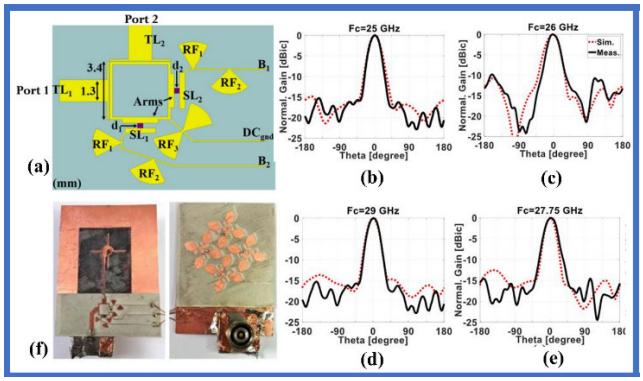

FIGURE 53. (a) Reconfigurable modified ring resonator BPF with integrated two PIN diodes with bias network. Simulated and measured radiation pattern at H-plane, (b) 11-state, (c) 10-state, (d) 01-state, (e) 00-state. (f) Prototype fabrication of array antenna [16].

rectangular shape) connected to circular shape series fed. The four elements are arranged at an angle of 90°, fed equally through a series-fed 50 Ω microstrip line, resulting in RHCP. The main feeding network on the lower substrate feeds the power to subarray arms through metallic vias.

The structure of BPF has a ring resonator with a capacitively coupled input and output port on two adjacent sides. The other two sides have varied-length open-ended stubs connected to the ring through the p-i-n diode (S1 and S2). These diodes are operated with two different bias lines supported by RF choke for wide-band operation, as shown in Figure 53(a). The feeding network is chosen with a thinner substrate to reduce radiation losses, whereas the radiator substrate is thicker to enhance the radiation efficiency and bandwidth. The results show the resonance at different frequencies based on the diodes state (ON/OFF state as 1/0): when both diodes are OFF (00-state), the antenna resonates at 28-30.1 GHz, at 10-state 26.7-28.4 GHz, 01-state 24.4-27.1 GHz, and 11-state 23.75-26.3 GHz with RHCP. The gain and 1 dB axial ratio resonance for these states are 13 dBic, 12 dBic, 10 dBic, and 12 dBic and 29 GHz, 26 GHz, 27.75 GHz, and 25 GHz in H-plane with HPBW of 20° as shown in Figure 53(b-e). The prototype fabrication is shown in Figure 53(f).

A frequency beam steering with high isolation leaky-wave array antenna developed on SIW is proposed in [67]. The design has two long rectangular patches on top of the Rogers RO3003 substrate with two feed lines on both ends as port-1 and -2. The bottom of the substrate has a full ground plane. The metallic vias are inserted at the patch's edges to connect the ground forming a SIW configuration. To reduce the leakage losses in SIW, meta-material (MTM) structure of seven E-shape slots is etched on top of each array. Another array also has an MTM structure etched in the reverse direction to reduce the mutual coupling. The coupling between two arrays can be further reduced by adding a traverse tapered slot MTM-shield on SIW, which also improves the radiation performance. In this design, MTM slots behave as series left-hand capacitance where are metallic vias as shunt left-hand inductors. The surface current distribution indicates that the coupling effect with MTM-shield has improved the isolation to 42.5 dB. The equivalent circuit analysis is performed based on the T-model and π-model of composite right/left-handed metamaterial transmission line (CRLH-MTM). The simulated bandwidth at reflection coefficient S11 < -10 dB is 55-65 GHz with isolation of -20 dB and higher, as shown in Figure 54(a). The radiation pattern is directional with beam steering at $-30°$, 0°, and $+30°$ at various frequencies with a gain of 8.5, 10.1, 9.5 dBi as shown in Figure 54(b-d). The proposed design is shown in Figure 55.

The merits and demerits of frequency reconfigurable array structures are discussed in Table 10. Also, Table 11, presents the summary of performance metrics of these array structures.

B. RADIATION PATTERN/ANGLE RECONFIGURABLE ARRAY

An array antenna can be designed to perform beam steering with a narrow beam in the desired direction by varying the

TABLE 10. Merits and demerits of frequency reconfigurable array structures.

References	Technique adapted	Merits	Demerits
[16]	Multilayer, uniform structure and spacing radiator, with RF diode and BPF	• Right-hand circular polarization. • Reduced transmission line losses and leaky wave losses. • Four tunable bands with wide bandwidth. • Suppressed SLL in H-plane. • Narrow beamwidth.	• Insertion losses due RF diodes. • External bias is required to operate RF diodes.
[67]	Multilayer, uniform structure and spacing radiator, with SIW and MTM structure, series feed	• Reduced leaky wave losses. • High isolation due to MTM. • Wide bandwidth. • Narrow beamwidth.	• Complex structure. • Structure is only simulated, not fabricated and measured.

TABLE 11. Performance metrics summary of frequency reconfigurable arrays.

Reference	Dimension (mm^2)	Center frequency (GHz)	Array Elements	Average Gain (dBi)	Bandwidth (GHz)	Isolation (dB)	Side Lobe Level (dB)	Efficiency (%)	Beam Squint	Beam steering angle	Beamwidth	Polarization
Frequency reconfigurable array												
[16]	43 x 32	29 / 26 / 27.75 / 25	16 – element	13 / 12 / 10 / 12	28-30.1 / 26.7-28.4 / 24.4-27.1 / 23.75-26.3	-	-17.5, -18, -19	-	0^0 at 29 / 26 / 27.75 / 25 GHz	-	20^0 in H-plane	RHCP
[67]	40 x 10	59	1 x 2	9.8	55 - 65	-33		76		-30^0, 0^0, $+30^0$	30^0 in E-plane	Linear

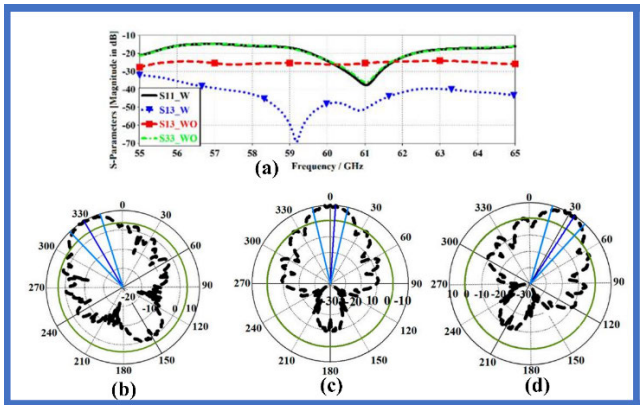

FIGURE 54. (a) Reflection coefficient and isolation before and after applying MTM-shield. Radiation pattern of 1 × 2 MTM-LWA array, (a) 55 GHz, (b) 60 GHz, (c) 65 GHz [67].

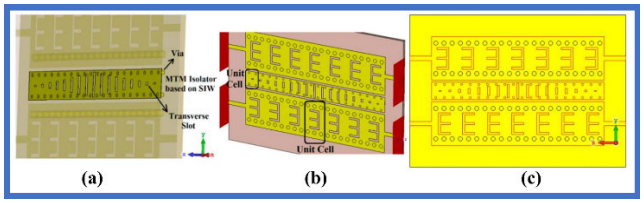

FIGURE 55. Proposed SIW-based leaky-wave antenna with MTM-shield. (a) Proposed MTM-SIW shield located between array antenna. (b) Top-view of leaky-wave array antenna. (c) Bottom-view of array antenna [67].

phase of a set of elements. An 8 × 24 and 32 × 24 right-hand-circular-polarization (RHCP) reconfigurable antenna to tune the frequency and radiation pattern is proposed in [17]. Each cell has four patch elements in this design arranged in a butterfly shape connected in series with a microstrip line. Each element in the cell is separated at a quadrature distance of λ/4 and placed in orthogonal orientation to obtain the RHCP. The cavity analysis is applied to analyze the radiation pattern on each patch in linear polarization (LP) [61]. The design is extended to two cells with adequate spacing (2λg) to maintain linearity and in-phase between cells, but this large inter-cell spacing has resulted in a higher grating lobe. Hence the distance is reduced to λg (where $\lambda g = 0.65\,\lambda 0$), which will overlap the elements but doesn't distort the radiation pattern. The surface current distribution and radiation efficiency are studied for 1 × 16, 1 × 24, and 1 × 32 linear arrays. In 1 × 32, the end cells' current density and radiation efficiency are reduced. Hence 1 × 24 array is chosen on which further parametric analysis on the width of elements and approximation of butterfly structure is performed using a transmission line model. The open-stopband (OSB) issue of leaky wave antenna is mitigated in this design due to the butterfly structure, which feeds sequentially with quadrature-phase to each element. The beam squint for the 1 × 24 structure resulted in the range from −5° at 84 GHz to +3° at 88 GHz in H-plane. An 8 × 24 is a combination of parallel-series feed which resulted in bandwidth from 84-88 GHz at S11 < −10 (Figure 56(a)) with the maximum beam squint of 6° in a bandwidth range of 85.2-86.3 GHz as shown in Figure 56(b-c). The prototype fabrication is shown in Figure 56(d).

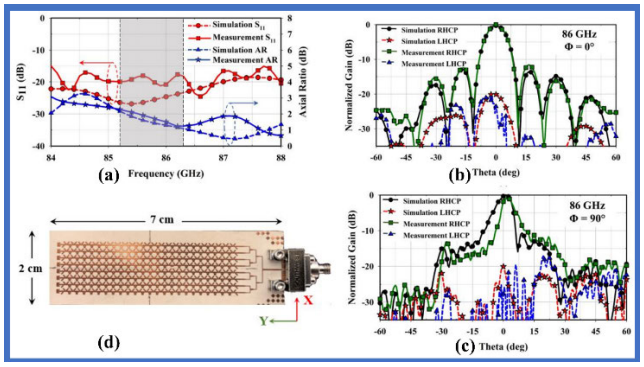

FIGURE 56. (a) Simulated and measured reflection coefficient of 8 × 24 butterfly planar array antenna, the shaded region from 85.2 to 86.3 GHz is the acceptable squint bandwidth. Simulated and measured normalized CP radiation pattern of 8 × 24 array (b) E-plane (c) H-plane. (d) Proposed prototype fabrication of array antenna [17].

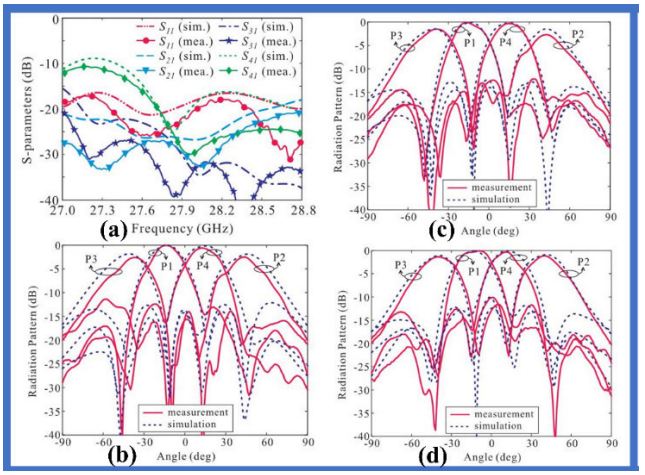

FIGURE 57. (a) Measured and simulated reflection coefficient S11 when port 1 is excited. Measured and simulated radiation pattern in E-plane at different frequencies. (b) 27.525 GHz, (c) 27.925 GHz, (d) 28.325 GHz [19].

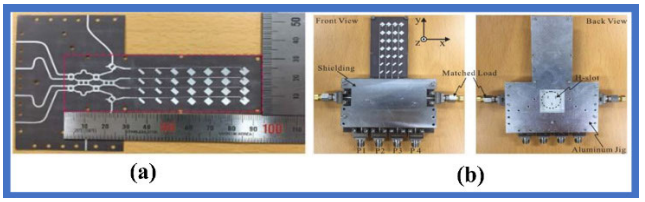

FIGURE 58. (a) Fabricated four-beam array antenna. (b) Assembled antenna [19].

In another design, a modified 4 × 4 butler matrix is used to steer the beam and reduce the sidelobe levels [19]. The butler matrix (BM) splits the power equally to all subarrays, which results in high sidelobe levels. This can be reduced either by implementing a power divider at the output of BM to split unequal power or implementing an attenuator at the output of BM to produce tapered amplitude distribution. Here the modified BM has; (a) four hybrid couplers with better isolation S41 between port-1 and −4 of −25 dB with 2.25° of phase difference between port 2 and 3. (b) two crossovers of better isolation of −22 dB between port-1 and −2, and port-1 and −4 in the desired frequency range of 27.52-28.32 GHz. (c) two 45° phase shifters at port-1 and -4. (d) two attenuators at the output of BM to produce tapered amplitude distribution. The attenuator is a four-port circular coupler, where port-2 is isolated by shorting to the ground plane through metallic vias, port-3 is terminated with matched load, and the attenuated output is taken from port-4.

The array antenna has rectangular patches at an angle of 45° to the right of the 100 Ω microstrip line connected in a comb-line structure to reduce the feeding losses, and the microstrip line is terminated by an inset feed patch, with that it becomes a 7-elements subarray. A rectangular slit in the microstrip line near to patch element is to reduce the reflection losses. The microstrip line of 100 Ω is connected through a 50 Ω transformer. The BM and array antenna are designed on the single layer of the TLY-5 substrate. Several H-slots are etched on the ground plane to improve the isolation between BM and array antenna. The design is extended to a 4 × 7 antenna array connected to BM, resulting in bandwidth at S11 < −10 dB is 27-28.8 GHz (Figure 57(a)) with beams steered at an angle of −16.2°, +40.8°, −39.4°, and +12.6° and reduced sidelobe levels of −16.7 dB, −10.3 dB, −10.9 dB, and −14.5 dB as shown in Figure 57(b-d). The prototype fabrication is shown in Figure 58. The limitation of the design is it has average bandwidth.

A wideband two layer 16-element array antenna is proposed in [18]. The single radiating element is a rectangular patch with inset feed on top of the lower substrate. The rectangular parasitic patch on top of the upper substrate is stacked above the lower substrate, separated by distance d for maximum power coupling, resulting in a wider bandwidth of 25.7-29.7 GHz. Both the substrates are Rogers 5880 of 0.254 mm thickness. Further, two element study is carried out by placing symmetrically and asymmetrically. The symmetric arrangement has resulted in 5° drifts in radiation pattern off the broadside, and whereas asymmetric has resulted in 0° radiation in broadside, hence, asymmetric design is extended to a 16-element array, where two subarrays of 8-elements each are placed in asymmetry, fed by corporate feed network.

To keep the coupling minimum between subarrays, adjacent elements are separated by a distance of 0.56λ0 at 28 GHz. With this, isolation between two ports is maintained at -19 dB. The two feeding networks are designed to radiate in different directions and maintain the SLL at −10 dB. One feeding network with no phase delay, and other with 180° phase delay. The port-1 delay is n-dphi+dphi delay, where dphi is 154°, n is even number element (1 to 16), and the port-2 delay is two n-times the dphi. The bandwidth at reflection coefficient S11 < −10 dB is 25-30.5 GHz for both the feeding networks, as shown in Figure 59(a-b). The radiation pattern results at broadside with HPBW of 60° and 10° in E- and H-plane, scan from −54° to +54° in H-plane

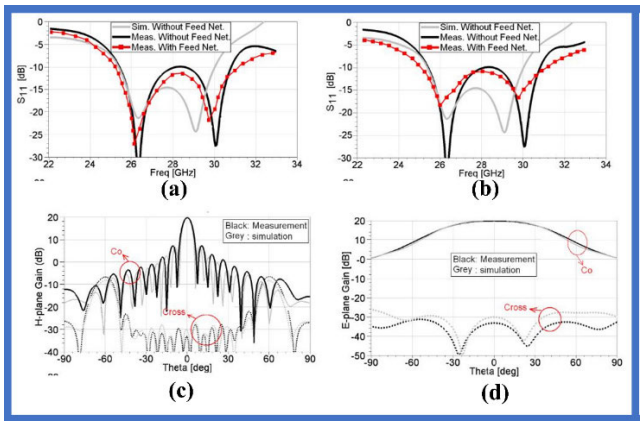

FIGURE 59. Simulated and measured reflection coefficient with and without feeding network, (a) dphi = 0° at 28 GHz. (b) dphi = 154° at 28 GHz. Simulated and measured radiation pattern with dphi = 0° at 28 GHz (c) H-plane, (d) E-plane [18].

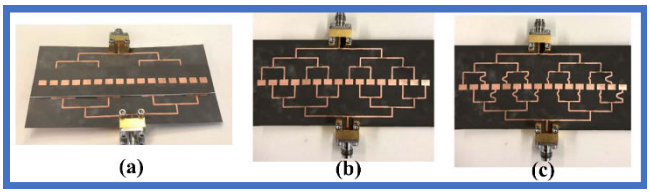

FIGURE 60. Prototype fabrication. (a) Excited elements covered with parasitic elements. (b) Feeding network for boresight pattern. (c) Feeding network for maximum scan (dphi = 154°) at 28 GHz [18].

with the total scan angle of 108° as shown in Figure 59(c-d). The prototype fabrication is shown in Figure 60.

Another series-fed design is proposed for wide bandwidth and beamforming ability [68]. Four rectangular patches are connected in series in this design through a microstrip line. The first two patches are optimized with inset feed, improving the impedance, and the latter two patch corners are truncated to degenerate the two modes and increase the bandwidth. These two modes result in left and right elliptical polarization, which can be combined to obtain linear polarization. The length of the microstrip line between patches is a half wavelength. The microstrip line is fed through a quarter wave transformer for impedance matching. The modified series-fed array's performance is compared with the conventional series-fed array, showing the 6.6% increment in bandwidth at S11 < -10 dB. The cross-polarization is minimized by an asymmetrical arrangement of modified series-fed arrays adjacent to each other, resulting a 4 x 16 array structure.

An active transmit/receive module (TRM) is connected to a 4 $\times$ 16 array through a 50 Ω microstrip line to perform the beam steering. The TRM has a 5-bit phase shifter, with a change in one least significant bit (LSB) resulting in phase shift and attenuation of 11.25° and 1 dB. Each modified series-fed array is connected to TRM, and phase accuracy is increased by implementing an interconnected digital algorithm in FPGA. The resulting bandwidth at reflection coefficient S11 < -10 dB is 36-39 GHz with an isolation

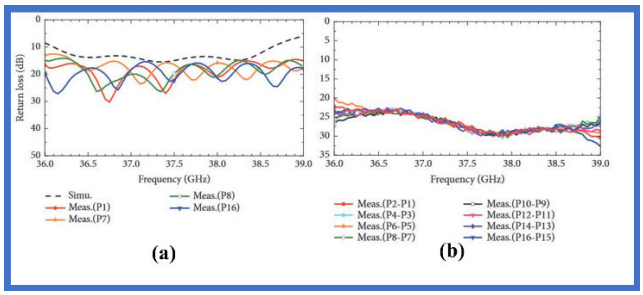

FIGURE 61. Measured and simulated 4 × 16 antenna array, (a) Reflection coefficient, (b) Isolation [68].

level of -20 dB and lower throughout the band, as shown in Figure 61. The radiation pattern has a beam width of 5.5° at boresight in H-plane with a beam scanning ability of $\pm$ 20° with the change in 10° and the SLL of -13 dB as shown in Figure 62(a-b). The prototype fabrication is shown in Figure 62(c-d). The limitations of the design are it used a commercial TR module for beam scanning.

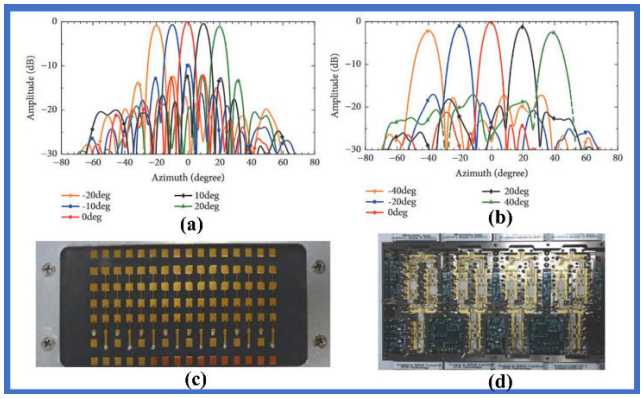

FIGURE 62. Simulation of scanned H-plane pattern, (a) transmitting pattern with uniform distribution, (b) receiving patterns with low sidelobes. (c) Prototype fabrication antenna. (d) Transcom T/R Module [68].

A simple 2 × 2 and 3 × 3 modified series-fed array antenna with beam steering ability is proposed in [69]. In the initial design, a single rectangular patch is designed to resonate at 28 GHz, which is fed by two 50 Ω transmission lines at adjacent sides, further connected to a quarter wave transformer. The excitation by two ports resulted in perpendicular and inline surface current with feedline. This analysis reveals that beam steering can be achieved by implementing phase shifters. Further, the design is extended to a 2 $\times$ 2 series-fed array with four ports, two in the x and y direction. When all the ports are excited with zero phases, it results in radiation in the broadside direction, with a maximum gain of 13.2 dBi and SLL of -20 dB. When a phase of $-110°$ is applied to port-1 while port-2 is maintained at zero phase resulting in $-24°$ beam direction in H-plane and vice-versa. The design is optimized to 3 $\times$ 3 elements with only four ports instead of six ports. In general, for an N $\times$ N array, only N+1 or N ports are required when N is odd or even. So, in this case, it requires

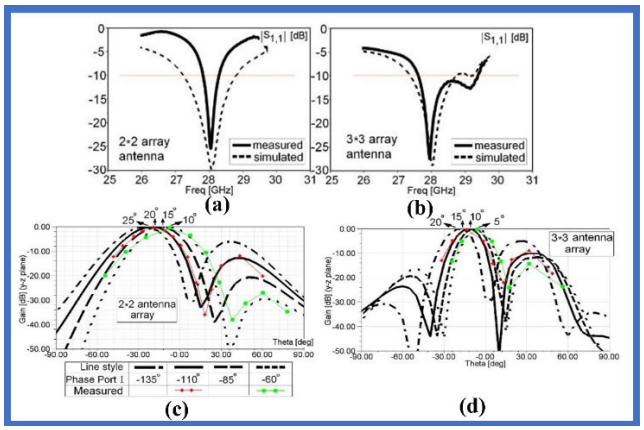

FIGURE 63. Measured S11 when port 1 is excited, (a) 2 × 2 array (b) 3 × 3 array. Normalized simulated and measured H-plane (c) 2 × 2 array, (d) 3 × 3 array [69].

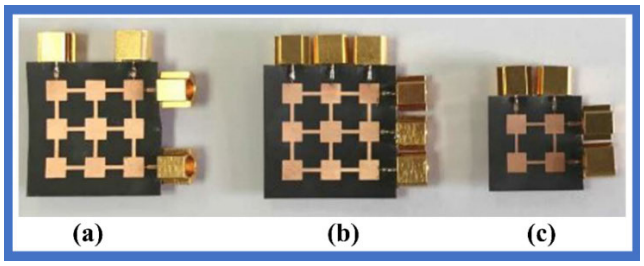

FIGURE 64. Prototype fabrication of array antenna, (a) 3 × 3 array with 4-ports, (b) 3 × 3 array with 6-ports, (c) 2 × 2 array with 4-ports [69].

only four ports, and the results are compared with six port configurations. The bandwidth at reflection coefficient S11 < -10 dB is 27.7-28.3 GHz and 27.5-29.4 GHz for 2×2 and 3×3 arrays as shown in Figure 63(a-b). The beam is steered at an angle of $\pm 25°$, and $\pm 20°$ for 2×2 and 3×3 array in the H-plane, HPBW of radiation pattern is 42° in H-plane as shown in Figure 63(c-d). The prototype fabrication is shown in Figure 64.

In another design, a 13-beam planar series-fed array antenna supported with a butler matrix (BM) and branch line coupler (BLC) is proposed [70]. The array antenna is designed to generate 7-beams from the butler matrix and 6-beams from two branch-line couplers compared to the conventional 4×4 butler and branch-line coupler, which could generate only 4+2 beams. The initial design is 1×10 rectangular tapered patches from center to end with a Chebyshev coefficient to minimize the SLL. These tapered arrays are fed by a series microstrip line. The spacing between elements is half-guided wavelength ($\lambda g/2$). The 4×4 butler matrix has four 3-db quadrature couplers, four phase shifters (two 180° and two 0°), two cross-overs, four input ports and four output ports. When power is fed to port-1 of coupler, the equally divided power with 90° phase shift appears across output, similarly when fed at port-2. But when the power of applied to both ports the output has equally divided power with in-phase, this contributes to the three switched beams from the

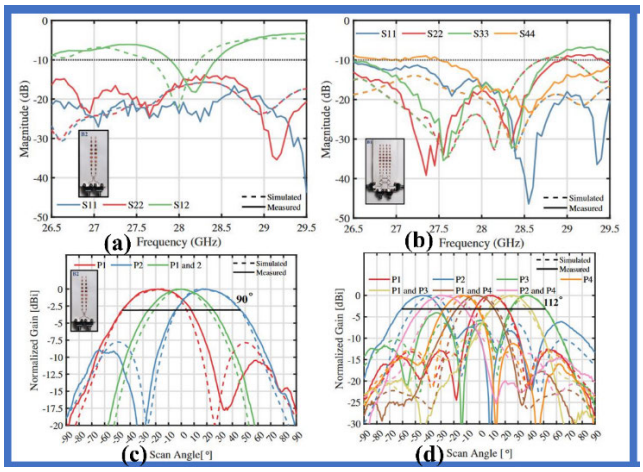

FIGURE 65. Measured and simulated reflection coefficient (left) (a) 2 × 10 BLC array antenna, (b) 4 × 10 BM array antenna. Measured and simulated radiation pattern of beam forming (right) (a) 2 × 10 BLC array antenna, (b) 4 × 10 BM array [70].

coupler. The 4×4 BM generates 4-beams with the progressive phase of 45°, −135°, 135°, −45° when power is separately fed to each of the four ports and additional 3 beams when two ports are excited simultaneously with a phase of 90°, 0°, −90°. The design is extended to a 4×10 and 2×10 BM and BLC array, where each subarray is placed at the distance of $\lambda_0/2$. The bandwidth of 2×10 BLC and 4×10 BM at reflection coefficient S11 < -10 dB is 27.85-28.4 GHz and 26.5-28.75 GHz, as shown in Figure 65(a-b). The beam of 2×10 and 4×10 array has HPBW of 60° at an angle of −20°, 0°, +20° and HPBW of 28° at an angle of −45°, −30°, −15°, 0°, 10°, 25°, 35° as shown in Figure 65(c-d). The overall beam steering ability of proposed array is ± 138° in space with average gain of 12 dBi and SLL of −15 dB. The prototype fabrication is shown in Figure 66.

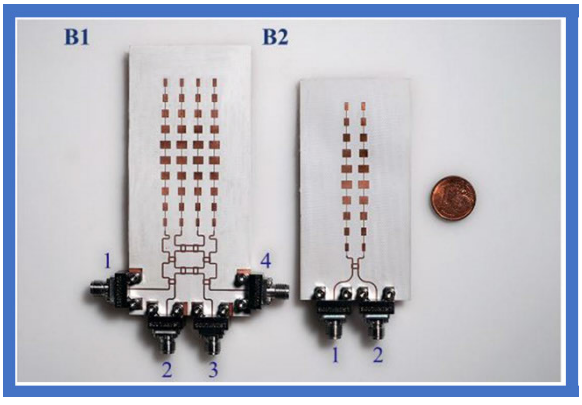

FIGURE 66. Prototype fabrication of array antenna. B1 – 4 × 10 BM array antenna, B2 – 2 × 10 BLC array antenna [70].

To reduce the radiation losses from the butler matrix, a compact and cost efficient two-layer structure is proposed in [35]. It has two substrates of polytetrafluoroethylene (PTFE) with different electrical properties, the above

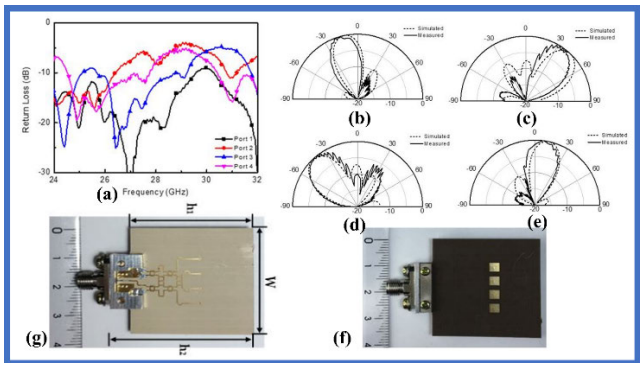

FIGURE 67. (a) Simulated and measured reflection coefficient of single patch. Simulated and measured radiation pattern when following ports are excited: (b) Port 1, (c) Port 2, (d) Port 3, (e) Port 4. Prototype fabrication of proposed antenna array, (f) top view, (g) bottom view [35].

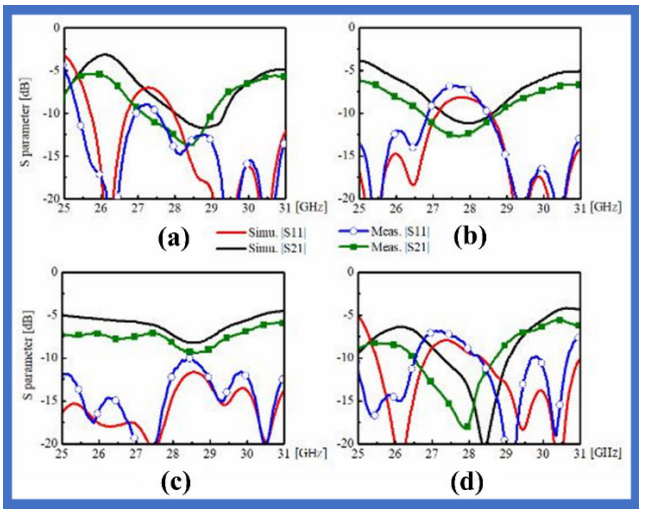

FIGURE 68. Simulated and measured S-parameter of four prototype with phase shift (left) of (a) −140°, (b) −90°, (c) 0°, and (d) 140° 71].

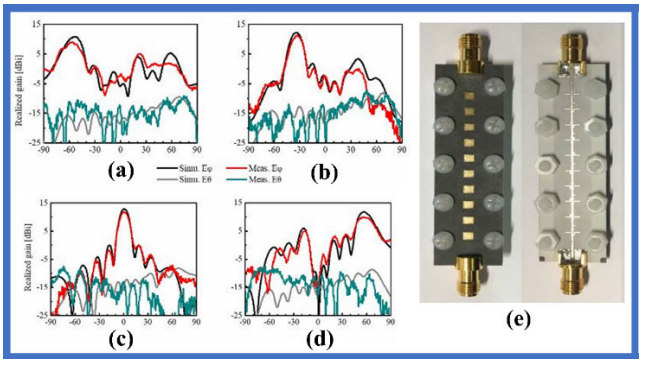

FIGURE 69. Simulated and measured realized gain of four prototype with phase shift of (a) −140°, (b) −90°, (c) 0°, and (d) 140°. (e) Fabrication of four prototypes with phase shift of −140° [71].

substrate-1 is TLY-5A with lower εr of 2.17 and below substrate-2 is RF-60A with a higher εr of 6.15. To reduce the effect of BM on radiators, the BM is printed on the bottom of substrate-2 and the rectangular radiating patches are printed on the top of substrate-1. The bottom and top of substrate-1 and 2 are ground planes joined by a prepreg layer. The BM has four input ports (P1, P2, P3, P4), and four output ports (P5, P6, P7, P8) with two BLC, two crossover, and two 45° phase shifters. The BM output signal is coupled to patches through metallic vias. The parametric analysis on patch dimension and spacing between elements are performed to improve the impedance match and gain. To reduce the size of BM, the substrate with higher permittivity is selected such that the overall calculated dimension of strip line reduces. The resulted bandwidth at reflection coefficient S11 < -10 dB is 24.1-25.1 GHz as shown in Figure 67(a). The BM generates the phase shift of −135°, −45°, +45°, and +135° this results in the beam steering at an angle of −45°, −15°, +15°, and 45° with SLL of −12, −6, −13.8 and −11.7 dB as shown in Figure 67(b-e). The prototype fabrication is shown in Figure 67(f-g).

A two-layer series-fed leaky-wave array antenna is proposed to steer the beam at the variable frequency with an active phase shifter [71]. The upper substrate is Rogers 5880, where ten rectangular patches are arranged in a straight line, the top of the second substrate (Rogers 4003C) has a ground plane with two rectangular slot lines beneath the patches to couple the power, and the bottom has the series feed structure. The feeding structure has a 50 Ω microstrip line with ten power-distributing structures, where each structure has two stubs crossing and two stubs opposite the microstrip line. These are connected through a switch (p-i-n diode) to control the phase. Four switches are connected between stubs, two on the left and two on the right of the microstrip line. The microstrip line exhibits periodic phase distribution along the line and 180° phase on either side, which gives the advantage for a 2-bit phase shifter to generate a phase difference of 0°, 90°, 180°, 270°. To mitigate the issue of impedance mismatch due to reflected power at input, five additional stubs are added to the microstrip line, which cancels the reflections produced by the phase shifters. The simulated beam steering angle at 27, 28, and 29 GHz has resulted in −56° to +55°, −65° to +66°, −57° to +68°.

In this work, due to fabrication limitation diodes are not implemented instead the switch positions are closed by shorting the metal strip, with that the four phase shifts are generated at −140°, −90°, 0°, 140° to steer the beam at different angle. The bandwidth at reflection coefficient S11 < -10 at these phases are 26-26.7 GHz and 28-31 GHz, 25-26.75 GHz and 28.6-31 GHz, 25-31 GHz, and 25-26.5 GHz and 28.8-30.4 GHz as shown in Figure 68. The radiation was obtained at −60°, −30°, 0°, and 60°. Figure 69(d) shows the beam steering at 24 GHz. The prototype fabrication is shown in Figure 69(e). The limitations of the design are: (a) The actual p-i-n diode configuration is not tested, (b) The radiation pattern has a large SLL, and (c) The design has poor isolation.

The reflection-canceling structure with a non-uniform spaced tapered series-fed array antenna is proposed with low

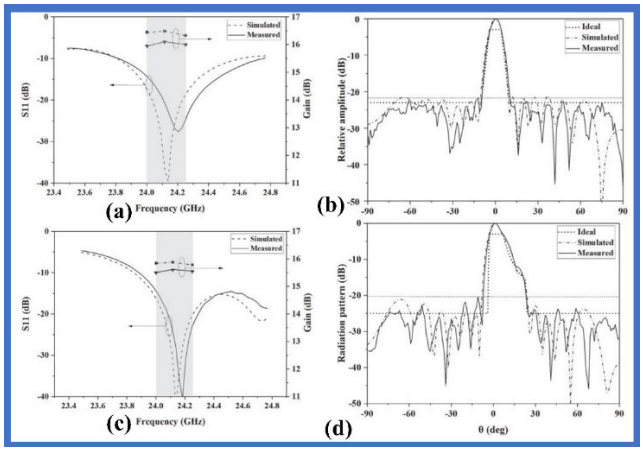

FIGURE 70. Simulated and measured parameters of low side-lobe array, (a) Reflection coefficient S11, (b) Radiation pattern at 24 GHz. Simulated and measured parameters of shaped-beam array, (c) Reflection coefficient S11, (d) Radiation pattern at 24 GHz [72].

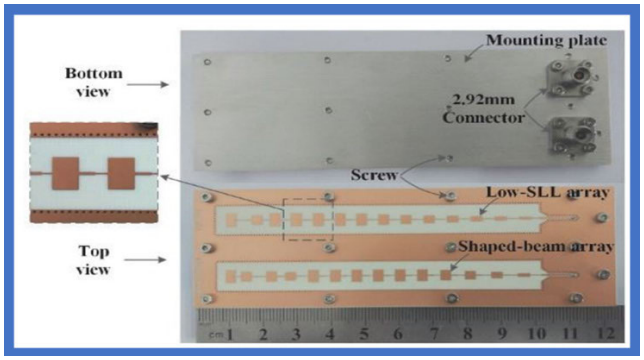

FIGURE 71. Proposed prototype fabrication of array antenna [72].

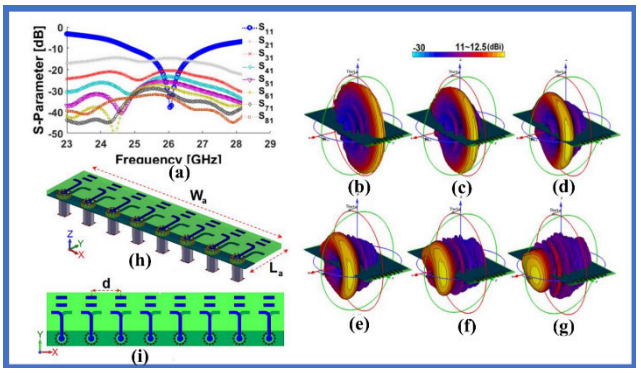

FIGURE 72. (a) Simulated reflection coefficient and isolation of mmWave 5G smartphone antenna. 3D radiation beams of 5G smartphone design at (b) 0°, (c) 15°, (d) 30°, (e) 45°, (f) 60°, and (g) 75°. Proposed design of linear phased array antenna. (h) 3D transparent and (i) top view [73].

side lobe levels, and a beam shaping pattern is proposed in [72]. The single element is a rectangular patch with two ports where the signal is fed through a quarter-wave transformer at port-1 to match the impedance. This also works as a reflected wave canceller. The patch radiates the power fed to it, and the remaining power is coupled to the next section through the microstrip line of port-2. The single element is extended to a linear array by arranging the patches in series fed by a microstrip line. The amplitude and phase distribution of linear array can be changed by varying the width and non-uniform spacing of patches. The residue in the transmission line is eliminated by terminating the line with a patch of inset feed. Here two types of arrays are designed, one for low sidelobe level and the second for beam shaping. In both cases, there are 14 radiating elements in series covered by GCPW, which requires a microstrip-to-GCPW-to-cable transition. The low side-lobe level array has bandwidth at reflection coefficient S11 < -10 dB is 23.9-24.7 GHz, with HPBW of 10° in the broadside direction and SLL of -21.7 dB as shown in Figure 70(a-b). The shaped-beam array has bandwidth at S11 < -10 dB is 23.9-25 GHz, and the main beam is shaped at $-3°$ and 23° with SLL of -20 dB, as shown in Figure 70(b-d). The prototype fabrication is shown in Figure 71. The limitations of design are: (a) The bandwidth is very narrow at low-side-lobe level design, (b) The gain and efficiency of the design are not verified, and (c) The design doesn't support beam steering ability.

In another design, end-fire radiation, highly directive, beam steerable quasi-Yagi array antenna is proposed in [73]. The single-element Yagi antenna consists of a driven element where half of the driven element is etched on the top of the Arlon Ad350 substrate, fed by coaxial-to-microstrip transition, and the other half is at the bottom of the substrate connected to a ground plane. Two directors of equal dimensions follow the driven element. Metallic vias cover the feed point to restrict the surface current. The parametric analysis on driven element length and width, and on the size of the director is performed. It reveals that by changing the length of the driven element, the resonating frequency can be changed, and director length directly impacts impedance matching. The design is extended to eight elements separated at distance d and fed by corporate feed. It is understood that large inter-element spacing results in better radiation characteristics, but it limits the scanning angle. Hence there should be a trade-off between both. In this case, the distance is slightly less than $\lambda/2$ to obtain a wide scanning angle by applying phase shifter. The bandwidth at reflection coefficient S11 < -10 dB is 24.85-27.1 GHz with isolation of -16 dB, as shown in Figure 72(a). The radiation pattern is in the end-fire direction with beam steering of 0°-75°, as shown in Figure 72(b-g). The proposed design is shown in Figure 72(h-i).

The next design has higher bandwidth and wide frequency scanning with a 7×8 array antenna, as proposed in [74]. The antenna is designed on a single-layer substrate of Rogers 4350B with a thickness of 0.508 mm. The radiating element is a curved microstrip line of length λg at the center frequency. Such seven radiating elements are connected in series with microstrip-SIW transmission lines to reduce the radiation losses, which constitute subarray. The radius of the curved radiating element is optimized for maximum radiation. Eight

such subarray structures are arranged parallel to each other and are fed by a parallel feeding network at both ends, resulting in two port structures. When port-1 is excited, port-2 is connected to absorber which is at the left and right of the structure, it results in left hand circular polarization (LHCP). The phase difference between adjacent radiating element is 2.36° at 30 GHz which is negligible, the phase difference increases with the frequency above 30 GHz. The power fed to the array antenna through coaxial connector, which uses a coaxial-to-SIW transition structure. The bandwidth at reflection coefficient S11 < -10 dB resulted in 26-34 GHz with a gain of 23 dBi as shown in Figure 73(a-b). The narrow radiation pattern of 10.0°, 9.1°, and 9.1° is steered with change in frequency at 28, 30, and 34 GHz in the direction of −14.5°, 0°, and +22.5° as shown in Figure 73(c-d). The prototype fabrication is shown in Figure 73(e).

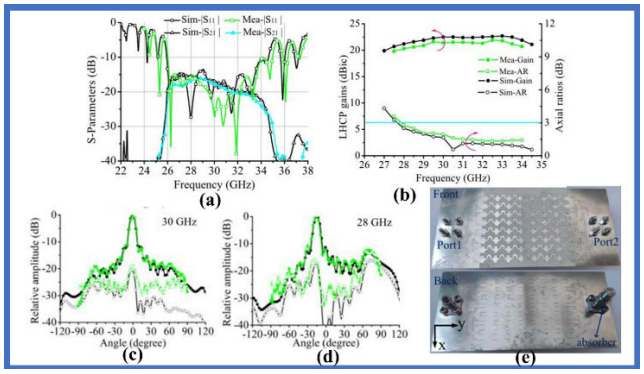

FIGURE 73. Measured and simulated results of proposed array antenna (left), (a) Reflection coefficient S11, (b) LHCP gain. Measured and simulated radiation pattern in H-plane at, (c) 30 GHz, (d) 28 GHz. Prototype fabrication of proposed antenna array [74].

In the next design, end-fire radiation with a wide beam scanning array antenna is proposed [75]. Here single-element structure has a dual function, it works as a radiator and power splitter. The design has a rectangular patch on top of the substrate with inset feed on the left and right as the input and output port. The metallic vias around the patch form the substrate-integrated waveguide cavity (SIWC) with a slit at the feeding point in an L-shape. The half dipole is etched on top, and another half at the bottom, which is connected to a ground plane of SIWC. This results in end-fire radiation. The power coupled to the next element is controlled by varying the length of a slit at port-2, so that required power at the output can be obtained, in this way the RAPR is controlled in array. The required resonance can be obtained by varying the length of the dipole. The design is extended to a 1×4 subarray connected in series through a mender line (phase shifter), and the optimum distance between elements is maintained to minimize the SLL.

The power from the output of one element is fed to next by varying the length of the feed slit to feed equal power to all the elements. With the varied length of the mender line, different phase constants can be achieved at all four elements, which results in beam steering ability in E-plane, in this case it is 90° to 110°. Eight subarrays are stacked onto two different corporate feed structures to obtain array-1 configuration for broadside radiation and array-2 for beam scanning. The array-1 feeding network offers 0° phase shift, whereas array-2 offers 120° phase shift at alternate ports. A slight difference is observed in the bandwidth with two feeding networks, 24.8-28 GHz for array-1, and 24.5-27.5 GHz for array 2, as shown in Figure 74(a). The radiation pattern is at 108° and 0° in E- and H-plane with HPBW of 15° for array -1. The beam is steered to 65° in H-plane for array-2, as shown in Figure 74(d-g). Both configurations have SLL of −15 dB with a gain of above 15 dBi. The prototype fabrication is shown in Figure74(b-c).

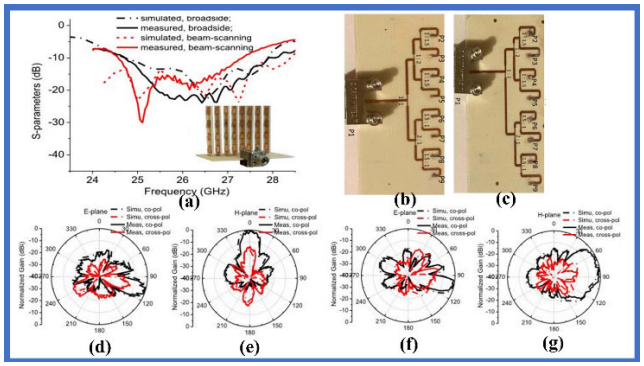

FIGURE 74. (a) Simulated and measured reflection coefficient of array antenna. Fabricated eight-way power splitters (b) Array-1 with zero phase, (c) Array-2 with 120° phase. Simulated and measured normalized radiation patterns at 26 GHz. (d) E-plane, array -1, (e) H-plane, array-1, (f) E-plane, array-2, (g) H-plane, array-2 [75].

An active device is used to steer the beam instead of phase shifter with 1-bit reconfigurable array antenna to reduce the phase quantization error [20]. The design has two substrate and four layers, where four rectangular patches are etched on top of Rogers 5880 substrate-1 with rectangular slots at the bottom underneath the patch. The substrate-2 is Rogers 4003C, top layer has ground plane and the bottom has parallel feeding network surrounded by SIW. The ground plane has a rectangular slot to couple the power from feed to radiator. The two substrates are bonded with prepreg layer of Rogers 4350F. The feed network has two p-i-n diode which acts as switch that controls the phase of radiator. The arrangement of these diodes is such that when DC voltage is applied only one of the diodes is ON and it results in phase of 0° or −180°.

The T-junction power divider has three one-to-two dividers. The main one-to-two divider is GCPW to reduce the radiation losses and ground length, and the other two dividers are stacked by the ground plane to reduce the radiation losses. The 1-bit array resulted in grating and high SLL when trying to change the beam's direction from 0°. This leads to a phase quantization error of $\pi/2$, which was tried to eliminate by applying a fixed phase to each element of the array. But still, the phase quantization error remains to be same. Hence, an invasive weed optimization algorithm (IWO) is used to find the optimum value for the fixed phase. The four elements

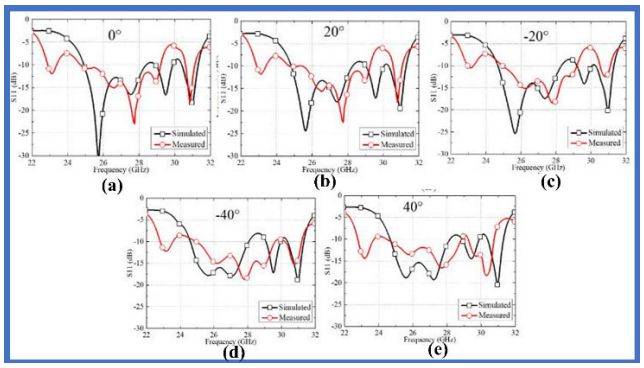

FIGURE 75. Simulated and measured parameters reflection coefficient within the range of 22-32 GHz (a-e) [20].

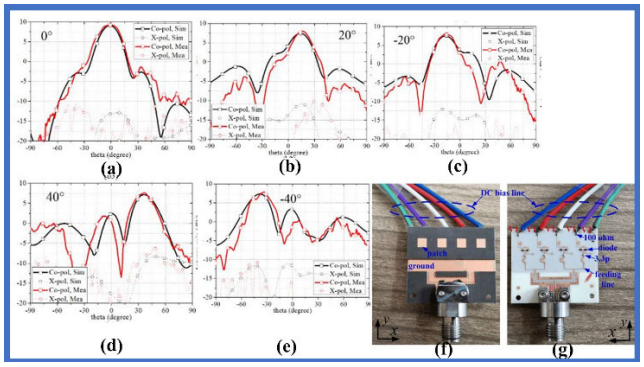

FIGURE 76. Radiation pattern in E-plane at 26 GHz in different direction (a-e). Prototype fabrication of 1-bit four element array, (f) top view, (g) bottom view [20].

of an array are applied with fixed phases of −36°, −75°, −68°, and −19° as resulted by IWO algorithm. With this, the four-element array could practically steer the beam at −70°, −42°, −36°, −18°, −2°, 14°, 19°, 37°, and 62°, out of which the five beam steering angles of ± 40° are selected, which results in no grating lobes. The bandwidth at reflection coefficient S11 < −10 dB is 25-29 GHz for all the states, as shown in Figure 75. Overall, the design has eight p-i-n diodes applied with three different voltages to operate in five states, resulting in five beams at 0°, 20° −20°, 40°, and −40°, as shown in Figure 76.

The prototype fabrication is shown in Figure 76(f-g). The limitation of the design is that at 40° and −40° the grating lobes are evident; therefore, the beam steering ability is restricted to −34° to +35°.

The modified Vivaldi antenna with tunable graphene nanoplates with variable resistivity in the range from 200 to 20 Ω is proposed in [21]. The design of single-element has an L-shaped 50 Ω microstrip feed line terminated with an inverted cone shape structure on the bottom of the substrate. The microstrip length and cone-shape radius are optimized for better impedance matching. The top of the substrate is etched with a circular slot extended to a rectangular slot, which is terminated with an open-ended tapered slit. This forms the tapered radiator. The top of the substrate also has

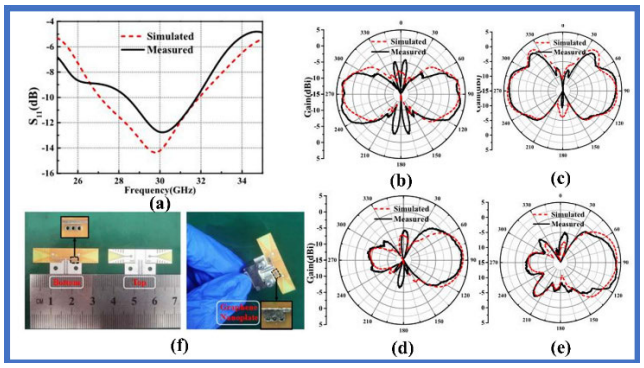

FIGURE 77. (a) Simulated and measured reflection coefficient. Simulated and measure radiation pattern, E-plane (b, d) in state 1 and 2, H-plane (c, e) in state 1 and 2 [21]. (f) Prototype fabrication of reconfigurable Vivaldi antenna array [21].

five rectangular tapered slits on either side of the radiator this is to improve the gain, directivity, and impedance match. The overlay position of the L-shaped strip line on the radiator slot is crucial to determine the resonant frequency.

Graphene is becoming popular in RF design circuits due to its flexible and tunable properties. This modified Vivaldi antenna is further upgraded with graphene nanoplates placed near the feed line and connected to the ground through metallic vias. The resistance of graphene nanoplates is at high state, which can be reduced by applying bias voltage which perturbs the surface current resulting in control of radiation in the antenna. The single-element design is extended to two elements connected back-to-back which is fed by parallel feed. The feed line is covered with GCPW to reduce the losses, and vertical slits separate two antennas to provide better isolation. The resulting bandwidth at reflection coefficient S11 < −10 dB is 28.2-31.9 GHz, resonating at 30 GHz, as shown in Figure 77(a). The beam steering is controlled by applying a bias voltage to two graphene nanoplates (Ga and Gb) of two radiators in three stages. When zero volts (state 1) is applied to Ga and Gb its resistance will be at 200 Ω, and the beam is directed at 90° and 270°. When Ga and Gb is applied with 4V and 0V (state 2), its resistance is 20 Ω and 200 Ω with the beam at 90°, and when Ga and Gb have 0V and 4V (state 3), their resistance changes to 200 Ω and 20 Ω with the beam at 270° as shown in Figure 77(b-e). The prototype fabrication is shown in Figure 77(f). The limitation of the design is it has a low gain of 3.8 dBi. The merits and demerits of radiation / beam reconfigurable arrays are discussed in Table 12. Also, the summary of performance metrics of these arrays are shown in Table 13.

C. POLARIZATION RECONFIGURABLE ARRAY

In a novel design, the array antenna could switch between RHCP and LHCP with the pair of active p-i-n diode and branch line coupler [23]. Here two Rogers 5880 substrates are glued with the bonding film. The bottom of substrate-2 has the T-junction power divider with two BLCs, and the top layer has four H-shaped slots etched on the ground

TABLE 12. Merits and demerits of radiation / beam reconfigurable arrays structures.

References	Technique adapted	Merits	Demerits
[17]	Uniform structure and spacing of butterfly radiator with hybrid feed	• Equal power distribution. • Right-hand CP. • Open stop band (OSB) issue of leaky wave antenna is mitigated. • Wide bandwidth. • Beam squint of 6^0 in bandwidth.	• Large geometrical structure. • Beam forming in only two directions.
[19]	Non-uniform structure and uniform spacing radiators with modified BM	• Equal power distribution from BM. • Reduced feed line losses due to inclined inset feed patch. • Wide bandwidth • Discrete beam steering from -16^0 to $+12.6^0$.	• Dominant SLL in E-plane.
[18]	Multilayer, uniform structure and spacing radiator with parallel feed.	• Asymmetrical design prevents the beam from drifting. • Wide bandwidth • Wide scanning angle of $\pm 54^0$ with narrow beamwidth in H-plane	• Wide beamwidth in E-plane.
[68]	Non-uniform structure and spacing radiator, with series feed	• Asymmetrical arrangement has reduced cross-polarization. • Wide bandwidth. • Narrow beamwidth in H-plane with $\pm 20^0$ scan angle.	• Dominant SLL in H-plane. • Commercial TGP2102 phase shifter is used.
[69]	Uniform structure and spacing radiator	• Two port excitation results in perpendicular and inline surface current with feedline. • Wide bandwidth. • Discrete scanning angle is $\pm 25^0$ with a narrow beam in H-plane.	• Requires separate phase shifter circuit.
[70]	Non-uniform structure and uniform spacing radiator, along with BM and BLC	• 13 beam scan angles. • Discrete scanning angle of $\pm 138^0$, with narrow beamwidth. • Suppressed SLL.	• Narrow bandwidth • Radiation losses due BM and BLC.
[35]	Multilayer, uniform structure and spacing radiator, along with BM	• Reduced radiation losses from BM due to the separation of planes. • Wide bandwidth. • Discrete scanning angle is $\pm 45^0$ with narrow beamwidth.	• Dominant SLL.
[71]	Uniform structure and spacing radiator, with series feed, RF diode	• Reduce impedance mismatch due to stubs. • Wide bandwidth. • Discrete scanning angle of $\pm 60^0$ with a narrow beam.	• Dominant SLL. • Measurement results are obtained by shorting pins rather than using actual RF diodes.
[72]	Non-uniform structure and spacing radiator with GCPW feed	• Suppressed SLL. • Wide bandwidth for shaped-beam array structure. • Beam shaping ability at 0^0 and 23^0.	• Narrow bandwidth for low SLL array structure. • No beam scanning ability.
[73]	Uniform structure and spacing radiator	• Wide bandwidth • Scanning angle from 0^0 to 75^0 with end-fire radiation.	• It required a microstrip-to-GCPW-to-cable transition.
[74]	Uniform structure and uniform spacing radiator with hybrid feed and SIW cavity	• Reduced transmission line losses. • LH and RH circular polarization. • Wide bandwidth. • Discrete scanning angle from -14.5^0 to $+22.5^0$ with narrow beam	• Phase difference of 2.36^0 between elements. • Requires coaxial-to-SIW transition structure.
[75]	Uniform structure and spacing radiator with SIW cavity and hybrid feed	• Controlled RAPR design. • Wide bandwidth. • Beam squint at 80^0 and 60^0. • Suppressed SLL.	• Coupling losses due to vertically stacked subarrays.
[20]	Multilayer, uniform structure and spacing of radiator with parallel feed and SIW cavity	• Reduced phase quantization error by the use of an RF device. • Discrete scanning angle of $\pm 34^0$	• Grating lobes at $\pm 40^0$. • Insertion losses due to eight RF p-i-n diodes.
[21]	Vivaldi radiator with graphene nanoplates, fed by GCPW	• Reduced transmission line losses. • Wide bandwidth. • Beamforming at four angles.	• External bias is required to change the resistance of graphene nanoplates. • Very low gain.

TABLE 13. Performance metric summary of radiation/ beam reconfigurable array structures.

Reference	Dimension (mm^2)	Center frequency (GHz)	Array Elements	Average Gain (dBi)	Bandwidth (GHz)	Isolation (dB)	Side Lobe Level (dB)	Efficiency (%)	Beam Squint	Beam steering angle	Beamwidth	Polarization
Radiation / Beam Reconfigurable Arrays												
[17]	70 x 2	86	8 x 24	11.5	84 – 88	-	-	75	-5^0 at 84 GHz, $+3^0$ at 88 GHz	-	10^0 in E- & H-plane	RHCP/ LHCP
[19]	30 x 32	28	4 x 7	16-17	27 – 28.8	-15	-16.7, -10.3, -10.9, -14.5	-	-	-16.2^0, $+40.8^0$, -39.4^0, $+12.6^0$	10^0 in E-plane	Linear
[18]	99.2 x 52.65	26	1 x 16	18	25 – 30.5	-19	-11.75, -12.1	86	-54.4^0 at 26 GHz, -49^0 at 28 GHz	-54^0 to $+54^0$	60^0 & 10^0 in E- & H-plane	Linear
[68]	-	37/39	4 x 16	21	36 – 39	-20	-13	-	-	-20^0 to $+20^0$ at angle of 10^0	30^0 & 5.5^0 in E- & H-plane	Linear
[69]	-	28	2 x 2 / 3 x 3	15.6	27.7 – 28.3 / 27.5 – 29.4	-	-10	75	-	-25^0 to $+25^0$ / -20^0 to $+20^0$ at angle of 5^0 in H – plane	42^0 in H-plane	Linear
[70]	90 x 45	28	2 x10 / 4 x 10	12	27.85 – 28.4 / 26.5 – 28.75	-	-15	-	-	± 138^0 at an angle of 15^0	8^0 in E-plane	Linear
[35]	36.2 x 36.2	24	1 x 4	7.4	24.1 – 25.1	-	-12, -6, -13.8, -11.7	-	-	-45^0, -15^0, $+15^0$, $+45^0$	15^0 in E-plane	Linear
[71]		27 / 28 / 29	1 x10	8.9, 11.1, 11.7, 9.8	26-26-7 and 28-31 / 25-26.75 and 28.6-31 / 25-31 / 25-26.5 and 28.8-30.4 (at various switches)	-	-	-	-56^0 to $+55^0$, -65^0 to $+66^0$, -57^0 to $+68^0$	-60^0, -30^0, 0^0, 60^0	20^0 in E-plane	Linear
[72]	125 x 45	24	2 x 14	15.5	23.9 – 24.7, 23.9 – 25	-	-21.7	-	-	-3^0 & 23^0	25^0 in E-plane	Linear
[73]	60 x 120	26	1 x 8	11	24.85 – 27.1	-16	-	90		0^0 to 75^0 at angle of 15^0	15^0 in E-plane	Linear
[74]	70 x 80	30	8 x 7	23	26 - 34	-16	-	-	10^0, 9.1^0, 9.1^0 at 28, 30, 34 GHz	-14.5^0, 0^0, $+22.5^0$	5^0 in E-plane	LHCP / RHCP
[75]	-	25	4 x 7	15	24.8 – 28 (array-1), 24.5 – 27.5 (array-2)	-	-15	80	80^0 & 60^0 at 24 & 27 GHz	-	108^0 & 0^0 in E- & H-plane	Linear
[20]	27 x 10	28	1 x 4	8	25 - 29		-10.5, -7.5, -5.6, -4.6, -7.6	-	0^0, 16^0, -18^0, 38^0, -34^0 at 26 GHz / -3^0, 17^0, -19^0, 37^0 at 27 GHz	± 40^0 at angle of 20^0	27^0 in E - plane	Linear
[21]	-	30	1 x 2	3.8	28.2 – 31.9	-	-	65 / 40	-	90^0 and 270^0 for different bias	80^0 in E-plane	Linear

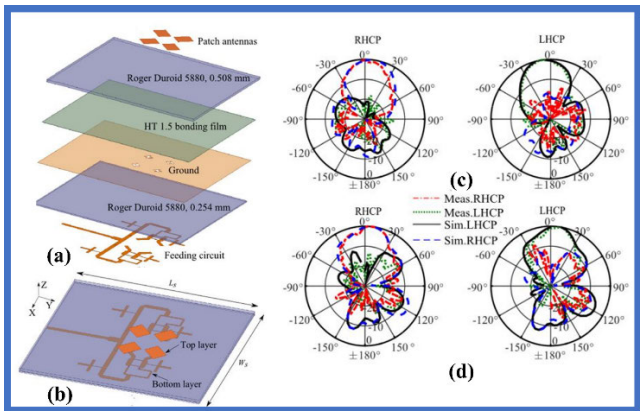

FIGURE 78. Polarization reconfigurable antenna array (a-b) 3-D exploded view of layers. Normalized simulated and measured radiation pattern at 28 GHz (c) E-plane, (d) H-plane. [23].

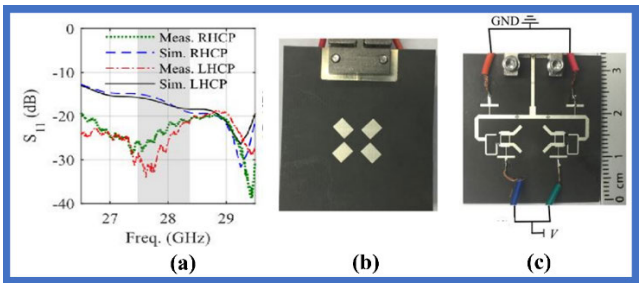

FIGURE 79. (a) Reflection coefficient S11 of proposed array. Prototype fabrication of proposed array antenna, (b) top view, (c) bottom view [23].

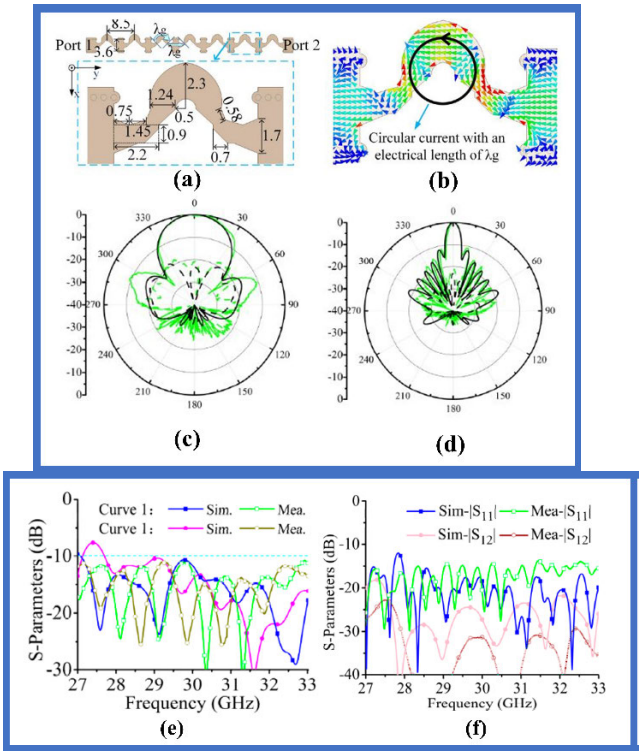

FIGURE 80. Radiation element and array, (a) structure and dimensions of array, (b) current distribution of curved microstrip line. Measured and simulated radiation pattern of array when port-1 is excited at 29.9 GHz (c) E-plane, (d) H-plane. (f) Measured and simulated reflection coefficient of array without feeding network. (f) Measured and simulated reflection coefficient and isolation with feeding network [24].

plane. The rectangular radiating patches are arranged in a circular fashion on top of substrate-1, as shown in the 3D view Figure 78(a-b). When these patches are excited in an anti-clockwise direction with the phase shift of 90°, it results in RHCP and vice versa for LHCP. This phase shift is obtained from the quadrature wavelength (λ/4) BLC connected at the two feeding ends of the T-junction power divider through the p-i-n diode for switching the ports of the coupler. When diode D1 is ON, and D2 is OFF, BLC splits the signal magnitude equally with a 90°-phase difference at port-2 and -3. Similarly, in the reverse condition, equal magnitude is split with a −90° phase difference at port −2 and −3.

The feeding arm length of power divider is variable from λg to λg/2. When the diode is OFF, the arm will be open stub with high input impedance, resulting in no disturbance in the other feeding arm. Hence, under this condition, the number of p-i-n diodes required is less, so insertion loss can be kept at a minimum because these diodes are not a perfect impedance match. The biasing to the p-i-n diode is achieved through the low-pass filter (LPF) to block the DC to feed arm. To obtain RHCP, D1 and D2 should be ON, and D3 and D4 should be OFF, and vice versa for LHCP. The bandwidth of RHCP and LHCP at reflection coefficient S11 < −10 dB is 26.5-29.5 GHz with a 3 dB bandwidth of 27-28.2 GHz, as shown in Figure 79(a). The average gain is 5 dBi with an efficiency of 56%. The radiation pattern is in a broadside direction, as in Figure 88(c-d). The prototype fabrication is shown in Figure 79(b-c). The limitation of the design is it has low gain, and low efficiency due to imperfect diodes and large back radiation.

In another design, the superposition of RHCP and LHCP with a feeding phase of ± 90° with equal magnitude is synthesized to obtain linear polarization at ± 45° [24]. The single-element is a semi-circular microstrip ring of varied diameter fed by SIW, as it has lower losses compared to the strip line. This results in CP radiation, as observed from the current distribution Figure 80(a-b). The single-element has been extended to seven such elements, which are connected in series fed by SIW, forming a subarray with two ports on both ends on Rogers 4350B. When both ports are excited simultaneously, the isolation of -20 dB is reported with a bandwidth of 29-31 GHz.

The dual linear polarization is obtained when both ports are excited with a phase difference of 0° and 90°, resulting in −45° linear polarization. When Port-1 and -2 are excited by 0° and −90°, it results in 45° linear polarization. The radiation is in the broadside direction but with large cross-polarization. This is due to unequal power radiation by elements when both ports are excited which has different phase center. To resolve this issue, another array is

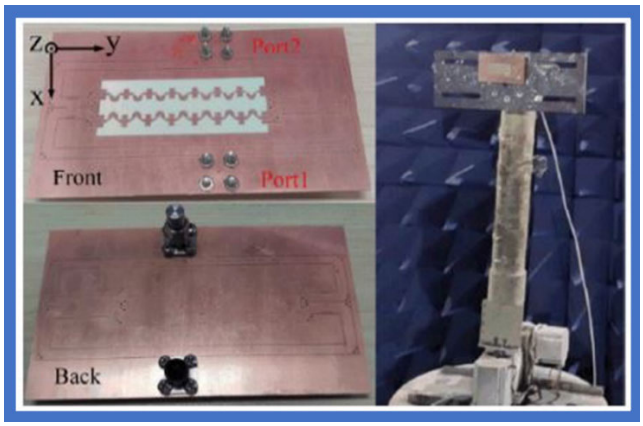

FIGURE 81. Prototype fabricaiton of proposed array antenna [24].

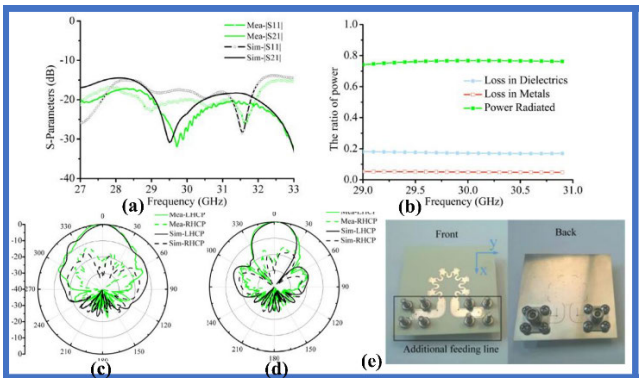

FIGURE 82. (a) Simulated and measure reflection coefficient and isolation. (b) Simulated ohmic, dielectric losses, and radiated power. Simulated and measure radiation patter (c) E-plane, (d) H-plane. (e)Proposed prototype fabrication of antenna [76].

placed adjacent to each other in an asymmetrical fashion where Port 1, 2, 3, and 4 has CP orientation of LH, RH, LH, and RH with feeding phase of 0°, 90°, 180°, 270° for −45° LP and 0°, −90°, −180°, −270° for +45° LP. The measured bandwidth at reflection coefficient S11 < −10 dB is 27-33 GHz with isolation of −15 dB between the ports, as shown in Figure 80(e). The radiation pattern is in broadside with HPBW of 36.8° and 8.3° in E- and H-plane at 29.9 GHz, as shown in Figure 80(c-d). For measurement purposes, in this article, the array antenna is connected to the feeding network because of which discrepancies can be seen in the measured and simulated results, as in Fig 80(f) In practice, the array antennas are directly connected to the RF chip with a phase control function. The prototype fabrication is shown in Figure 81.

In another design, the complexity of a multilayer substrate-integrated waveguide (SIW) is simplified to a single-layer, series-fed, 7-element structure [76]. Each unit consists of U-shape radiator connected to a phase shift transmission line (PSTL) separated at an angle of 45° which are engraved on top of Rogers RO4350B substrate. To make the PSTL as a non-radiating element, SIW concept is adopted, where the edges of PSTL having metallic vias are connected to the ground. This structure is extended to 7 radiating elements with 6 phase shifters arranged circularly. Whenever the signal is coupled at port 1, the signal flows with a phase shift in an anti-clockwise direction, resulting in left-hand-circular polarization (LHCP) in the z-axis. Similarly, when the signal is fed at port-2, it results in RHCP. The U-shape radiator is a non-uniform structure with a wider strip at the bottom of the U-shape. A parametric analysis is performed to study the radiated power.

The power radiation analysis from the radiating elements 1, 2, and 3 and 5, 6, and 7 are categorized as two subarrays where most of the power is radiated by the first three elements. This also results in beam deflection due to uneven power distribution and phase error with variation in frequency. An additional coaxial-to-SIW structure is added to feed the power, which also adds up to additional losses. With all these losses, the bandwidth at S11 < −10 dB resulted in 27-33 GHz, and isolation S12 of −20 dB is throughout the band, as shown in Figure 82(a). The simulated ohmic and dielectric losses are shown in Figure 82(b). The LHCP/RHCP resulted in HPBW of 33.5° and 35° in the E- and H-plane, as shown in Figure 82(c-d). The prototype fabrication is shown in Figure 82(e). The merits and demerits of polarization reconfigurable arrays are discussed in Table 14. Also, the summary of performance metrics of these arrays are presented in Table 15.

VI. DISCUSSION

The above sections have presented a detailed review of various array antennas based on feeding methods and shown how these antennas can be extended to reconfigurable arrays. The series-fed network offers an advantage in terms of low transmission line losses and compact design, but this method suffers from unequal power distribution to elements, narrow bandwidth, high return losses, and no control over individual elements. In series-fed planar arrays, the radiating element works as a power divider and radiator. When elements are uniformly arranged, most of the radiation takes place only by the first few radiators due to high input power. This results in unequal power distribution. In [36] and [40], the issue of unequal power distribution and narrow bandwidth is addressed with tapered shape elements and non-uniform positioning of the radiating elements, which also resulted in reduced SLL. The gain improvement with the ladder structure is shown in [37]. The signal in the series microstrip line has a periodic electric and magnetic field. If these are not radiated completely through radiators, this gives rise to return loss and cancels the magnetic field. Adding a stub to the transmission line at every λg period [38] or terminating the microstrip line with perfect match/radiator [39] can reduce the return losses. The CPW is another technique to reduce transmission line losses [41]. The SIW series-fed method has low radiation losses which are controlled by metallic vias around the transmission line and the structure. This also allows operating at higher modes at ease [42].

TABLE 14. Merits and demerits of polarization reconfigurable array structures.

References	Technique adapted	Merits	Demerits
[23]	Multilayer, uniform structure and spacing radiator, fed by parallel feed, additionally RF switch and BLC are used	• RH and LH circular polarization. • Wide bandwidth	• Introduces insertion loss due to RF diodes. • Low gain.
[24]	Non-uniform structure, uniform spacing with series-fed, along with SIW cavity	• Reduced leaky waves due to SIW. • Dual linear polarization. • Wide bandwidth. • Narrow beamwidth in E- and H-plane.	• Complex structure.
[76]	Non-uniform structure, uniform spacing radiator with SIW cavity and series-fed	• RH and LH circular polarization. • Wide bandwidth. • Narrow beamwidth in E-and H-plane.	• Resulted in uneven power distribution and phase error. • Requires coaxial-to-SIW structure to feed power.

TABLE 15. Performance metric summary of polarization reconfigurable structures.

Reference	Dimension (mm^2)	Center frequency (GHz)	Array Elements	Average Gain (dBi)	Bandwidth (GHz)	Isolation (dB)	Efficiency (%)	Beamwidth	Polarization
[23]	33 x 33	28	2 x 2	5	26.5 – 29.5	-	56	30^0 in E- & H-plane	RHCP / LHCP
[24]	-	30	2 x 7	11.8	27 -33	-15	-	36.8^0 & 8.3^0 in E- & H-plane	-45^0 LP / $+45^0$ LP
[76]	35 x 28	30	7x1	11.3 dBi at 30 GHZ	27 – 33	-20	-	33.5^0 & 35^0 in E - & H-plane	RHCP/LHCP

The parallel feed is the simplest to apply because it is easy to feed the required power and phase to each element. In [43], [44], [45], and [46] are a planar array in which equal power is applied through T-junction and bandwidth is enhanced by defecting the ground to partial ground. The parallel-fed method introduces high transmission line loss due to multiple feeding arms in an array structure. This can be resolved by etching the feed network on the bottom of the multilayer structure where the ground plane is shared between layers [47], [50], [51], and power to the radiator may be coupled through slots. The combination of coplanar strips and CPW can also reduce transmission line losses [48]. The other issue with array antenna is the coupling losses due to adjacent elements. With proper spacing between the elements, this can be reduced. In Vivaldi arrays, a notch between the elements [54] or comb-like element structure [55] can perturb the current flow, due to which the coupling can be reduced. The ME dipole [57] with pill box transmission structure [14] is also efficient in controlling radiation losses. A ridge gap waveguide (RGWG) with ME can be used to mitigate the substrate losses in a parallel transmission structure [59].

The benefits of series-fed and parallel-fed can be combined as a hybrid structure to make efficient transmission structure and to improve the radiation performance [60], [61], [62]. Our studies show that the hybrid feeding network of CPW [63], slot coupled [64], or SIW [65] structure has resulted in narrow or average bandwidth. The graphene is gaining attention due to its flexible and high conductive nature. With the CVD method, the radiating element can be formed, and these radiating elements have shown interesting results in radiation patterns with a high directive beam of 10.3° and 5.1° in E- and H-plane with low side-lobe levels of −24 dB, but it resulted in narrow bandwidth. The above feeding methods and radiating structures can be extended to a reconfigurable array by incorporating RF switches or phase shifters. The frequency can be tuned by designing BPF with the combination of a p-i-n diode and ring resonator [16]. The metamaterial structure can also be used to tune the frequency [77]. The beam steering can be continuous or discrete. To obtain these, the arrays are designed with hybrid feeding along with the radiating element. In such cases, the inter-element spacing plays a pivotal role because of which grating lobes may occur [17]. The butler matrix, along with BLCs [19], [70], [35] and or fixed phase shifter [18], can able to steer the beam in discrete steps. The active transmit/receive module can be used for continuous beam steering [68]. Active RF diodes [71] with extended stubs can steer the beam. Such structures also result in beam squint. The graphene nanoplates can be used in place of active RF switches to steer the beam [21]. The polarization can be changed when the phase at each element is changed in clockwise or anti-clockwise manner. For this,

RF switches, along with stubs, can be used to change the polarization [23]. The polarization can be changed when fed by either one of two port SIW feed networks with curved radiator, resulting in RHCP or LHCP [24] and when both ports are fed, it superimposes RHCP and LHCP, resulting in LP.

VII. CONCLUSION AND FUTURE SCOPE

A comprehensive review of array antennas based on the feeding method and reconfigurability is presented. The series and parallel feed methods have their own advantages and disadvantages. The tapered structures, CPW, and stubs along the transmission line may help in reducing return loss, and SIW technique can be used to overcome the demerits of series feed. Likewise, by separating the feed network and radiator into a multilayer structure, defected ground structure, CPS with CPW, pill box transmission, and RGWG can be used in parallel feed. The array with a combination of series and parallel can improve performance in terms of bandwidth, directivity, and low side-lobe level. The arrays with hybrid feed along with active RF switches, fixed phase shifter, or butler matrix with branch line coupler, could be able to tune the frequency, beam pattern, or polarization.

As graphene is gaining attraction due to its properties, it can be used as a radiator, or it can be used to tune the array antennas. The future scope is to extend the work on the reconfigurable array using graphene material, as only limited work can be seen. The major issue which is noticed in the reconfigurable array is that most designs have resulted in narrow bandwidth. Hence, a novel approach is required to enhance the bandwidth while maintaining the beam steering ability. The reconfigurable arrays can be extended to MIMO antennas, as the demand for 5G is to have a high gain, narrow beam, higher data rate, and wide bandwidth with steerable beam capacity both at the base station and mobile device.

REFERENCES

[1] X. Wang, L. Kong, F. Kong, F. Qiu, M. Xia, S. Arnon, and G. Chen, "Millimeter wave communication: A comprehensive survey," *IEEE Commun. Surveys Tuts.*, vol. 20, no. 3, pp. 1616–1653, 3rd Quart., 2018, doi: 10.1109/COMST.2018.2844322.

[2] F. Norouzian, E. Marchetti, M. Gashinova, E. Hoare, C. Constantinou, P. Gardner, and M. Cherniakov, "Rain attenuation at millimeter wave and low-THz frequencies," *IEEE Trans. Antennas Propag.*, vol. 68, no. 1, pp. 421–431, Jan. 2020, doi: 10.1109/TAP.2019.2938735.

[3] Z. Qingling and J. Li, "Rain attenuation in millimeter wave ranges," in *Proc. 7th Int. Symp. Antennas, Propag. EM Theory*, Guilin, China, Oct. 2006, pp. 1–4, doi: 10.1109/ISAPE.2006.353538.

[4] M. Marcus and B. Pattan, "Millimeter wave propagation: Spectrum management implications," *IEEE Microw. Mag.*, vol. 6, no. 2, pp. 54–62, Jun. 2005, doi: 10.1109/MMW.2005.1491267.

[5] G. R. MacCartney, J. Zhang, S. Nie, and T. S. Rappaport, "Path loss models for 5G millimeter wave propagation channels in urban microcells," in *Proc. IEEE Global Commun. Conf. (GLOBECOM)*, Atlanta, GA, USA, Dec. 2013, pp. 3948–3953, doi: 10.1109/GLOCOM.2013.6831690.

[6] S. Sun, G. R. MacCartney, and T. S. Rappaport, "Millimeter-wave distance-dependent large-scale propagation measurements and path loss models for outdoor and indoor 5G systems," in *Proc. 10th Eur. Conf. Antennas Propag. (EuCAP)*, Davos, Switzerland, Apr. 2016, pp. 1–5, doi: 10.1109/EuCAP.2016.7481506.

[7] I. Rosaline, A. Kumar, P. Upadhyay, and A. H. Murshed, "Four element MIMO antenna systems with decoupling lines for high-speed 5G wireless data communication," *Int. J. Antennas Propag.*, vol. 2022, pp. 1–13, Jun. 2022, doi: 10.1155/2022/9078929.

[8] A. I. Sulyman, A. Alwarafy, G. R. MacCartney, T. S. Rappaport, and A. Alsanie, "Directional radio propagation path loss models for millimeter-wave wireless networks in the 28-, 60-, and 73-GHz bands," *IEEE Trans. Wireless Commun.*, vol. 15, no. 10, pp. 6939–6947, Oct. 2016, doi: 10.1109/TWC.2016.2594067.

[9] E. Levine, G. Malamud, S. Shtrikman, and D. Treves, "A study of microstrip array antennas with the feed network," *IEEE Trans. Antennas Propag.*, vol. 37, no. 4, pp. 426–434, Apr. 1989, doi: 10.1109/8.24162.

[10] R. Simons and R. Lee, "Coplanar waveguide feeds for phased array antennas," in *Proc. Conf. Adv. SEI Technol.*, Sep. 1991, p. 3422.

[11] M. Henry, C. E. Free, B. S. Izqueirdo, J. Batchelor, and P. Young, "Millimeter wave substrate integrated waveguide antennas: Design and fabrication analysis," *IEEE Trans. Adv. Packag.*, vol. 32, no. 1, pp. 93–100, Feb. 2009, doi: 10.1109/TADVP.2008.2011284.

[12] L. Yan, W. Hong, G. Hua, J. Chen, K. Wu, and T. J. Cui, "Simulation and experiment on SIW slot array antennas," *IEEE Microw. Wireless Compon. Lett.*, vol. 14, no. 9, pp. 446–448, Sep. 2004, doi: 10.1109/LMWC.2004.832081.

[13] Y. Yang, C. Zhang, S. Lin, and A. E. Fathy, "Development of an ultra wideband Vivaldi antenna array," in *Proc. IEEE Antennas Propag. Soc. Int. Symp.*, Washington, DC, USA, Jul. 2005, pp. 606–609, doi: 10.1109/APS.2005.1551392.

[14] G.-H. Sun and H. Wong, "A planar millimeter-wave antenna array with a pillbox-distributed network," *IEEE Trans. Antennas Propag.*, vol. 68, no. 5, pp. 3664–3672, May 2020, doi: 10.1109/TAP.2020.2963931.

[15] Z.-C. Hao, Q. Yuan, B.-W. Li, and G. Q. Luo, "Wideband *W*-band substrate-integrated waveguide magnetoelectric (ME) dipole array antenna," *IEEE Trans. Antennas Propag.*, vol. 66, no. 6, pp. 3195–3200, Jun. 2018, doi: 10.1109/TAP.2018.2820503.

[16] M. Patriotis, F. N. Ayoub, Y. Tawk, J. Costantine, and C. G. Christodoulou, "A millimeter-wave frequency reconfigurable circularly polarized antenna array," *IEEE Open J. Antennas Propag.*, vol. 2, pp. 759–766, 2021, doi: 10.1109/OJAP.2021.3090908.

[17] G. Mishra, S. K. Sharma, and J.-C.-S. Chieh, "A high gain series-fed circularly polarized traveling-wave antenna at *W*-band using a new Butterfly radiating element," *IEEE Trans. Antennas Propag.*, vol. 68, no. 12, pp. 7947–7957, Dec. 2020, doi: 10.1109/TAP.2020.3000567.

[18] M. Khalily, R. Tafazolli, P. Xiao, and A. A. Kishk, "Broadband mm-wave microstrip array antenna with improved radiation characteristics for different 5G applications," *IEEE Trans. Antennas Propag.*, vol. 66, no. 9, pp. 4641–4647, Sep. 2018, doi: 10.1109/TAP.2018.2845451.

[19] S. Trinh-Van, J. M. Lee, Y. Yang, K.-Y. Lee, and K. C. Hwang, "A sidelobe-reduced, four-beam array antenna fed by a modified 4 × 4 Butler matrix for 5G applications," *IEEE Trans. Antennas Propag.*, vol. 67, no. 7, pp. 4528–4536, Jul. 2019, doi: 10.1109/TAP.2019.2905783.

[20] Y. Wang, F. Xu, Y.-Q. Jin, and Z. Du, "Low-cost reconfigurable 1 bit millimeter-wave array antenna for mobile terminals," *IEEE Trans. Antennas Propag.*, vol. 70, no. 6, pp. 4507–4517, Jun. 2022, doi: 10.1109/TAP.2022.3140508.

[21] C. Fan, B. Wu, Y. Hu, Y. Zhao, and T. Su, "Millimeter-wave pattern reconfigurable Vivaldi antenna using tunable resistor based on graphene," *IEEE Trans. Antennas Propag.*, vol. 68, no. 6, pp. 4939–4943, Jun. 2020, doi: 10.1109/TAP.2019.2952639.

[22] J. Perruisseau-Carrier, "Graphene for antenna applications: Opportunities and challenges from microwaves to THz," in *Proc. Loughborough Antennas Propag. Conf. (LAPC)*, Loughborough, U.K., Nov. 2012, pp. 1–4, doi: 10.1109/LAPC.2012.6402934.

[23] E. A. Abbas, N. Nguyen-Trong, A. T. Mobashsher, and A. M. Abbosh, "Polarization-reconfigurable antenna array for millimeter-wave 5G," *IEEE Access*, vol. 7, pp. 131214–131220, 2019, doi: 10.1109/ACCESS.2019.2939815.

[24] Q. Lv, Y.-H. Yang, S.-G. Zhou, C. Shao, D. Zhou, and C.-Y.-D. Sim, "Design of a single-layer ±45° dual-polarized directional array antenna for millimeter wave applications," *Sensors*, vol. 21, no. 13, p. 4326, Jun. 2021, doi: 10.3390/s21134326.

[25] I. Rahman, S. M. Razavi, O. Liberg, C. Hoymann, H. Wiemann, C. Tidestav, P. Schliwa-Bertling, P. Persson, and D. Gerstenberger, "5G evolution toward 5G advanced: An overview of 3GPP releases 17 and 18," *Ericsson Technol. Rev.*, vol. 2021, no. 14, pp. 2–12, Oct. 2021.

[26] L. Wei, R. Q. Hu, Y. Qian, and G. Wu, "Key elements to enable millimeter wave communications for 5G wireless systems," *IEEE Wireless Commun.*, vol. 21, no. 6, pp. 136–143, Dec. 2014, doi: 10.1109/MWC.2014.7000981.

[27] J. Zhao, J. Liu, L. Yang, B. Ai, and S. Ni, "Future 5G-oriented system for urban rail transit: Opportunities and challenges," *China Commun.*, vol. 18, no. 2, pp. 1–12, Feb. 2021, doi: 10.23919/JCC.2021.02.001.

[28] T. Yuan, N. Yuan, and L.-W. Li, "A novel series-fed taper antenna array design," *IEEE Antennas Wireless Propag. Lett.*, vol. 7, pp. 362–365, 2008, doi: 10.1109/LAWP.2008.928487.

[29] A. Mansoul, F. Ghanem, M. R. Hamid, and M. Trabelsi, "A selective frequency-reconfigurable antenna for cognitive radio applications," *IEEE Antennas Wireless Propag. Lett.*, vol. 13, pp. 515–518, 2014, doi: 10.1109/LAWP.2014.2311114.

[30] M. Sun, Z. Zhang, F. Zhang, and A. Chen, "L/S multiband frequency-reconfigurable antenna for satellite applications," *IEEE Antennas Wireless Propag. Lett.*, vol. 18, no. 12, pp. 2617–2621, Dec. 2019, doi: 10.1109/LAWP.2019.2945624.

[31] C. Y. Rhee, J. H. Kim, W. J. Jung, T. Park, B. Lee, and C. W. Jung, "Frequency-reconfigurable antenna for broadband airborne applications," *IEEE Antennas Wireless Propag. Lett.*, vol. 13, pp. 189–192, 2014, doi: 10.1109/LAWP.2014.2301036.

[32] H. Hashemi, X. Guan, A. Komijani, and A. Hajimiri, "A 24-GHz SiGe phased-array receiver-LO phase-shifting approach," *IEEE Trans. Microw. Theory Techn.*, vol. 53, no. 2, pp. 614–626, Feb. 2005, doi: 10.1109/TMTT.2004.841218.

[33] B. Biglarbegian, M.-R. Nezhad-Ahmadi, M. Fakharzadeh, and S. Safavi-Naeini, "A wideband 90° continuous phase shifter for 60 GHz phased array transceiver in 90 nm CMOS technology," in *Proc. Eur. Microw. Conf. (EuMC)*, Sep. 2009, pp. 1–4.

[34] I. B. Mabrouk, M. Al-Hasan, M. Nedil, T. A. Denidni, and A. Sebak, "A novel design of radiation pattern-reconfigurable antenna system for millimeter-wave 5G applications," *IEEE Trans. Antennas Propag.*, vol. 68, no. 4, pp. 2585–2592, Apr. 2020, doi: 10.1109/TAP.2019.2952607.

[35] S. Kim, S. Yoon, Y. Lee, and H. Shin, "A miniaturized Butler matrix based switched beamforming antenna system in a two-layer hybrid stackup substrate for 5G applications," *Electronics*, vol. 8, no. 11, p. 1232, Oct. 2019, doi: 10.3390/electronics8111232.

[36] H. Wang, K. E. Kedze, and I. Park, "A high-gain and wideband series-fed angled printed dipole array antenna," *IEEE Trans. Antennas Propag.*, vol. 68, no. 7, pp. 5708–5713, Jul. 2020, doi: 10.1109/TAP.2020.2975882.

[37] L. Malviya and P. Gupta, "Millimeter wave high-gain antenna array for wireless applications," *IETE J. Res.*, vol. 2021, pp. 1–10, Mar. 2021, doi: 10.1080/03772063.2021.1903346.

[38] Y. Q. Guo, Y. M. Pan, and S. Y. Zheng, "Design of series-fed, single-layer, and wideband millimeter-wave microstrip arrays," *IEEE Trans. Antennas Propag.*, vol. 68, no. 10, pp. 7017–7026, Oct. 2020, doi: 10.1109/TAP.2020.3008668.

[39] U. Ullah, M. Al-Hasan, S. Koziel, and I. B. Mabrouk, "A series inclined slot-fed circularly polarized antenna for 5G 28 GHz applications," *IEEE Antennas Wireless Propag. Lett.*, vol. 20, no. 3, pp. 351–355, Mar. 2021, doi: 10.1109/LAWP.2021.3049901.

[40] Y. Kang, E. Noh, and K. Kim, "Design of traveling-wave series-fed microstrip array with a low sidelobe level," *IEEE Antennas Wireless Propag. Lett.*, vol. 19, no. 8, pp. 1395–1399, Aug. 2020, doi: 10.1109/LAWP.2020.2989916.

[41] C.-P. Chao, S.-H. Yang, C.-M. Tung, C.-F. Yang, W.-H. Lin, C.-Y. Chai, and I. Lin, "A series-fed cavity-back patch array antenna for a miniaturized 77 GHz radar module," in *Proc. IEEE Int. Symp. Antennas Propag. USNC-URSI Radio Sci. Meeting*, Atlanta, GA, USA, Jul. 2019, pp. 657–658, doi: 10.1109/APUSNCURSINRSM.2019.8888699.

[42] L. Li and J.-B. Yan, "A low-cost and efficient microstrip-fed air-substrate-integrated waveguide slot array," *Electronics*, vol. 10, no. 3, p. 338, Feb. 2021, doi: 10.3390/electronics10030338.

[43] M. E. Munir, A. G. A. Harbi, S. H. Kiani, M. Marey, N. O. Parchin, J. Khan, H. Mostafa, J. Iqbal, M. A. Khan, C. H. See, and R. A. Abd-Alhameed, "A new mm-wave antenna array with wideband characteristics for next generation communication systems," *Electronics*, vol. 11, no. 10, p. 1560, May 2022, doi: 10.3390/electronics11101560.

[44] M. M. Kamal, S. Yang, S. H. Kiani, M. R. Anjum, M. Alibakhshikenari, Z. A. Arain, A. A. Jamali, A. Lalbakhsh, and E. Limiti, "Donut-shaped mmWave printed antenna array for 5G technology," *Electronics*, vol. 10, no. 12, p. 1415, Jun. 2021, doi: 10.3390/electronics10121415.

[45] I. Ahmad, H. Sun, U. Rafique, and Z. Yi, "Triangular slot-loaded wideband planar rectangular antenna array for millimeter-wave 5G applications," *Electronics*, vol. 10, no. 7, p. 778, Mar. 2021, doi: 10.3390/electronics10070778.

[46] H. Ullah and F. A. Tahir, "A high gain and wideband narrow-beam antenna for 5G millimeter-wave applications," *IEEE Access*, vol. 8, pp. 29430–29434, 2020, doi: 10.1109/ACCESS.2020.2970753.

[47] J. Xu, W. Hong, Z. H. Jiang, H. Zhang, and K. Wu, "Low-profile wideband vertically folded slotted circular patch array for *Ka*-band applications," *IEEE Trans. Antennas Propag.*, vol. 68, no. 9, pp. 6844–6849, Sep. 2020, doi: 10.1109/TAP.2020.3005028.

[48] D. Liu and R. Sirdeshmukh, "A patch array antenna for 60 GHz package applications," in *Proc. IEEE Antennas Propag. Soc. Int. Symp.*, San Diego, CA, USA, Jul. 2008, pp. 1–4, doi: 10.1109/APS.2008.4618961.

[49] T. S. Mneesy, R. K. Hamad, A. I. Zaki, and W. A. E. Ali, "A novel high gain monopole antenna array for 60 GHz millimeter-wave communications," *Appl. Sci.*, vol. 10, no. 13, p. 4546, Jun. 2020, doi: 10.3390/app10134546.

[50] W. Ma, W. Cao, R. Hong, J. Jin, and B. Zhang, "Planar broadband higher-order mode millimeter-wave microstrip patch antenna array with low sidelobe level," *IEEE Antennas Wireless Propag. Lett.*, vol. 20, no. 12, pp. 2225–2229, Dec. 2021, doi: 10.1109/LAWP.2021.3103532.

[51] J. Jiang and B. Feng, "Chinese-characters Jin-shaped patch antenna array for 5G millimeter wave communications," in *Proc. Cross Strait Radio Sci. Wireless Technol. Conf. (CSRSWTC)*, Shenzhen, China, Oct. 2021, pp. 251–253, doi: 10.1109/CSRSWTC52801.2021.9631743.

[52] Y.-J. Kim, Y.-B. Kim, and H. L. Lee, "mmWave high gain planar H-shaped shorted ring antenna array," *Sensors*, vol. 20, no. 18, p. 5168, Sep. 2020, doi: 10.3390/s20185168.

[53] B. Hammu-Mohamed, Á. Palomares-Caballero, C. Segura-Gómez, F. G. Ruiz, and P. Padilla, "SIW cavity-backed antenna array based on double slots for mmWave communications," *Appl. Sci.*, vol. 11, no. 11, p. 4824, May 2021, doi: 10.3390/app11114824.

[54] P. Ramanujam, M. Ponnusamy, and K. Ramanujam, "A compact wide-bandwidth antipodal Vivaldi antenna array with suppressed mutual coupling for 5G mm-wave applications," *AEU-Int. J. Electron. Commun.*, vol. 133, May 2021, Art. no. 153668, doi: 10.1016/j.aeue.2021.153668.

[55] A. S. Dixit, S. Kumar, S. Urooj, and A. Malibari, "A highly compact antipodal Vivaldi antenna array for 5G millimeter wave applications," *Sensors*, vol. 21, no. 7, p. 2360, Mar. 2021, doi: 10.3390/s21072360.

[56] R. Ullah, S. Ullah, F. Faisal, R. Ullah, D.-Y. Choi, A. Ahmad, and B. Kamal, "High-gain Vivaldi antenna with wide bandwidth characteristics for 5G mobile and Ku-band radar applications," *Electronics*, vol. 10, no. 6, p. 667, Mar. 2021, doi: 10.3390/electronics10060667.

[57] A. Dadgarpour, N. Bayat-Makou, M. A. Antoniades, A. A. Kishk, and A. Sebak, "A dual-polarized magnetoelectric dipole array based on printed ridge gap waveguide with dual-polarized split-ring resonator lens," *IEEE Trans. Antennas Propag.*, vol. 68, no. 5, pp. 3578–3585, May 2020.

[58] J. D. Baena, J. Bonache, F. Martín, R. M. Sillero, F. Falcone, T. Lopetegi, and M. A. G. Laso, "Equivalent-circuit models for split-ring resonators and complementary split-ring resonators coupled to planar transmission lines," *IEEE Trans. Microw. Theory Techn.*, vol. 53, no. 4, pp. 1451–1461, Apr. 2005, doi: 10.1109/TMTT.2005.845211.

[59] W. Tan, Y. Xiao, C. Li, K. Zhu, H. Luo, and H. Sun, "A wide-band high-efficiency hybrid-feed antenna array for mm-wave wireless systems," *Electronics*, vol. 10, no. 19, p. 2383, Sep. 2021, doi: 10.3390/electronics10192383.

[60] B. T. Mohamed and H. Ammor, "A 16-elements corporate-series feed rectangular patch antenna array at 28 GHz, for future 5G applications," in *Proc. Int. Conf. Wireless Technol., Embedded Intell. Syst. (WITS)*, 2019, pp. 1–4.

[61] C. A. Balanis, *Antenna Theory: Analysis and Design*, 4th ed. Hoboken, NJ, USA: Wiley, 2016.

[62] Y. Liu, G. Bai, and M. C. E. Yagoub, "A 79 GHz series fed microstrip patch antenna array with bandwidth enhancement and sidelobe suppression," in *Proc. Int. Conf. Radar, Antenna, Microw., Electron., Telecommun. (ICRAMET)*, Nov. 2020, pp. 155–158.

[63] V. Harini, M. V. S. Sairam, and R. Madhu, "16-element CPW series fed millimeter-wave hexagonal array antenna for 5G femtocell applications," *Int. J. Microw. Wireless Technol.*, vol. 2021, pp. 1–15, Aug. 2021, doi: 10.1017/S1759078721001185.

[64] Z. Wang and Z. Huang, "A microwave/millimeter wave dual-band shared aperture patch antenna array," *IEEE Access*, vol. 8, pp. 218585–218591, 2020, doi: 10.1109/ACCESS.2020.3040250.

[65] H. Jin, G. Q. Luo, W. Wang, W. Che, and K.-S. Chin, "Integration design of millimeter-wave filtering patch antenna array with SIW four-way anti-phase filtering power divider," *IEEE Access*, vol. 7, pp. 49804–49812, 2019.
[66] R. Song, Z. Wang, H. Zu, Q. Chen, B. Mao, Z. P. Wu, and D. He, "Wideband and low sidelobe graphene antenna array for 5G applications," *Sci. Bull.*, vol. 66, no. 2, pp. 103–106, Jan. 2021, doi: 10.1016/j.scib.2020.09.028.
[67] M. Alibakhshikenari, B. S. Virdee, C. H. See, R. A. Abd-Alhameed, F. Falcone, and E. Limiti, "High-isolation leaky-wave array antenna based on CRLH-metamaterial implemented on SIW with ±30° frequency beam-scanning capability at millimetre-waves," *Electronics*, vol. 8, no. 6, p. 642, Jun. 2019, doi: 10.3390/electronics8060642.
[68] H.-C. Chen, T. Chiu, and C.-L. Hsu, "Design of series-fed bandwidth-enhanced microstrip antenna array for millimetre-wave beamforming applications," *Int. J. Antennas Propag.*, vol. 2019, pp. 1–10, Jun. 2019, doi: 10.1155/2019/3857964.
[69] M. Khalily, R. Tafazolli, T. A. Rahman, and M. R. Kamarudin, "Design of phased arrays of series-fed patch antennas with reduced number of the controllers for 28-GHz mm-wave applications," *IEEE Antennas Wireless Propag. Lett.*, vol. 15, pp. 1305–1308, Dec. 2015, doi: 10.1109/LAWP.2015.2505781.
[70] A. M. A. Najafabadi, F. A. Ghani, and I. Tekin, "Low-cost multibeam millimeter-wave array antennas for 5G mobile applications," *IEEE Trans. Veh. Technol.*, early access, Aug. 16, 2022, doi: 10.1109/TVT.2022.3198878.
[71] C. Deng, D. Liu, B. Yektakhah, and K. Sarabandi, "Series-fed beam-steerable millimeter-wave antenna design with wide spatial coverage for 5G mobile terminals," *IEEE Trans. Antennas Propag.*, vol. 68, no. 5, pp. 3366–3376, May 2020, doi: 10.1109/TAP.2019.2963583.
[72] H. Yi, L. Li, J. Han, and Y. Shi, "Traveling-wave series-fed patch array antenna using novel reflection-canceling elements for flexible beam," *IEEE Access*, vol. 7, pp. 111466–111476, 2019, doi: 10.1109/ACCESS.2019.2934652.
[73] N. O. Parchin, M. Alibakhshikenari, H. J. Basherlou, R. A. Abd-Alhameed, J. Rodriguez, and E. Limiti, "MM-wave phased array Quasi-Yagi antenna for the upcoming 5G cellular communications," *Appl. Sci.*, vol. 9, no. 5, p. 978, Mar. 2019, doi: 10.3390/app9050978.
[74] Y.-H. Yang, B.-H. Sun, and J.-L. Guo, "A single-layer wideband circularly polarized antenna for millimeter-wave applications," *IEEE Trans. Antennas Propag.*, vol. 68, no. 6, pp. 4925–4929, Jun. 2020, doi: 10.1109/TAP.2019.2951518.
[75] C. Mao, M. Khalily, P. Xiao, L. Zhang, and R. Tafazolli, "High-gain phased array antenna with endfire radiation for 26 GHz wide-beam-scanning applications," *IEEE Trans. Antennas Propag.*, vol. 69, no. 5, pp. 3015–3020, May 2021, doi: 10.1109/TAP.2020.3028181.
[76] Y.-H. Yang, B.-H. Sun, and J.-L. Guo, "A low-cost, single-layer, dual circularly polarized antenna for millimeter-wave applications," *IEEE Antennas Wireless Propag. Lett.*, vol. 18, no. 4, pp. 651–655, Apr. 2019, doi: 10.1109/LAWP.2019.2900301.
[77] B. K. Ledimo, P. Moaro, R. Ramogomana, M. Mosalaosi, and B. Basutli, "Design procedure of a frequency reconfigurable metasurface antenna at mmWave band," *Telecom*, vol. 3, no. 2, pp. 379–395, Jun. 2022, doi: 10.3390/telecom3020020.

B. G. PARVEEZ SHARIFF received the B.E. degree in telecommunication engineering and the M.Tech. degree in digital electronics and communication systems from Visvesvaraya Technological University, Belagavi, India. He is currently pursuing the Ph.D. degree with the Department of Electronics and Communication Engineering, Manipal Institute of Technology, Manipal, India. His research interests include microstrip antennas and metamaterials. He is a member of LMISTE, India.

TANWEER ALI (Senior Member, IEEE) is currently working as an Associate Professor with the Department of Electronics and Communication Engineering, Manipal Institute of Technology, Manipal Academy of Higher Education, Manipal. He is an active researcher in the field of microstrip antennas, wireless communication, and microwave imaging. He has been listed in top 2% scientists across the world for the year 2021 and 2022 by the prestigious list published by Stanford University, USA, indexed by Scopus. He has published more than 130 papers in reputed web of science (SCI) and Scopus indexed journals and conferences and has filed seven Indian patents, of which three have been published. He has H-index of 23 and i-10 index of 39. He is on the Board of a Reviewer of journals, such as the IEEE TRANSACTIONS ON ANTENNAS AND PROPAGATION, IEEE ANTENNAS AND WIRELESS PROPAGATION LETTERS, IEEE ACCESS, *IET Microwaves, Antennas and Propagation*, *IET of Electronics Letter*, *Wireless Personal Communications* (WPCs) (Springer), *AEU-International Journal of Electronics and Communications*, *Microwave and Optical Technology Letters* (MOTL) (Wiley), *International Journal of Antennas and Propagation* (Hindawi), *Advanced Electromagnetics*, *Progress in Electromagnetics Research* (PIER), *KSII Transactions on Engineering Science*, *International Journal of Microwave and Wireless Technologies*, *Frequenz*, *Radioengineering*, and IEEE OPEN JOURNAL OF ANTENNAS AND PROPAGATION.

PALLAVI R. MANE (Senior Member, IEEE) received the B.E. degree in electronics and communication engineering from the Gogte Institute of Technology, India, in 1996, the M.Tech. degree in digital electronics and advanced communication from the National Institute of Technology, Surathkal Karnataka, India, in 2002, and the Ph.D. degree in electronics and communication engineering from the Manipal Institute of Technology, Manipal-MAHE for the thesis in network coding, in 2014. She is currently a Professor with the Department of ECE, MIT-MAHE. She has authored several papers in international conferences and journal proceedings. Her research interests include network coding, source, and channel coding, and communication engineering.

PRADEEP KUMAR received the bachelor's, M.E., and Ph.D. degrees in electronics and communication engineering, in 2003, 2005, and 2009, respectively. He was a Postdoctoral Researcher at the Autonomous University of Madrid, Spain. He is currently with the University of KwaZulu-Natal, South Africa. He has over 15 years of experience in academics and research. He has held various positions, such as a lecturer, a senior lecturer, an assistant professor, and an associate professor. He is the author of many research papers published in various peer-reviewed journals/conferences. His current research interests include antennas, antenna arrays, and wireless communications. He is registered as a Professional Engineer with the Engineering Council of South Africa. He received various awards/fellowships, such as the MHRD Fellowship, the A4U Fellowship, the Research Excellence Award, the J. W. Nelson Fund Research Award, and the CAES Research Award. He is serving as a Reviewer/a TPC Member for many journals/conferences, such as IEEE TRANSACTIONS ON ANTENNAS AND PROPAGATION, IEEE ACCESS, *Progress in Electromagnetics Research*, *ACES Journal*, IEEE SYSTEMS JOURNAL, *SAIEE Africa Research Journal*, the *International Journal of Electronics*, SATNAC, and IEEE Africon.